

Investigating properties of cerebro-spinal fluid contacting cells in rodents; can they influence ependymal cell proliferation?

Charlotte Natasha Marx-Carr

Submitted in accordance with the requirements for the degree of Masters by Research

The University of Leeds

-

School of Biomedical Sciences

March 2022

The candidate confirms that the work submitted is her own and that appropriate credit has been given where reference has been made to the work of others

This copy has been supplied on the understanding that it is copyright material and that no quotation from the thesis may be published without proper acknowledgement

Acknowledgements

I would like to acknowledge and give thanks to Professor Jim Deuchars, my supervisor and Susan Deuchars my co-supervisor who both guided and advised me through this year. Their ideas and passion of the subject maintained my interest throughout and encouraged me to be creative with ideas which were always all discussed and considered helping me shape this masters project. They were always available to answer questions and check over anything I was uncertain of.

Also to the members of the Deuchars lab who were extremely helpful in assisting me with techniques and offered guidance for the duration I was in the lab. In particular I would like to thank Marilyn Clark for teaching me every key technique I used throughout this project and continually assisted me with any difficulties I faced and was always on hand to answer any questions and to help resolve any issues.

Importantly, this masters wouldn't have been possible without the support of my family and friends, Nici who believed in me and facilitated my move to Leeds this year. My dad has provided support throughout. Thanks to Matthew for the encouragement when completing the write up at every hour of the day and to Alex for help with presenting data.

It wouldn't have been possible to complete this project without all the help and support, particularly starting during the pandemic. All the belief and encouragement is greatly appreciated and I really enjoyed every aspect of completing this masters.

Abstract

The spinal cord is part of the central nervous system which contributes to many physiological functions. There is a possible neurogenic niche located within the central canal of the spinal cord, within which there are a subtype of cells proliferating at baseline. These cells demonstrate plasticity via an increased rate of proliferation following spinal cord injury (SCI). Neighbouring these dividing cells are cerebro-spinal fluid contacting cells (CSFcCs) which have a poorly defined function within rodents. This study assesses properties of CSFcCs, validates a novel transgenic mouse line and uses viral tracing to demonstrate the length and direction of their extensions. It also assessed whether CSFcCs can be manipulated to influence the activity of the cells proliferating within the ependymal layer.

Antibody labelling revealed CSFcCs also labelled with GCaMP6f expressed by the vesicular gamma-aminobutyric acid transporter (VGAT) promoter and a synaptic vesicle protein revealing they have the apparatus to load GABA into vesicles and release vesicular content from their terminals within the central canal (CC). They also co-labelled with an antibody to the glucagon-like peptide 1 receptor (GLP1R), offering a novel input for stimulation.

Intraperitoneal injection of the GLP1R agonist liraglutide with the proliferative marker 5-ethynyl-2'-deoxyuridine (EdU) resulted in a reduced number of EdU positive cells in the ependymal cell layer (ECL), compared to mice with EdU and vehicle only injections. This suggests there is a relationship between CSFcCs and ependymal cells (EpCs) which has not previously been shown.

Mice expressing cre-recombinase under control of the PKD2L1 promoter, which are shown here to be specifically expressed in CSFcCs in the CNS, were intraspinally injected with a floxed virus expressing diphtheria toxin subunit-A (DTA). There was a remarkable increase in the number of EdU+ cells around the CC in most regions of the spinal cord compared to uninjected mice or mice injected with a virus that did not express DTA. Markers of cell death indicated that the expression of DTA in CSFcCs resulted in the death of EpCs, further indicating an essential trophic relationship between these cells.

This connection between CSFcCs and dividing ependymal cells (EpCs) may be utilised for therapeutic benefit in disorders of the spinal cord where modulating proliferation may be used to restore cell populations.

Table of Contents

Acknowledgements	2
Abstract.....	3
Table of Contents	4
List of Figures	7
List of Tables	10
Abbreviations	11
Chapter 1: Introduction	13
1.1. The spinal cord.....	13
1.2. Central canal	13
1.3. Is the central canal region of the spinal cord a neurogenic niche?.....	13
1.3.1 Ependymal cells may be these neural stem cells	14
1.3.2 Cell proliferation after spinal cord injury	16
1.4. What is the role of cerebro-spinal fluid contacting cells?	17
1.4.1. CSFcs can respond to changes in pH	19
1.4.2. Do CSFcs have neuronal properties?.....	20
1.4.3. A mechanosensory function for CSFcs?	21
1.4.4. Do CSFcs receive synaptic inputs?.....	23
1.5. Glucagon like peptide 1 may influence CSFcs activity	25
1.5.2. GLP1 analogues are useful tools to study the role of these receptors.....	26
1.6. Conclusion	27
1.7. Hypothesis and Aims	28
1.8. General Methods	30
1.8.1. Animals.....	30
1.8.2. Preparation of the virus and tools.....	30
1.8.3. Surgery and Injection	31
1.8.4. Perfusions.....	32
1.8.5. Tissue preparation.....	32
1.8.6. Gelatin embedding.....	33

1.8.7. Immunohistochemistry	33
1.8.8. Mounting.....	37
1.8.9. Microscopy	37
Chapter 2: Exploring CSFcC distribution and properties	38
2.1. Introduction	38
2.2. Aims.....	39
2.3. Methods	41
2.3.1. Animals.....	41
2.3.2. Tissue used for staining and counts	42
2.3.3. Comparison of immunohistochemistry methods.....	43
2.3.4. Biotinylated antibodies	46
2.3.5. DAB.....	46
2.3.6. TSA.....	46
2.3.7. Dehydration.....	47
2.3.8. Counts and analysis	47
2.3.9. Virus.....	48
2.3.10. Tissue sectioning	48
2.4. Results	49
2.4.1. Different immunohistochemistry methods to label PKD2L1+ CSFcCs.....	49
2.4.2. GCaMP6f expression within PKD2L1+ CSFcCs	52
2.4.3. Double labelling of CSFcCs infers novel properties	59
2.4.4. Viral tracing of CSFcC projections along ventral fissure	64
2.5. Discussion	67
2.5.1. CSFcCs can be clearly and selectively visualised using antibodies for PKD2L1.....	67
2.5.2. CSFcC distribution in PKD2L1:GCaMP6f mice.....	68
2.5.3. Antibody labelling for other markers in PKD2L1+ CSFcCs	69
2.5.4. Projections from PKD2L1+ CSFcCs along ventral fissure	71
2.5.5. Conclusions.....	72
Chapter 3: Does manipulation of CSFcCs influence EpC proliferation?.....	73
3.1. Introduction	73
3.2. Hypothesis and Aims.....	75
3.3. Methods	76
3.3.1. Animals.....	76

3.3.2. Liraglutide and EdU Injections.....	76
3.3.3. Virus and Injections.....	76
3.3.4. Immunohistochemistry.....	77
3.3.5. Tissue used.....	78
3.3.6. Imaging.....	78
3.3.7. Counts and analysis.....	78
3.4. Results.....	80
3.4.1. Liraglutide decreased proliferation within the spinal cord.....	80
3.4.2. Viral expression of DTA in CSFcCs increased EpC proliferation.....	82
3.5. Discussion.....	100
3.5.1. Liraglutide injections dampened EpC proliferation in the spinal cord.....	100
3.5.2. Viral expression of DTA influenced CSFcCs, increasing EpC proliferation.....	102
3.5.3. Conclusions.....	104
4. Future Experiments.....	105
5. Conclusions.....	107
6. References.....	108

List of Figures

Figure 1: The ependymal zone	14
Figure 2: GLP1R mRNA expression within CSFcCs?	26
Figure 3: Summary of CSFcC and EpC functions	28
Figure 4: Intraspinal injections.....	31
Figure 5: Anatomical planes of the spinal cord.....	32
Figure 6: Indirectly conjugated antibodies	43
Figure 7: Biotinylated antibody binding	44
Figure 8: DAB labelling.....	45
Figure 9: TSA process	46
Figure 10: CSFcCs are primarily distributed around the CC	49
Figure 11: Biotinylated antibody labelling revealed labelling outside of CC.....	50
Figure 12: TSA labelling shows extensive axonal labelling in the ventral fissure	51
Figure 13: Prominent axons and CSFcC somata outside CC.....	51
Figure 14: GCaMP6f expression in CC and VF co-localised with PKD2L1.....	52
Figure 15: CSFcCs distributed along the entire CC.....	53
Figure 16: GCaMP6f not expressed in the brain	54
Figure 17: High CSFcC expression within various brainstem nuclei	55
Figure 18: Axonal projections across transverse brainstem sections	56
Figure 19: DAB staining of axons in brainstem nuclei	57
Figure 20: GCaMP6f expression in kidney tubules.....	58
Figure 21: PKD2L1 co-localises with VGAT:GCaMP6f+ CSFcCs.....	59
Figure 22: CSFcC terminals express SV2	60
Figure 23: CSFcCs express the GLP1R	60

Figure 24: High GLP1R expression in CSFcCs	61
Figure 25: CSFcCs express neuronal marker Hu C/D	62
Figure 26: Distribution of CSFcCs within ependymal zone	63
Figure 27: mCherry expression reveals rostral axon projections from CSFcCs	64
Figure 28: mCherry expression within CC and VF immediately below injection site.....	65
Figure 29: Axonal projections are observed in sacral sections, caudal to injection	66
Figure 30: Liraglutide and/or EdU injection schedule	76
Figure 31: Virus and EdU injection timeline.....	77
Figure 32: Significant decrease in the number of EdU+ cells after Liraglutide treatment ..	81
Figure 33: Viral expression of mCherry across whole spinal cord at injection site in DTA mouse 1	82
Figure 34: Viral expression of mCherry reaching CC at the injection site in DTA mouse 2 .	83
Figure 35: Significant increase in the number of proliferating EdU+ cells around the CC after viral injection	84
Figure 36: No caspase-3+ in any region of control mouse 1, little variation in EdU+ between regions.....	85
Figure 37: Viral injection into the spinal cord doesn't cause caspase-3 expression	85
Figure 38: Regional changes in EdU+ around CC of DTA mouse 1.....	86
Figure 39: Caspase-3+ CC and changes in CSFcC morphology in DTA cord 1	87
Figure 40: High number of EdU+ cells around CC DTA mouse 2	88
Figure 41: Caspase-3+ around CC of many regions from DTA mouse 2 and unusual morphology of CSFcCs	89
Figure 42: GCaMP6f+ CSFcCs in a control animal with typical morphology	91
Figure 43: GCaMP6f+ CSFcCs in DTA mouse 1 with notable morphological changes in GCaMP6f+ CSFcCs	92
Figure 44: GCaMP6f+ CSFcCs in DTA mouse 2 with some unusual morphological features	93

Figure 45: mCherry+ within motor and somatosensory areas of the brain	95
Figure 46: Brain sections were not caspase-3+	96
Figure 47: mCherry+ cells and axons in the NTS	97
Figure 48: mCherry+ projections in the region of GCaMP6f+ CSFcs in brainstem and within raphe nuclei.....	99
Figure 49: Manipulation of CSFcs can result in increased or decreased EpC proliferation	104

List of Tables

Table 1: Receptors and channels expressed by CSFcCs	23
Table 2: Peptides present within CSFcCs	29
Table 3: List of primary antibodies, concentrations and justifications	35
Table 4: List of secondary antibodies and concentrations.	36
Table 5: Tissue used for labelling and counts.	42
Table 6: Tissue used for Liraglutide and DTA counts and analysis.....	78

Abbreviations

AAV	Adeno-associated virus
ACh	Acetylcholine
aCSF	Artificial CSF
ASIC3	Acid sensing ion channel 3
BrdU	Bromodeoxyuridine
cAMP	Cyclic adenosine monophosphate
CARD	Catalysed reporter deposition
CC	Central canal
ChR	Channel rhodopsin
CNS	Central nervous system
cre	Cre recombinase
CSF	Cerebro-spinal fluid
CSFcC	Cerebro-spinal fluid contacting cells
DAB	Diaminobenzidine
dH ₂ O	Distilled water
DT	Diphtheria toxin
DTA	Diphtheria toxin subunit-A
EDU	5-ethynyl-2'-deoxyuridine
EGF	Epidermal growth factor
EpCs	Ependymal cells
FGF	Fibroblast growth factor
GABA	Gamma-aminobutyric acid
GABA _A	Gamma-aminobutyric acid – A type receptor
GFP	Green fluorescent protein
GLP1	Glucagon like peptide 1
GLP1R	GLP1 receptors
GM	Grey matter
HRP	Horse radish peroxidase
IP	Intraperitoneal
KO	Knock out
LiGluR	Light gated ionotropic glutamate receptor
MCA	Mecamylamine
mRNA	Messenger RNA
MS	Multiple sclerosis

NSC	Neural stem cell
NTS	Nucleus tractus solitarius
PFA	Paraformaldehyde
PBS	Phosphate buffered saline
PBST	Phosphate buffered saline with Triton
PKD2L1	Polycystic kidney disease 2 type 1
PVN	Paraventricular nucleus
RF	Reissner's fibre
RO	Nucleus raphe obscurus
SCI	Spinal cord injury
SEM	Standard error of the mean
SV2	Synaptic vesicle glycoprotein 2
tdT	Tandem dimer tomato
TSA	Tyramide signal amplification
VGAT	Vesicular GABA transporter
VF	Ventral fissure
WM	White matter

Chapter 1: Introduction

1.1. The spinal cord

The spinal cord is an essential part of the central nervous system (CNS) relaying information between the brain and the periphery and generating reflex responses via intra spinal circuits. The spinal cord is encased in the vertebral column, extending from the medulla oblongata to the conus medullaris.

The grey matter of the spinal cord is organised into apparent zones, termed laminae, which have cytoarchitectonic boundaries dividing this area into 10 laminae (Rexed, 1954). The neural circuitry of the spinal cord contributes to essential body functions. The importance of the spinal cord and associated circuitry is apparent when disorders arise compromising normal function, such as spinal cord injury (SCI) or degenerative diseases including Multiple Sclerosis (MS).

1.2. Central canal

The central canal is a fluid filled, elliptical cavity derived from the neural tube which originates at the fourth ventricle and extends throughout the spinal cord. It is surrounded by the ependymal zone consisting of at least three distinct cell types; tanycytes, ependymal cells (EpCs) and cerebro-spinal fluid contacting cells (CSFcCs), as shown in Figure 1. EpCs are the most populous cell type in this region (Hugnot and Franzen, 2011) providing the interface between the cerebro-spinal fluid (CSF) and parenchyma (Moore, 2016).

CSF is an ultra-filtrate of plasma, primarily produced by the choroid plexus. CSF circulates through the ventricles and central canal, transporting its contents between the brain and spinal cord and clearing cellular excretions. The biologically active substances contained within the CSF include hormone releasing factors from the hypothalamus, ions, neurotransmitters and neuropeptides (reviewed by Di Terlizzi and Platt, 2006).

1.3. Is the central canal region of the spinal cord a neurogenic niche?

A neurogenic niche refers to the specialised microenvironment composed of cells and matrix that surrounds progenitor cells, maintaining their undifferentiated state. It is essential in regulating the survival of progenitors and may be capable of influencing their proliferation and/or division.

Neural stem cells (NSC) are multipotent, self-renewing cells located within niches of the CNS. They are important for the maintenance and repair of tissues (Hamilton *et al.*, 2009). These regions are characterised by high vascular density and often interact with the CSF which may provide signalling molecules to the progenitor cells surrounding the CC (Figure 1). There are two primary regions identified as neurogenic niches in the brain; the subventricular zone and the sub granular zone of the dentate gyrus (Xu *et al.*, 2017). Cells expressing neural stem cell markers, have also been isolated from the ependymal zone in the spinal cord that surrounds the central canal, then shown to have the capacity to proliferate and differentiate (Weiss *et al.*, 1996, Johansson *et al.*, 1999, Martens *et al.*, 2002). Weiss *et al.* (1996) isolated cells from the thoracic, lumbar and sacral regions of the spinal cord by dissecting out the cord, sectioning it to around 1 mm³, enzymatically dissociating these sections and then culturing the different cells. They reported greater numbers of proliferating cells in the lumbar and sacral regions. From these cultures, they dissociated a single sphere, which is likely to have originated from a neural stem cell and plated the single sphere with epidermal growth factor and fibroblast growth factor. The neural stem cells dissociated from cultures, generated neurospheres that were immunopositive for MAP-2, GFAP and O4 indicating these cells differentiated into neurones, astrocytes and oligodendrocytes respectively, demonstrating their multipotency.

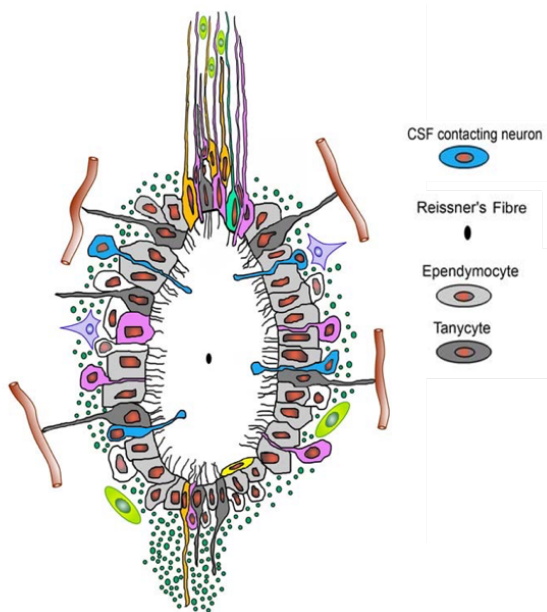


Figure 1: The ependymal zone surrounding the central canal of the spinal cord consisting of various cell types in close proximity to one another. EpCs (termed ependymocytes in this figure) are said to have neural stem cell properties based on their expression of markers of plasticity thus the different local cell types may be differentially contributing to the neurogenic niche.

Image adapted from Hugnot and Franzen (2011).

1.3.1 Ependymal cells may be these neural stem cells

Cells within the ependymal cell layer are the primary source of stem cells within the spinal cord (Meletis *et al.*, 2008), which was determined using genetic fate mapping of the proliferating cells, indeed they appear to facilitate the extensive recovery seen post spinal

cord injury. Although sometimes broadly referred to as EpCs, it is possible that the dividing cells are a subpopulation of cells within the regions of the ependymal zone that have phenotypic markers of NSCs.

Alfaro-Cervello *et al.* (2012) characterised EpCs as cuboidal cells organised in a pseudostratified arrangement, with two motile cilia and which were immunopositive for vimentin, CD24, FoxJ1, SOX2 and CD133, all of which are typically expressed in neural stem cells.

Horner *et al.* (2000) assessed the proliferative capacity of these cells *in vivo* by injecting bromodeoxyuridine (BrdU) intraperitoneally (IP) into mice and visualising the cells that had divided and incorporated this. BrdU is a thymidine analogue incorporated into the DNA of dividing cells, which is then detected using immunolabelling (Kempermann and Gage, 1997).

They observed BrdU labelling in the central canal, suggesting the proliferation of EpCs

Hamilton *et al.* (2009) found these BrdU cells were also positive for Ki67, a marker expressed by actively proliferating cells at multiple stages of the cell cycle – G1, S, G2 and M (Gerdes *et al.*, 1983). Significantly there were 2-3 times more Ki67 positive cells located in the dorsal pole of the central canal compared to the ventral region. This suggests EpCs refers to a heterogeneous population of cells, of which only a subtype are possible neural stem cells. They subsequently concluded that EpCs reside in a quiescent state of self-renewal as opposed to actively dividing to produce transit-amplifying progenitors. Quiescent stem cells are in a dormant state and are seen to have minimal basal rates of division.

Hamilton *et al.* (2009) observed cells within the ependymal zone of the spinal cord were immunopositive for nestin, SOX2 and CD133, all markers of neural stem cells. They also generated neurospheres, cultured neural stem cells that proliferate to form clusters of cells, from the lumbar spinal cord of an adult mouse. Following dissociation of 16 mm regions of lumbar spinal cord containing the central canal, cells rapidly expanded and differentiated *in vitro*, expressing immunofluorescent markers of neurones, astrocytes and oligodendrocytes. This affirms previous thoughts that multipotent neural stem cells with neurogenic potential exist within the spinal cord, however by dissociating whole spinal cord sections, it doesn't show which region the proliferating cells originated from.

In each of the examples described above, expansion of the cells within the ependymal layer population was induced by the addition of exogenous factors such as epidermal growth factor; this shows they are responsive to their environment, which within the spinal cord refers to the CSF. It is subsequently important to consider the receptors on EpCs that may be targeted in order to harness and increase their proliferative potential. Corns *et al.* (2013) reported a depolarisation of EpCs when spinal cord slices from mice are bathed in GABA.

When repeated in the presence of bicuculline, a GABA_A antagonist, this response was reduced indicating the presence of these receptors. Further experiments by this group revealed similar responses to acetylcholine (ACh) antagonised by a nicotinic receptor antagonist mecamylamine (MCA), indicating the presence of nicotinic acetylcholine receptors later defined to have the alpha 7 subunit. These experiments show EpCs are able to respond to different neurotransmitters, this is a concept I will harness throughout this project; the release of neurotransmitters and other molecules from cells located close to EpCs such as CSFcCs.

Considering the neural stem cell properties of ependymal cells, they may have therapeutic potential to replace lost or damaged cells in disorders of the spinal cord. It is subsequently of significance that the physiologically restricted capacity for proliferation differs greatly from their activity in disease states (Moore, 2016).

1.3.2 Cell proliferation after spinal cord injury

Spinal cord injuries (SCI) cause debilitating, long term changes to a patient's life and with limited therapeutic options to restore the loss of function, it leaves individuals with a poor prognosis.

Through analysis of spinal cord injury cases in a hospital over 12-month period, it was anticipated that each case costs £1.12 million. Coupled with approximately 1270 new cases of SCI each year in the UK (McDaid *et al.*, 2019), this has a tremendous economic impact. The complex cascade of events following the initial injury pose difficulty in determining the appropriate therapeutic targets as there is a significant primary insult followed by various cellular level changes that result in further cell death, impaired recovery and regeneration. However, there are endogenous repair mechanisms that restore some function, EpCs may contribute to this.

When comparing the activity of EpCs *in vitro* removed from injured and control groups, there are significant differences in their proliferative ability (Moreno-Manzaro *et al.*, 2009). EpCs isolated from injured rats display a significant increase in their ability to form neurospheres. This was quantified by the rate of proliferation shown to be 10-fold greater in the injured group compared to the control. This suggests that EpCs are no longer in the quiescent state following spinal cord injury. *In vivo*, this may compensate for the extensive cell loss.

In spite of this, it has been shown that the EpC proliferative response is not always present and this varies based on the model of injury used (Ren *et al.*, 2017). In a crush injury, generated using forceps at spinal level T10, EpC progeny labelled with tandem dimer

Tomato (tdT), a red fluorescent protein (RFP), under the promoters FoxJ1 and Nestin remained in close proximity to the ependymal zone and accounted for less than 2 % of the newly proliferating cells in the scar region. This largely differed from the response of EpCs to a longitudinal penetrating stab injury along the midline of the spinal cord directly injuring the ependymal region. In this context, EpC progeny made up the majority of proliferating cells. Significantly, a similar stab injury lateral to the midline that didn't directly impact the ependymal region didn't induce an EpC response, which means EpCs only respond when they are directly injured. Therefore they may not be an endogenous source of recovery or regeneration in all injury/disease states.

1.4. What is the role of cerebro-spinal fluid contacting cells?

In the early 1920s, Kolmer (1921) and Agdhur (1922) identified one of the cell types within the ependymal region of the central canal contacting the CSF, common to 200 vertebrate species; CSFcCs. Significantly, as shown in Figure 1, CSFcCs are located in the ependymal zone, in close proximity to the EpCs. This places them in an optimal location to contribute to the neurogenic niche found in this region. These cells possess a unique morphology, a bulb-like soma close to the central canal with microviliated apical extensions that terminate in the CSF. These ciliated neurones were described as sensory cells based on this morphology, facilitating constant sensing of the CSF. Since this finding, the role of CSFcCs has been greatly expanded, they appear to contribute to mechano- and chemosensory systems however there is still ambiguity surrounding their circuitry and physiological function.

Immunocytochemical localisation of GABA in the spinal cord of *Xenopus* embryos labelled neurones which shared a similar morphology to those described by Kolmer and Agdhur. Light microscopy revealed both ipsilateral and rostral axon projections extending from these cells with those projections reaching the CSF covered in microvilli (Dale *et al.*, 1987). More recent findings reveal two distinct populations of CSFcCs in river lamprey (Jalalvand *et al.*, 2014). They were labelled using injections of Alexa fluorescence 488-dextran to the lateral region of the spinal cord. Type 1 CSFcCs have protrusions extending into the central canal with bulb-like endings and lateral processes as above. Type 2 differ from these with flat endings on the projections into the central canal. When quantitative comparisons were made, this group determined that type 2 had smaller somata and were located further from the central canal. Immunohistochemical analysis revealed further differences, type 1 co-localised with GABA, somatostatin, glutamate receptors and GABA receptors whereas type 2 were immunopositive for taurine but not GABA or somatostatin. Whole patch cell

recordings determined electrophysiological differences with type 1 spontaneously firing action potentials whereas type 2 did not display these neuronal properties, suggesting they may be more characteristic of a glial cell. Within this thesis I will be discussing type 1, referred to as CSFcCs.

An important characteristic of CSFcCs is their expression of the polycystic kidney disease 2 type 1 (PKD2L1) ion channel. This was first noticed when Huang *et al.* (2006) characterised the anatomical expression of PKD2L1 using *in situ* hybridisation and antibody labelling. PKD2L1 is a transient receptor potential, non-selective cation channel involved in sour taste responses. *In situ* hybridisation of PKD2L1 revealed labelling of spinal neurons with the characteristic CSFcC morphology. PKD2L1 has since been established as a marker for CSFcCs, exclusively and consistently marking these cells in the spinal cord in the central canal region of embryonic, postnatal and adult mice, macaque and zebrafish larvae (Djenoune *et al.*, 2014). In each species, the PKD2L1⁺ CSFcCs show typical morphology with an apical extension into the central canal and a basal axon contacting other neurones. Subsequently, throughout this thesis, antibodies against the PKD2L1 receptor are used to immunofluorescently label CSFcCs within the CNS.

Stoeckel *et al.* (2003) used immunoperoxidase labelling of P2X2, another receptor subtype only expressed within CSFcCs within the spinal cord, to describe CSFcCs location and morphology in the spinal cord of rats. Notably after observing the typical distribution of these cells around the CC interlaced with EpCs, they noticed labelling in the ventral fissure (VF). They described the labelling in this region as bundles of axons that appear to contact the P2X2 labelled CSFcCs around the CC, extending all the way down to the ventral fissure. It was only when sectioned in a horizontal plane that they noticed this labelling ran along the cord within the VF. The VF is a groove along the midline of the anterior spinal cord, within which the anterior spinal artery is positioned (Bican *et al.*, 2015). There are axon tracts within this region, possibly the rostral reticulospinal tract and lateral vestibulospinal tract (Watson and Harrison, 2012). However the VF hasn't been defined with a specific functional role, therefore it is unclear why CSFcCs send axons along this region.

An important consideration is how these cells vary depending on the age of the animals. Orts-Del'Immagine *et al.* (2017) demonstrate notable changes between CSFcCs depending on the age of the animal using immunohistochemical techniques to label CSFcCs in PKD2L1-IRES-Cre mice. They found that in newborn mice, CSFcCs express DCX, PSA-NCAM and phosphor-CREB which all indicate an early maturation state. This differed from

adult spinal cords in which CSFcCs had reduced immunoreactivity for DCX and no PSA-NCAM labelling. Furthermore, the cell bodies migrated away from the central canal with larger distances from the central canal to CSFcC somata in adults. There was also an overall decline in CSFcC number from 17.5 to 6.6 cells/10 μm tissue depth.

1.4.1. CSFcCs can respond to changes in pH

CSFcCs have an acute sensitivity to changes in pH, shown by Huang *et al.* (2006) following their discovery of this receptor within CSFcCs in the spinal cord. Recordings of CSFcCs in a cell attached configuration revealed dependent increases in the frequency of action potential firing in response to pH stimulation between 6.5 and 7.4. This altered response to changes in proton concentration suggests that this may form an aspect of their physiological role. The pH of CSF is 7.33 (Kazemi and Johnson, 1986), which falls within the range of pH CSFcCs can respond to, suggesting these cells may have a role in maintenance of pH as they have the ability to fire action potentials when changes are detected.

When citric acid, pH 2.8 was applied under pressure to brainstem slices for 10 seconds, all the recorded CSFcCs exhibit a biphasic response, fast inward, rapidly desensitising current followed by a sustained inward current (Orts-Del'Immagine *et al.*, 2012). To assess whether this channel independently responds to acidification and alkalinisation, Orts Del'Immagine *et al.* (2016) tested these responses in knock out (KO) mouse models. Patch clamp recordings were taken from PKD2L1 KO CSFcCs within brainstem slices. The response to application of pH 5 solution was remarkably similar compared to wild type with fast inward currents recorded. However, the current response in wild type slices seen upon application of an alkaline solution pH 9 was abolished in the KO model. This suggests PKD2L1 channels are responsible for the responses to alkalinisation however the fast inward currents triggered by acidification appear to be initiated by an independent mechanism such as the acid sensing ion channel 3.

Another pH sensitive channel expressed in CSFcCs is acid sensing ion channel 3 (ASIC3). Jalalvand *et al.* (2016) tested the response of CSFcCs to lowered pH, 6.9 in river lamprey, this elicited an increase in spontaneous action potentials. This pH dependent response was lost in the presence of APETx2, an ASIC3 channel blocker. This correlates with the aforementioned study with PKD2L1 channels responding to alkalinisation and ASIC3 detecting acidic changes in pH.

1.4.2. Do CSFcCs have neuronal properties?

CSFcCs have been labelled with various neuronal markers and display characteristic firing patterns when patch clamp recordings are performed. This suggests that they communicate with neighbouring cell types, determining their circuitry may offer a clearer understanding of function.

Marichal *et al.* (2009) investigated CSFcCs surrounding the central canal region of the spinal cord of neonatal rats. Within this group of cells, they reported variation in electrophysiological responses and immunostaining indicating that these neurones persist at different stages of differentiation. CSFcCs co-labelled with Hu C/D, a protein expressed in early neurones, along with DCX and PSA-NCAM, markers of plasticity. In the patch clamp configuration, some neurones passively responded to depolarising current pulses whereas others actively respond to depolarisation with slow or fast potentials. Finally, when looking at the response of these neurones to GABA, they found that gabazine, a GABA_A inhibitor, blocked the GABA induced currents.

When electrophysiologically assessing the baseline membrane properties in mouse brainstem slices, CSFcCs displayed depolarising events likened to post synaptic potentials able to trigger action potentials (Orts-Del'Immagine *et al.*, 2012). This was said to be indicative of synaptic inputs. These currents were blocked in the presence of gabazine, supporting prior findings in spinal cord that CSFcCs are responding to GABAergic inputs via GABA_A receptors. Additionally, the pressure application of potassium chloride induced two primary responses; tonic or phasic firing – trains of action potentials or individual spike responses respectively. These properties suggest that CSFcCs receive inputs and transmit signals, leading to experiments in this project aiming to resolve some of the associated circuits.

Fidelin *et al.* (2015) initially demonstrated in transgenic (pkd2l1:Gal4)^{icm10} zebrafish larvae, that CSFcCs express synaptophysin by injecting UAS:synaptophysin-GFP, visualising the presynaptic boutons in the ventral axon of PKD2L1 positive CSFcCs, projecting away from the central canal. These boutons surround V0-v interneurons, activated during spontaneous, slow locomotion events. Light activation of CSFcCs expressing channel rhodopsin (ChR) caused inhibitory post synaptic currents in the V0-v interneurons demonstrating a transmission of activity between these cell types. Significantly, the PKD2L1 positive CSFcCs labelled with synaptophysin along with the presence of presynaptic boutons

discussed here, suggests CSFcCs have the capacity to release neurotransmitters and/or other signalling molecules from their terminals.

Patch clamp recordings from CSFcCs at baseline reveal spontaneous activity through PKD2L1 channels, capable of triggering action potentials (Orts-Del'Immagine *et al.*, 2016). When coupled with the apparent lack of excitatory inputs to CSFcCs this suggests PKD2L1 channels are an important source of excitation.

Concluding from these studies, it is shown that CSFcCs possess some neuronal like properties in firing action potentials and expressing various immunohistochemical markers of neurones at different stages of maturation. Neurones tend to have synaptic inputs, to receive signals, and outputs in order to transmit information to other cells, so it is important to look at possible routes of input and output on CSFcCs relating to their circuitry.

1.4.3. A mechanosensory function for CSFcCs?

Active locomotion in zebrafish larvae elicits calcium responses in CSFcCs, consistent with a mechanosensory role (Bohm *et al.*, 2016). Specifically, unilateral tail bends induced calcium transients in the dorsally populated CSFcCs ipsilateral to the side contracting. A response was also initiated in CSFcCs when larvae embedded in agarose were pressed with a glass probe. It appears that these responses were mediated by changes in PKD2L1 channel activity since PKD2L1 null mutants didn't show responses to either passive or active bending. These PKD2L1 null mutant larvae also showed a reduced tail beat frequency when freely swimming. This suggests a role of CSFcCs in relating information regarding movement and spine position which optimises locomotion. This was later assessed in the context of CSF flow which is affected by such movements. Zebrafish larvae with a mutation affecting the recruitment of dynein arms results in reduced cilia motility and subsequent limited CSF flow (Sternberg *et al.*, 2018). This reduced flow correlated with a loss of spontaneous calcium activity within CSFcCs, suggesting these cells respond to the CSF flow.

Orts-Del'Immagine *et al.*, (2020) focused on the contribution of CSFcCs to the more active role of CSF in the development of the body axis, spinal morphogenesis and transducing movement signals. Escape responses were induced in zebrafish larvae by puffing artificial CSF (aCSF) onto the otic vesicle, a component of the inner ear of zebrafish larvae formed within 16 hours post fertilisation (Haddon and Lewis, 1997). This caused calcium transients

in dorsolateral and ventral CSFcC populations. Both the magnitude of this response and the proportion of CSFcCs responding was reduced in mutant models that caused defective polarity and motility of cilia, reiterating the link between CSF flow and CSFcC activity. Mutations in the cilia decreased the flow of CSF, transport, the central canal diameter and prevented Reissner's fibre (RF) from forming. The RF is an extracellular structure which runs through the CC. Since CSFcC endings within the central canal are closely located to the RF, this relationship was further explored as a source of the lost activity in CSFcCs. A hypomorphic mutation in the scospondin gene was generated, preventing the aggregation of protein into the RF. In these mutants the CSFcC activity in response to tail bending was lost, suggesting that the movement of the RF is linked to activity in the CSFcCs.

As an alternative to recording CSFcC activity in response to mechanical stimuli, some groups have looked at optogenetic activation of CSFcCs expressing ChR and the subsequent changes in behaviour. Wyart *et al.* (2009) activated spinal neurones expressing a light gated glutamate receptor (LiGluR) in zebrafish larvae which resulted in robust tail oscillations similar to the spontaneous forward swimming motion observed in wild type animals. Immunohistochemical analysis of these neurones revealed positive labelling with GABA, GAD65/67 and somatostatin, leading to the conclusion that they are CSFcCs. They then expressed LiGluR solely in CSFcCs, activation of which led to alternating symmetrical tail beats. LiGluR is a genetically modified ion channel that can be activated with light. The number of oscillations in 4 out of 8 larvae was reduced in the presence of bicuculline, a selective GABA_A antagonist, in the other 4 the activity was abolished. Similarly, light activation of ChR expressing CSFcCs resulted in slow swimming motion in larvae that were initially stationary whereas motion was terminated in larvae that were already swimming upon light stimulation (Fidelin *et al.*, 2015).

The previously discussed evidence suggests that CSFcCs are activated in response to contusions of the spinal cord however the targets of these responses are unclear. Hubbard *et al.* (2016) resolved some of these targets in zebrafish. They assessed the projections from CSFcCs from which they concluded that most axonal projections extended ventrally however some had dorsally extending axons which appear to terminate around other cells. They also noticed the ventral extensions labelled with synaptophysin, a presynaptic component suggesting they are innervating a local cell. CSFcCs expressing ChR were activated, simultaneously whole patch cell clamp recordings were taken from the nearest cell bodies – caudal primary motor neurones. There were large inhibitory post synaptic potentials recorded in these neurones. This response was lost in the presence of gabazine suggesting GABA is

released from the CSFcCs. Smaller responses were also recorded from non-caudal primary motor neurones. Following this they investigated the dorsal projections which terminated onto primary ascending glutamatergic interneurons involved in modulating the sensory motor circuit and recruiting effector motor neurones. After their initial description as sensory cells (Kolmer and Agdhur, 1921) CSFcCs have now been shown to respond to mechanical stimuli and neurotransmitters, it is important to understand the physiological inputs to these cells, building an idea of their circuitry.

1.4.4. Do CSFcCs receive synaptic inputs?

Responses have been elicited within CSFcCs in response to various compounds, as discussed above, which offer some insight into their possible physiological role. This also provides mechanisms by which they can be exogenously manipulated for possible therapeutic benefit (Table 1).

Receptor/Channel	Evidence	RNAseq score
<i>GLP1R</i>	Rosenberg <i>et al.</i> , 2018 Ghazale <i>et al.</i> , 2019	333.9
<i>Glycine</i>	Orts'Del-Immagine <i>et al.</i> , 2012	66.8
<i>GABA-A</i>	Marichal <i>et al.</i> , 2009	GABRA1 - 1 GABRA2 – 262.5 GABRA3 – 8.3 GABRA4 – 75.6
<i>GABA-B</i>	Margeta-Mitrovic1999 (rat)	GABRB1 – 2022.5 GABRB2 – 17.4 GABRB3 - 92.7
<i>NPR2</i>	Rosenberg <i>et al.</i> , 2018	48.6
<i>Neogenin</i>	Rosenberg <i>et al.</i> , 2018	209.3
<i>NR3C1 - glucocorticoid</i>	Rosenberg <i>et al.</i> , 2018	58.3
<i>VIPR2</i>	Rosenberg <i>et al.</i> , 2018	15.9
<i>PKD2L1</i>	Huang 2006	2424.3
<i>ASIC3</i>	Jalalvand <i>et al.</i> , 2016	1
<i>P2x2</i>	Stoeckel <i>et al.</i> , 2003	1

Table 1: Receptors and channels expressed by CSFcCs providing possible targets to induce activity and the release of vesicles.

Corns *et al.* (2015) recorded depolarisation in CSFcCs following pressure ejection of ACh onto mouse spinal cord slices. This response was mediated by nicotinic acetylcholine

receptors demonstrated by the significantly reduced response in the presence of MCA, a selective antagonist.

As well as responding via changes in the electrophysiology, neurones tend to release signalling molecules such as neurotransmitters in order to relay information to other cells. A more recent discovery within CSFcCs, expanding their functional role is their proposed ability to secrete peptides from the terminal within the central canal. Prendergast *et al.* (2019) demonstrate this in the context of CSFcCs responding to an infection of the CSF. *Streptococcus pneumoniae* was injected into the hindbrain ventricles of zebrafish larvae, within 12 hours, large calcium transients were recorded in CSFcCs. To assess the contribution of CSFcCs to the immune response, RNA sequencing of CSFcCs was carried out which revealed the presence of several genes encoding peptides associated with the immune response (Table 1). Furthermore, a significant decrease in the survival was recorded when botulinum toxin B light chain was applied to CSFcCs inhibiting their capacity to release such peptides via vesicular fusion. This may result from the release of peptides however, here it was only shown that CSFcCs have the ability to produce such peptides, not that they are released from the terminals.

CSFcCs have also been discussed as GABAergic. This is due to the overlapping immunocytochemical labelling between P2X₂ and GABA in rats, using P2X₂ as a marker of CSFcCs (Stoeckel *et al.*, 2003). There was a similar overlap in labelling between glutamic acid decarboxylase (GAD), the enzyme responsible for producing GABA, with PKD2L1 in a transgenic zebrafish larvae line expressing mCherry under the control of a PKD2L1 promoter (Fidelin *et al.* 2015). Combining this evidence, it suggests that CSFcCs have some properties that may facilitate response to physiological signals as well as the release of signalling molecules which could influence local cells.

Other receptors expressed by CSFcCs offers a route of exogenously targeting their ability to release signalling molecules into their local environment. A receptor shown to be highly expressed in CSFcCs, 300 times greater than EpCs, is the glucagon like peptide 1 receptor (GLP1R) determined using mRNA sequencing of CSFcCs (Rosenberg *et al.*, 2018).

1.5. Glucagon like peptide 1 may influence CSFcC activity

Glucagon like peptide 1 (GLP1) is an incretin hormone involved in regulating insulin secretion from beta cells of the pancreas following nutrient ingestion. It is released from L-cells of the colon and ileum (Koole *et al.*, 2013) which results in various responses including delayed gastric emptying, lower glucagon levels in the plasma and decreased food intake (Lee and Jun, 2016). It is also produced by neurones in the brainstem with roles in the central nervous system extending to modulation of both blood pressure and heart rate (reviewed by Trapp and Hisadome, 2011). GLP1 binds to GLP1R, a G-protein coupled receptor expressed on the surface of cells associated with various intracellular signalling cascades. Stimulation of this receptor leads to activation of adenylyl cyclase and subsequently an increase in cyclic adenosine monophosphate (cAMP) (Carlessi *et al.*, 2017).

GLP1Rs expressed in the brain are involved in suppressing feeding behaviours after food ingestion, an anorexigenic effect. Katsurada *et al.* (2014) injected a retrograde tracer into the paraventricular nucleus (PVN) of the hypothalamus revealing inputs from GLP1 expressing neurones of the nucleus tractus of solitarius (NTS).

Chen *et al.* (2017) observed GLP1R immunopositive cells in the spinal cord were also immunopositive for NeuN which indicated some of this receptor expression was in neurones. Quantitative analysis of receptor expression using Western blotting after injury revealed greater GLP1R expression within the spinal cord. There is widespread expression of this receptor within various regions of the body however expression within the spinal cord may present a candidate therapeutic target for regeneration and recovery in spinal cord injury or disease patients. The associated signalling cascades following activation of this receptor have beneficial effects in the context of inflammation, injury and diseases of the CNS as reviewed by Zhang *et al.* (2018).

Significantly, GLP1Rs are expressed in CSFcCs. I initially detected this in the Allen Spinal Cord Expression atlas, GLP1R mRNA is shown in cells around the central canal ideally located to be CSFcCs as shown in Figure 2. Subsequently, sequencing of mRNA from CSFcCs, also showed that they express GLP1R (Rosenberg *et al.*, 2018, Ghazale *et al.*, 2019). Targeting this receptor within this population of neurones in the spinal cord may allow exogenous manipulation of their activity, with the potential for changes in cells that they influence.

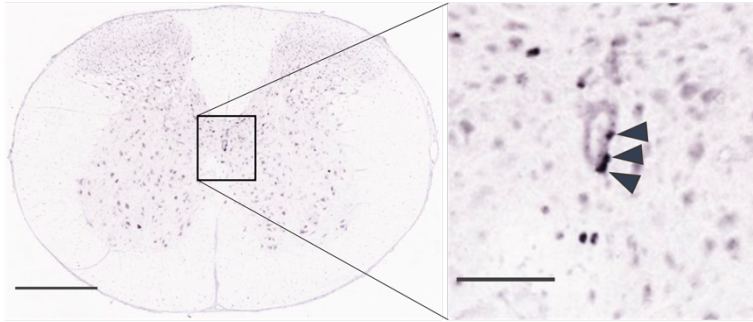


Figure 2: *GLP1R mRNA expression within CSFcCs?* In situ hybridisation of the GLP1 receptor in the mouse spinal cord showing expression in cells around in central canal (Allen Institute, 2008). Left whole cervical transverse section, scale bar 500 µm. Right, enlarged CC from section, scale bar 100 µm.

GLP1R expression has not yet been well defined within the spinal cord of mice and it is unclear which cells within the spinal cord express these receptors. The receptor is implicated in complex second messenger cascades and therefore its presence around the CC (Figure 2) may provide a tool for influencing cells causing effects in neighbouring cells within this region such as EpCs, previously discussed to respond to changes within their environment. Resolving this in rodents may also reveal the therapeutic potential of targeting these receptors, something I aim to test within this project.

1.5.2. GLP1 analogues are useful tools to study the role of these receptors

The physiological role of GLP1 provides a therapeutic avenue in the context of type 2 diabetes in which exogenous application of analogues can assist glucose control. Currently analogues in clinical use include Exendin-4, Liraglutide and Lixisenatide (Sharma *et al.* 2018). However, it has been documented that there are various off target effects expanding the possible applications of these therapeutics clinically.

Liraglutide improved functional recovery after spinal cord injury in mice which may prove to be a therapeutic used in humans (Chen *et al.*, 2017). At a cellular level, various changes appear to have contributed to the improved motor scores and inclined plane tests including reduced apoptosis, increased autophagy and microtubulin acetylation. Motor scores were generated from the Basso, Beattie, Bresnahan test, an assessment of locomotor function in an open field. The cavity diameter and extent of motor neurone loss, seen using nissl staining were also reduced in the treated group. Liraglutide exacerbated the autophagic response seen within the injury group compared to SHAM which was measured using markers of autophagy including LC-II/LC3-I ratios and Beclin1. They verified that these changes resulted from GLP1R signalling using siRNA GLP1R knockdown mice. In this group the treatment made no difference to recovery compared to the untreated group. This study

exemplifies the varied effects of GLP1R signalling and the potential therapeutic application of GLP1 analogues. By administering Liraglutide subcutaneously near to the injury site, it is not clear where the effects of this are occurring within the animal in order to improve functional outcome. It is important to decipher where GLP1Rs are expressed within the spinal cord and on which cells as this may provide more information regarding the mechanism of action by which Liraglutide improved functional recovery after SCI.

1.6. Conclusion

In summary, an accumulation of this knowledge compiles to form a picture of the roles of the cells within the region surrounding the central canal of the spinal cord, as depicted in Figure 3. Most significantly, I have discussed the possible role of CSFcCs in responding to changes of pH in the CSF contributing to the maintenance of homeostasis, as a result of their location and morphology. This includes their ability to produce peptides and release contents of vesicles from their end bulb within the CSF (Prendergast *et al.*, 2019, Fidelin *et al.*, 2015, Hubbard *et al.*, 2016). Furthermore, unpublished preliminary data from the laboratory shows the CSFcC bulb terminal extending into the CSF expressing synaptic markers, reiterating the suggestion that these cells are able to release molecules from their end bulb. The location of CSFcCs, in close proximity to EpCs i.e. progenitor cells, suggests they may be contributing to the neurogenic niche which maintains the state of progenitor cells and influences their division rate. The primary gaps in our knowledge are whether CSFcC secretions have the ability to modulate EpC activity and which, if any, neuronal circuits the CSFcCs are part of.

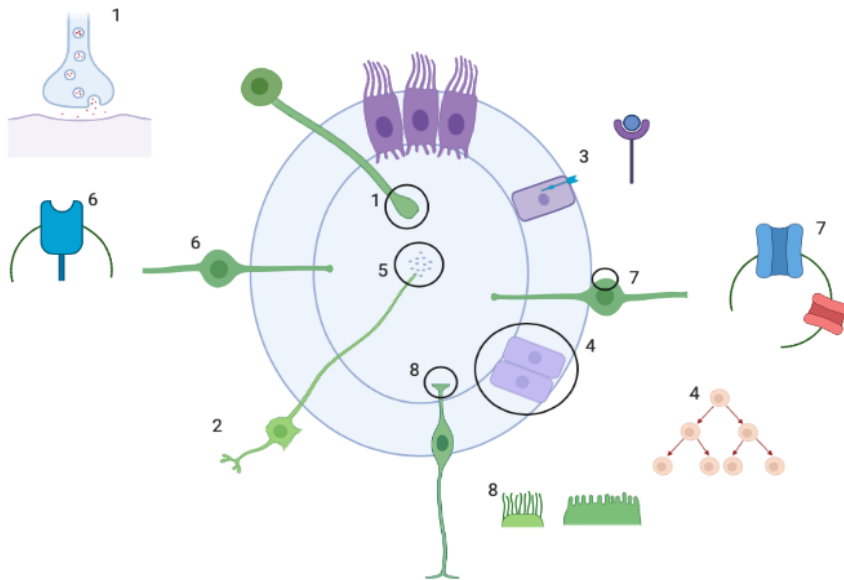


Figure 3: Summary of CSFcC and EpC functions. By accumulating all of the functions of CSFcCs determined within different species, alongside those of the closely located EpCs, an overall hypothesis can be considered, which leads to the aims of this project.

1 = Synaptic release from CSFcC terminals (Prendergast *et al.*, 2019, Fidelin *et al.*, 2015) (Table 1)

2 = Projections away from CC, synapses with other cell types, neurotransmitter secretions (Table 2) (Dale *et al.*, 1987, Djenoune *et al.*, 2014, Fidelin *et al.*, 2015, Hubbard *et al.*, 2016)

3 = Receptors on EpCs (Table 2)

4 = Proliferation of EpCs (Weiss *et al.*, 1996, Johansson *et al.*, 1999, Martens *et al.*, 2002)

5 = Contacts with RF and response to CSF flow (Sternberg *et al.*, 2018, Orts-Del'Immagine *et al.*, 2020, Wyart *et al.*, 2009)

6 = Receptors on CSFcCs (Table 1)

7 = Channels facilitating response to pH – PKD2L1 and ASIC3 (Huang *et al.*, 2006, Orts-Del'Immagine *et al.*, 2012, Djenoune *et al.*, 2014, Jalalvand *et al.*, 2014)

8 = Ciliated endings (Kolmer and Agdhour 1921, Dale *et al.*, 1987) Image created using Biorender

1.7. Hypothesis and Aims

This knowledge has led to the hypothesis; CSFcC activation through exogenous receptor stimulation will cause the release of substances such as GABA into the CSF that may influence the proliferation and/or differentiation of EpCs. The mechanisms for exploiting this possible relationship depend on receptors on CSFcCs (Table 1) which can be activated using exogenous drugs, their subsequent secretions (Table 2) and the receptors on EpCs (Table 2) that facilitate a response to such secretions. I aim to demonstrate select receptors expressed on CSFcCs using immunohistochemical techniques and describe their distribution within the CNS of rodents. Subsequently, utilise such receptors to manipulate CSFcCs and influence cells within the CC region. Furthermore, using viral tracing methods, I aim to resolve the CSFcC projections in rodents including the direction in which they travel, yet to be identified. In turn, this will assist in understanding their physiological function and provide opportunity for exogenous manipulation of such functions for therapeutic benefit.

CSFcCs		Ependymal cells			
Genes/mRNA expressed (evidence)	Protein produced by gene	Receptor of protein	Gene encoding receptor	RNAseq score within EpCs (Rosenberg <i>et al.</i> , 2018)	Present in EpCs?
<i>Nppc</i> (Prendergaast <i>et al.</i> , 2019)	Natriuretic peptide C	Natriuretic peptide receptor	NPR3	1	No
			NPR2	19.1	Yes
<i>Sst1.1</i> (Prendergaast <i>et al.</i> , 2019, Jalalvand <i>et al.</i> , 2014)	Somatostatin 1	Somatostatin receptor 1	Sstr1	1	No
		Somatostatin receptor 4	Sstr4	10.6	Yes
<i>Ntn1b</i> (Prendergaast <i>et al.</i> , 2019)	Netrin 1b	Neogenin	Neo1	190.3	Yes
<i>Txn</i> (Prendergaast <i>et al.</i> , 2019)	Thioredoxin	Glucocorticoid receptor		146.5	Yes
<i>Sst3</i> (Prendergaast <i>et al.</i> , 2019)	Somatostatin 3	Somatostatin receptor 3		1	No
<i>Ramp1</i> (Prendergaast <i>et al.</i> , 2019)	Receptor activity modifying protein	Secretin	SCTR	291.1	Yes
		Calcitonin	CALCR	22.4	Yes
		Vasoactive intestinal peptide	VIPR1	1	No
<i>GABA</i> (Orts'Del-Immagine <i>et al.</i> , 2012, Stoeckel <i>et al.</i> , 2003)	-	$GABA_{A/B}$	GABRA1 GABRA2 GABRA3 GABRA4 GABRB1 GABRB2 GABRB3	1 262 8.32 75.6 2002 17.4 92.7	Yes (Corns <i>et al.</i> , 2013)

Table 2: Peptides present within CSFcCs (Prendergaast *et al.*, 2019, Orts'Del-Immagine *et al.*, 2012, Stoeckel *et al.*, 2003, Jalalvand *et al.*, 2014). These peptides have the potential to act as the output signalling molecules within CSFcCs to transmit messages to local cells. EpCs are a populous local cell type, therefore the table also includes information about whether EpCs have the receptors needed to respond to any signals released by CSFcCs.

1.8. General Methods

1.8.1. Animals

Handling of animals and experiments were carried out in accordance with the UK Home Office guidelines and the requirements of the United Kingdom Animals (Scientific Procedures) Act 1986. Licence number P1D97A177. Handling of mice was conducted by Jim Deuchars as I was unable to train for a licence during the pandemic. Mice were housed with a 12-hour light, 12-hour dark cycle, with water and food freely accessible. To minimize the suffering of animals, close observations were made after surgery to administer analgesia when required or terminating any animals that did not fully recover. The number of animals used was the minimum required for experimental analysis. Three different transgenic mouse lines were used for this research.

Vesicular GABA transporter (VGAT)-IRES-Cre mice (VGAT.Cre, stock 028862, B6J.129S6(FVB)-Slc32a1,tm2(cre)) crossed with floxed GCaMP6f mice (GCaMP6f.flox, stock 028865, B6J.CGt(ROSA)26Sor<tm95.1 (CAGGCaMP6f)). These two mouse lines were originally sourced from Jackson Laboratory (Maine, USA). This generated VGAT:GCaMP6f mice.

Polycystic kidney disease 2-like 1 (PKD2L1)-IRES-Cre mice (PKD2L1.Cre, MGI:6451758, (C57BL/6J-129X1/SvJ)F1<tm1(cre)) crossed with floxed GCaMP6f mice (GCaMP6f.flox, stock 028865, B6J.CGt(ROSA)26Sor<tm95.1 (CAGGCaMP6f)). This generated PKD2L1:GCaMP6f mice as referred to throughout this thesis. The PKD2L1-IRES-Cre mice were gifted from Sue Kinnamon labs (University of Colorado, USA).

1.8.2. Preparation of the virus and tools

Tools used in surgery were sterilised in an autoclave before the surgery. These included fine forceps, crocodile forceps, small scissors, haemostat locking clamps, scalpel and blades, tissue retractors, 1 mL syringe, gauge needles, vicryl absorbable sutures, curved needle and a high temperature cautery. Glass electrodes were used for the viral injections, these were pulled using a micropipette puller (Sutter Instruments) prior to the surgery. 1 mL glass syringe was used to provide pressure for ejection.

1.8.3. Surgery and Injection

Mice were anaesthetised with intraperitoneal injections of 75 mg/kg ketamine and 1 mg/kg medetomidine. Pedal withdrawal reflex tests were used to ensure the animals were anaesthetised before surgery. Clippers were used to shave 2-3 cm of hair around the surgery site. The animals were kept on a heated table at 37 °C during surgery to maintain body temperature. Looking down a surgical microscope, a scalpel blade was used to make an incision on the dorsal surface at the lumbar region of the spinal cord through the skin and muscular layers covering the spinal column. Retractors were used to open this region. Once a portion of the spinal column was visible through the vertebra, the dura and pia were removed from the surgical region using a 30 gauge needle. The pia matter was removed using the same needle. The glass microelectrode was inserted 1 mm into the spinal cord at the midline, the region was estimated visually in relation to the vertebrae starting above the lumbar enlargement, into the intervertebral foramen between the vertebrae. Approximately 50-100 nL was injected initially, followed by a 30 s wait time, the electrode was moved dorsally by approximately 0.1 mm, another 50-100 nL was injected, this was continued until the 500 nL was injected. The surgery and injection are summarised in Figure 4.

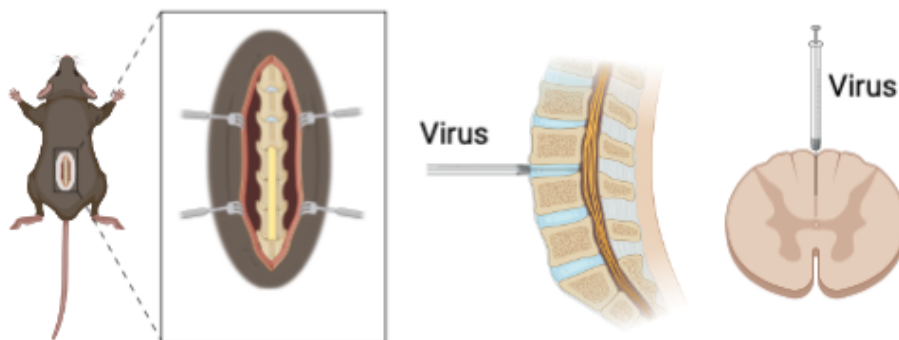


Figure 4: *Intraspinal injections*, showing an overview of the injections into the spinal cord through the intervertebral space (Biorender).

After surgery, subcutaneous injections were administered of 1 mg/kg atipamezole to reverse the anaesthesia and muscle relaxant effects previously induced. Buprenorphine (Vetergesic, 0.3 mL/mg, 0.1 mg/kg) was injected IP for analgesia following the surgery. Postoperative observations were carried out after the surgery to observe for any further signs of pain or discomfort. Once recovered, mice were placed back into cages with other mice. Observations continued for the first few days post-surgery.

1.8.4. Perfusions

Mice were administered 60 mg/kg pentobarbitone intraperitoneally, after a few minutes this was followed by a test for absence of the pedal withdrawal reflex to check they were anaesthetised. Transcardial perfusions were carried out while under anaesthetic to fix the tissue. The circulation was flushed with 50 mL 0.1 M PB, then approximately 200 mL 4 % paraformaldehyde (w/v) 0.1 M PB (PFA). The brain and vertebral column were removed from each animal and post fixed in PFA overnight at 4 °C before being stored in 0.1 M PB at 4 °C.

1.8.5. Tissue preparation

After fixation, using fine scissors, the vertebrae were cut to remove the spinal cord from the vertebral column. The meninges were subsequently removed with fine forceps under a dissecting microscope. 50 µm transverse sections were produced using a Leica VT1000S microtome by mounting short sections of spinal cord, approximately 5 mm, onto the stage. Sections were collected into a well plate containing phosphate buffered saline (PBS). The same process was carried out for brain and brainstem sections. In order to visualise cells around the central canal and the distribution of cells at each level of the spinal cord, sections were cut in a transverse plane (Figure 5). It was also beneficial to visualise the axons from cells projecting between spinal cord levels, therefore tissue was also sectioned in coronal and sagittal planes (Figure 5) after gelatin embedding.

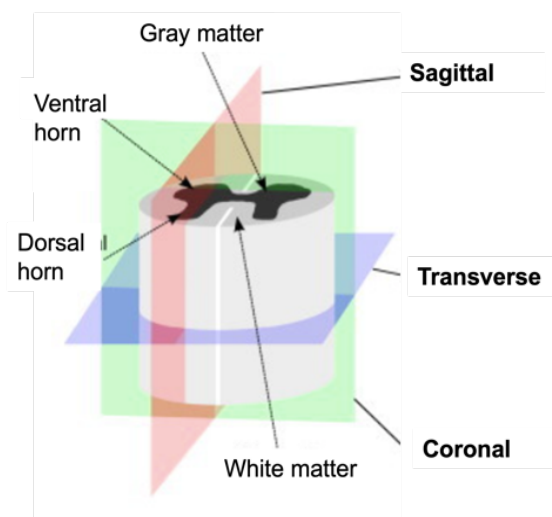


Figure 5: Anatomical planes of the spinal cord. This shows the different planes of the spinal cord tissue was sectioned in during this project depending on what was being observed. The key regions of the spinal cord are also labelled; ventral horn, dorsal horn, white matter and grey matter. Image adapted from Koser *et al.* (2015).

1.8.6. Gelatin embedding

In order to section spinal cord tissue in the coronal and sagittal planes, the cord was embedded in gelatin. 10 % (w/v) porcine gelatin (Sigma-Aldrich, 04055) was dissolved in distilled water (dH₂O) at 100 °C whilst continuously stirred. The spinal cord was cut into 4 sections; cervical, thoracic and lumbar and sacral, using a single edged blade before submerging in gelatin and cooling on a cold plate in the fridge. Once solidified, these individual blocks of gelatin were left in 4 % PFA, 0.25% (w/v) glutaraldehyde overnight at 4 °C to fix the gelatin for sectioning. The individually embedded spinal cord sections were cut on the vibrating microtome, as described above, at 50 µm in either coronal or sagittal planes.

1.8.7. Immunohistochemistry

Primary antibodies raised against a specific epitope were incubated with the sections at 4 °C overnight. They were diluted (Table 3) in PBS 0.1% (v/v) Triton X-100 (Thermofisher, 85111) (PBST 0.1 %) in order to permeabilise the cell membranes. Sera of the animal that the secondary antibody is raised in (Table 4) were added to the primary solutions to reduce non-specific binding. These sections were washed 3 times in PBS to remove the primary antibody. Following this they were left in secondary antibodies, diluted in PBS (Table 4) for 2-4 hours resulting in the binding of a molecule attached to a fluorophore which can be detected under the fluorescent microscope. The different fluorophores used permitted visualisation of 2 or 3 antibodies within the same tissue. The tables below detail the antibodies used in this project, their source and catalogue number and evidence of what each antibody labels. Throughout, antibody labelling within tissue will be referred to as antibody+, indicating a sample is positive for the antibody binding for example CSFcCs immunopositive for PKD2L1 are PKD2L1+.

Target	Host	Company (catalogue no./LOT)	Dilution	Cell	Why?
PKD2L1	Rabbit	Proteintech (13711-2- AP/00003999)	1:500	CSFcCs	A calcium permeable transient receptor potential channel expressed in the membrane of CSFcCs within the CNS (Huang <i>et al.</i> 2006).
ChAT	Goat	Millipore corp (AB144P/22808 14)	1:500	Cholinergic neurones	Choline acetyltransferase is an enzyme required for the synthesis of acetylcholine (Cozzari and Hartman, 1980).
SV2	Mouse	DSHB	1:100	Synaptic vesicles	Monoclonal antibody generated of SV2 binds the protein in all synaptic vesicles of all transmitters. (Feany <i>et al.</i> , 1992).
GLP1R	Mouse	DSHB (Mab 7F38-S/1ea)	1:500	GLP1 receptors	Specific antibody to the GLP1 receptor located on the surface of various cells located in the gastrointestinal tract as well as in the central nervous system (Heppner <i>et al.</i> , 2015).
GFP	Chicken	Abcam (ab13970/GR33 61051-9)	1:1000	Cells expressing GFP	Antibody binds to the GFP expressed within specific cell lines of transgenic mice, enhancing the fluorescence. This includes GCaMP6f.
Iba1	Rabbit	Thermofisher (PA5- 27436/SK24786 38E)	1:500	Microglia	Iba1 is a molecule involved in the ruffling of cell membranes in activated microglia,

					capable of binding actin (Ohsawa <i>et al.</i> , 2004). Iba1 mRNA is specifically expressed in microglia (Ito <i>et al.</i> , 1998).
Synaptophysin	Rabbit	Proteintech (17785-1-AP)	1:200	Synaptic vesicles	A membrane glycoprotein located in neuronal presynaptic vesicles (Wiedenmann <i>et al.</i> , 1986).
mCherry	Rabbit	Badrilla (A010-mCherry-50/0612-2)	1:1000	Cells expressing mCherry or Channel rhodopsin	A monomeric red fluorescent protein, derived from DsRed, the first RFP (Shaner <i>et al.</i> , 2004).
SOX2	Rabbit	Milipore corp (SC-17320/K1115)	1:1000	Ependymal cells	A transcription factor implicated in determining cell fate. Found in pluripotent stem cells, influences their differentiation (Zhang <i>et al.</i> , 2014).
Hu C/D	Rabbit	Proteintech (13032-1-AP/000039630)	1:1000	Neurones	RNA binding protein that regulates the identity and maturation of neuronal cells (Akamatsu <i>et al.</i> , 2005).
Cleaved caspase-3	Rabbit	Cell signalling (96615)	1:400	Apoptotic cells	Caspase-3 is a frequently activated death protease which catalyses cellular protein cleavage, instigating apoptosis (Porter and Jänicke, 1999)

Table 3: List of primary antibodies, concentrations and justifications. Sections were incubated in primary antibodies overnight. Secondary antibodies conjugated to fluorophores were then incubated with the sections for 2 hours in order to generate a detectable signal from the labelled targets.

Secondary Antibody		Target	Serum (5%)	Company (Catalogue no./LOT)	Dilution
Alexa 488	Donkey anti rabbit	Rabbit	Donkey	Thermofisher (A21206/127 5888)	1:1000
	Donkey anti sheep	Sheep/Goat	Donkey	Invitrogen (A11039/230 4258)	1:1000
	Streptavidin	Biotin	-	Invitrogen (S11223/236 9183)	1:500
Alexa 555	Donkey anti mouse	Mouse	Donkey	Invitrogen (A31570/190 5844)	1:1000
	Goat anti chicken	Chicken	Goat	Invitrogen (A11039/230 4258)	1:1000
	Donkey anti rabbit	Rabbit	Donkey	Invitrogen (A32794/U12 84002)	1:1000
	Streptavidin	Biotin	-	Invitrogen (S11223/236 9183)	1:1000
Biotinylated	Donkey anti mouse	Mouse	Donkey	Bethyl (A90- 337B)	1:500
	Donkey anti rabbit	Rabbit	Donkey	Invitrogen (A16039/42- 152-070814)	1:500
	Donkey anti chicken	Chicken	Donkey	Jackson (703-065- 155/103674)	1:500
HRP	Streptavidin	Biotin	-	Thermofisher (FP1043/337 655)	1:500

Table 4: List of secondary antibodies and concentrations. Sections were incubated in one of the above secondary antibodies for 2-4 hours resulting in the binding of a molecule attached to a fluorophore or an element that can then be visualised using staining techniques such as tyramide signal amplification (TSA) or diaminobenzidine (DAB).

1.8.8. Mounting

After the above staining procedures, sections were lifted out of solution and placed onto microscope slides. Once dry, a drop of Vectashield with DAPI (Vector laboratories, H-1200-10) was added and a cover slip lowered over the section. The edges were sealed with nail varnish.

1.8.9. Microscopy

Once mounted, using a Leica DMRE the slides were checked for fluorescent signals in the appropriate channels to ensure successful staining. Following this, images were taken on various microscopes depending on the required magnification and image clarity.

For large batches of images required for 5-ethynyl-2'-deoxyuridine (EdU) counting, an automated slide scanner, Zeiss Axioscan Z.1, was used with a 20 x objective in either a single plane, or multiple planes depending on the cells being imaged. For overview, to visualise lower power images of entire sections, the EVOS Auto 2 Fluorescent Microscope was used. Whereas, to attain high power images, Zeiss LSM880 laser scanning confocal microscope was used at either 20 x objective, or the 40 x objective. This captured detailed images revealing co-localisation.

These images were viewed and edited in Fiji. Only brightness and contrast were adjusted to enhance the visibility of the labelling.

Chapter 2: Exploring CSFcC distribution and properties

2.1. Introduction

CSFcCs contribute to the heterogeneous cell population around the central canal which extends from the medulla to the sacral spinal cord. With their unique morphology they possess a soma, located in the ependymal zone and an apical extension projecting into the central canal, contacting the CSF (Kolmer, 1921, Agdhur, 1922, Dale *et al.*, 1987).

CSFcCs have a diversity of properties. These include a mechanosensory role (Kolmer, 1921, Agdhur 1922), responses to changes in pH (Huang *et al.*, 2006, Orts-Del'Immagine *et al.*, 2012, Jalalvand *et al.*, 2016) and neuronal properties (Marichal *et al.*, 2008, Jalalvand *et al.*, 2014, Fidelin *et al.*, 2015). More recently, they have been associated with roles in locomotion (Wyart *et al.*, 2009, Bohm *et al.*, 2016) and modulating CSF flow (Sternberg *et al.*, 2018, Orts-Del'Immagine *et al.*, 2020). However, most of these studies are restricted to invertebrates and lower vertebrates with few defining these cells in rodents. Similarly, the functional studies describe their activity in lower vertebrates.

In this chapter, a novel transgenic mouse line was used assess CSFcC distribution in mice. Transgenic models have altered genomes in order to study specific proteins in isolation within a physiological system. This use of tissue or cell specific gene expression under the control of a gene promoter was first demonstrated by Gordon *et al.* (1980). Here, a transgenic model was used with a genetically encoded calcium indicator, green fluorescent protein (GFP) fused to calmodulin (CaM) referred to as GCaMP6f, expressed under the promoter PKD2L1, a channel only expressed in CSFcCs within the CNS. This will facilitate describing the distribution of CSFcCs along the rostral caudal axis in the brainstem and brain. PKD2L1-IRES-Cre mice were crossed with floxed GCaMP6f mice resulting in PKD2L1:GCaMP6f mice in which GCaMP6f is expressed in all cells containing PKD2L1. This will label all CSFcCs with a fluorescent protein which can be enhanced with the use of immunohistochemistry. Notably, GCaMP6f is a calcium indicator *in vivo* and *in vitro*, however in this thesis, it is observed in fixed tissue and used solely as a form of GFP for marking the cells it is genetically expressed within, PKD2L1+ CSFcCs.

After visualising CSFcCs using various immunohistochemical processes and demonstrating the transgenic PKD2L1-Cre mouse line is expressing cre recombinase (cre) in CSFcCs, the next stage was to further investigate their circuitry. Viral tracing methods are a process by

which the circuitry of a unique cell type, in this case CSFcCs can be isolated. The use of a floxed virus in a cre animal, results in the expression of a specific protein only within cells expressing cre. The adeno-associated virus (AAV) expressed hCHR2-mCherry, a fusion protein of two molecules; channel rhodopsin (ChR2) and mCherry. mCherry permits the visualisation of the protein expression as it is a monomeric red fluorescent protein derived from DsRed (Shaner *et al.*, 2004). Injecting this floxed virus into PKD2L1-Cre mice, should lead to restricted expression of the fluorescent proteins in CSFcCs, the transport of which along their axons should reveal where they project to and cells onto which they terminate. Channel rhodopsin is a light activated channel which can be stimulated using optogenetics (Boyden *et al.*, 2005) however in this aspect of the project this will not be utilised, the expression of this fusion protein will solely be used as a marker of where the virus is expressed. Studies of CSFcCs principally occur in Zebrafish and Drosophila with fewer murine studies, restricting our understanding of these unique cells in higher vertebrates.

2.2. Aims

This part of the project is aimed at optimising visualisation of CSFcCs and assessing where they project to, from specific regions of the spinal cord. Using various immunohistochemistry methods with the PKD2L1 antibody to label CSFcCs in the CNS, I will qualitatively compare the visualisation of the cells, aiming to achieve best visualisation of the axons projecting from the somata around the CC. I expect methods that amplify the signal from the initial antibody binding the epitope to result in more apparent staining in the finer regions of the cell including the axons.

Additionally, I expect to see expression of CSFcCs throughout all spinal cord levels of mice which has not yet been clearly shown. The introduction of a novel transgenic mouse line to demonstrate this element of the project requires validation of the model which I will test through labelling of CSFcCs using anti-PKD2L1 co-currently with anti-GFP. The GFP antibody is used to enhance the fluorescence from the GCaMP6f protein encoded within the transgenic animals, promoted by PKD2L1. The use of double labelling of GCaMP6f with a PKD2L1 antibody will verify GCaMP6f expression is unique to CSFcCs and allow us to define their expression along the rostral caudal axis, within the brain and brainstem. High expression of this receptor should be seen in the kidney therefore this tissue will also be used to visualise GCaMP6f expression and further verify the model.

The function of CSFcCs could be in releasing signals into the CSF via vesicles secreted from their terminals. To test this, I will use immunohistochemistry to label CSFcCs along with other markers observed within synaptic terminals, using the transgenic mice previously validated.

There may be a neuronal role for these cells, in order to show this we need to look at where they project to and then what cells they output signals to. The viral injections into the lumbar region of the spinal cord will be used to map the projections from CSFcCs within this level of the spinal cord. This will reveal the extent and location of projections, which isn't clear from the faint axonal labelling previously seen in transverse sections.

2.3. Methods

2.3.1. Animals

VGAT:GCaMP6f female and male C57Bl/6 mice at 12 weeks were used to compare each of the discussed immunohistochemistry methods to improve visualisation of CSFcCs. 3 PKD2L1:GCaMP6f female and male mice at 12 weeks were used to characterise CSFcC expression throughout the central nervous system and kidneys. After perfusion of the mice, the abdomen was opened by incision through the skin at the midline and pinning aside the flesh. Following this, scissors were used to decapitate the mice and cut along either side of the midline removing the limbs. Then the intestine and organs were cut away until reaching the ventral surface of the spinal cord leaving the kidneys attached. The nerves connecting to the kidneys were cut to detach them. The brain was obtained by using a blade to cut the skin at the top of the head and expose the skull. Then the skull was cut using fine scissors, starting at the caudal brainstem, through the midline to the eye sockets. The skull was lifted off using a fine spatula and the brain was lifted out of the ventral skull. The olfactory bulb was cut off from the brain using a single edge blade. The kidney and olfactory bulb were gelatin embedded before sectioning as discussed above. 3 PKD2L1:Cre animals were used to assess CSFcC projections using viral tracing. The tissue used and number of sections for each staining process are detailed in Table 5.

2.3.2. Tissue used for staining and counts

Phenotype	N	Age (weeks)	Antibody	Number of sections per animal			Other tissue
				C	T	L	
VGAT:GCaMP6f	3	12	GFP and PKD2L1	3	3	3	-
			PKD2L1 (indirect)	5	5	5	
			PKD2L1 (biotinylated)	5	5	5	
			PKD2L1 (TSA)	5	5	5	
			PKD2L1 (DAB)	5	5	5	
PKD2L1:GCaMP6f	3	8-12	GFP and PKD2L1	5	5	5	Brain, brainstem, kidney
	2	8-12	GFP and Hu C/D	3	3	3	-
			GFP and SOX2	3	3	3	-
	3	8-12	GFP and GLP1R	6	6	6	-
			PKD2L1 and GLP1R	6	6	6	-
	PKD2L1-IRES-Cre	3	12	mCherry	5	5	5

Table 5: Tissue used for labelling and counts. Displaying all of the tissue used with number of mice, age of mice at perfusion, the antibody used to label the sections and the number of sections per animal and the subsequent regions from which the sections are cut. C = cervical, T = thoracic, L = lumbar. Also includes any tissue outside of the spinal cord sectioned and labelled. This tissue was used for co-localisation to verify CSFfC phenotypes and to verify the transgenic phenotype of the new mouse line. C = cervical, T = thoracic and L = lumbar.

2.3.3. Comparison of immunohistochemistry methods

Indirectly conjugated antibodies

Indirectly conjugated antibody labelling is the first form of immunohistochemistry I used to visualise CSFcCs within the spinal cord, shown in Figure 6. This refers to a two-step process, first the primary antibody, specific to the desired epitope is incubated with the tissue. Following this, the secondary antibody is added, specifically binding to the primary antibody. The secondary antibody is bound to a fluorophore which allows the antibody binding to be visualised under a fluorescence microscope. This amplifies the signal as multiple secondary antibody molecules bind to each primary antibody and therefore to each epitope. Additionally, conjugation to a fluorophore creates a larger molecule, this would make it difficult to bind the epitope, a small region of interest, if bound directly to the primary antibody.

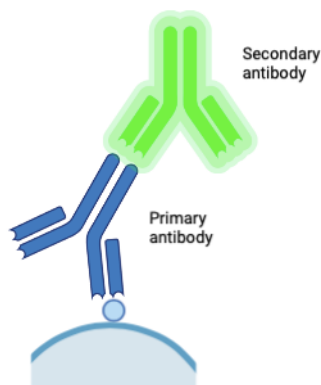


Figure 6: *Indirectly conjugated antibodies.* This shows the process by which indirectly conjugated antibodies label the epitope of interest permitting visualisation of a specific part of the tissue. The primary antibody binds first to the protein it has been raised against, followed by incubation with the secondary antibody which is conjugated to a fluorophore which can be visualised microscopically.

Biotinylated antibodies

The next antibody labelling technique aimed to improve the quality of the staining of CSFcC processes, principally those projecting away from the CC towards the ventral fissure (VF) region. Biotinylated antibody protocols are reported to improve the labelling compared to the indirect method, as shown in Figure 7. This is due to the additional step further amplifying the signal. This process is typically used to locate low abundance proteins within the tissue. The binding of a biotinylated secondary antibody to the streptavidin conjugated to a fluorophore is a strong, non-covalent interaction (Strachan *et al.*, 2004).

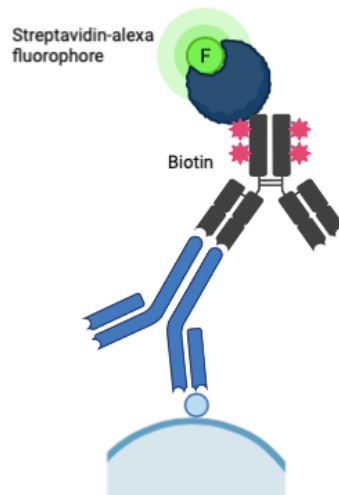


Figure 7: Biotinylated antibody binding. Detailing the additional step within this process compared with the indirectly conjugated antibody process. Following the primary antibody binding, the tissue is incubated with biotinylated secondary antibodies and then a Streptavidin molecule conjugated to the alexa fluorophore which binds the biotinylated secondary antibody. It is of note that the biotinylated step amplifies the signal with multiple biotinylated secondary molecules binding to each primary antibody bound to the epitope.

Diaminobenzidine (DAB)

DAB visualisation uses a catalysed reporter deposition (CARD) method of immunohistochemistry, permitting amplification of the signal relative to indirect methods of immunohistochemistry. The primary antibody is added first to bind the epitope, followed by the biotinylated secondary, as above. This is followed by Streptavidin, which strongly binds the biotin (Figure 8), forming the complex used for visualisation, however in this case it is bound to horseradish peroxidase (HRP). The addition of a solution containing DAB and hydrogen peroxidase to an antibody bound HRP results in oxidation of the DAB depositing a brown precipitate at the location of the epitope. This precipitate is insoluble in alcohol and doesn't degrade therefore it is a permanent form of antibody labelling, unlike the fluorescence techniques in which the fluorescence fades and bleaches over time. This is visualised using brightfield microscopy and can often be imaged at a low magnification due to the stark contrast between the brown precipitate and the light-coloured background. It is the biotinylation step that amplifies the initial binding of the primary antibody as multiple biotinylated secondary antibodies bind each primary antibody (Fahimi and Herzog, 1973).

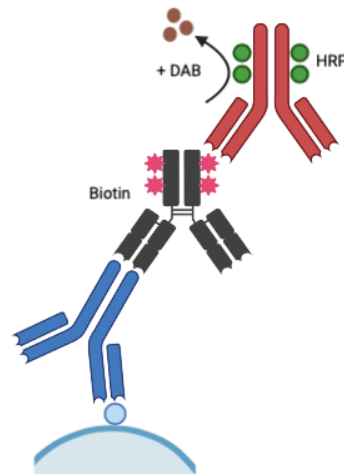


Figure 8: DAB labelling. Demonstrates the stages involved in DAB staining, including the final stage which differs from biotinylated antibody labelling. Significantly, it is the addition of the DAB solution at the end of the protocol which results in the brown pigment forming which permits visualisation of the initial antibody binding.

Tyramide signal amplification (TSA)

TSA is an example of enzyme linked signal amplification, enhancing the detection of the protein target, particularly targets of low abundance. It follows similar stages to those discussed in DAB labelling however, results in a fluorescent signal. Once again, HRP is used to catalyse the depositing fluorescently labelled tyramide to the target protein (Figure 9). Notably, this method of immunohistochemistry is highly specific, sensitive and permits multiple fluorescent labels to be added simultaneously (Faget and Hnasko, 2015). Compared to DAB, a possible carcinogen and irritant, TSA is safer, and uses fluorescence which has the capacity to label multiple targets in a single section. Additionally, the amplification of the primary antibody binding permits the use of this at a lower concentration with a 2-50-fold decrease compared to the concentrations required in the indirectly conjugated antibody methods (Hunyady *et al.*, 1996). Chao *et al* (1996) demonstrate that the use of Cy3.89-tyramide in catalysed reporter deposition protocols lead to an 8.5 fold enhanced signal when compared with the use of biotinylated antibodies followed by Cy3.18-Streptavidin for visualisation.

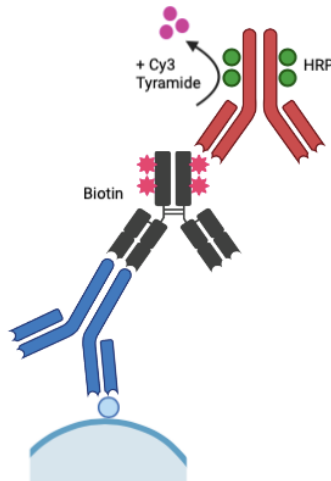


Figure 9: TSA process. Displays the differing final stage in this process in which the Cy3 conjugated tyramide reacts with the HRP resulting in fluorescent labelling of the antibody binding which had formerly been amplified by the biotinylated secondary antibody.

2.3.4. Biotinylated antibodies

After the primary antibodies bound to the tissue, secondary antibodies, conjugated to biotin were washed on the sections for 2 hours. This was followed by incubation with Streptavidin bound to a fluorophore (Table 4) for visualisation of the amplified signal.

2.3.5. DAB

Prior to incubation with the primary antibodies, sections used for DAB labelling had an additional quenching step. Sections were flooded with 3 % hydrogen peroxidase in PBS at room temperature for 30 minutes to saturate endogenous peroxidases to eliminate staining of erythrocytes, granulocytes or neurones (Bussolati *et al.*, 2011) within the tissue. After incubation with primary antibodies as above, secondary antibodies conjugated to biotin were added for 2 hours. This is replaced with streptavidin-HRP (Table 4). Sections are finally incubated with DAB solution (Vector Laboratories, SK-4100) 0.15 M hydrogen peroxide in buffer stock solution, DAB reagent and dH₂O covers the sections and is left for 5-10 minutes, until the sections appear brown.

2.3.6. TSA

The same quenching step is required for TSA as it also uses hydrogen peroxide as the catalyst. Following the same steps as for DAB, after incubation with Streptavidin-HRP, Cy3

tyramide (APExBIO, K1050) 1:100 in TSA amplification diluent was washed over the sections for 10 minutes. TSA amplification diluent; 100 μ M boric acid, 294 μ M hydrogen peroxide, 56.1 M dH₂O, 0.1 % (v/v) Tween20.

2.3.7. Dehydration

Sections stained with DAB can undergo a further step to improve the visualisation. Sections were placed onto gelatinised slides. Once dried, they were placed sequentially into solutions: 50 %, 70 %, 90 % and 100 % ethanol (v/v) dH₂O, left for 1 minute in each to remove the water content of the tissue. Finally, the slide is placed into Histo-clear II (Geneflow, A2-0105) for 3 minutes. DPX mounting media (Sigma-aldrich, 06522) is used as this is non-aqueous which preserves the dehydration steps.

2.3.8. Counts and analysis

These sections used to test visualisation of CSFcCs using different processes were imaged using EVOS Auto 2 Fluorescent Microscope at 10 x, 20 x and 40 x magnification. This was due to COVID-19 restricting training on the confocal microscope at this point of my project.

For counts of overlapping antibody staining, the Leica DMRE was used at 40 x magnification using the variable focus to check whether each CSFcC labelled with either GCaMP6f or PKD2L1 was also labelled with GLP1R. The number of CSFcCs labelled with the GLP1R antibody was calculated as a percentage of the total number labelled with either PKD2L1 (PKD2L1+) or GCaMP6f (GCaMP6f+) in each 50 μ m section.

The other co-localisation analysis within this chapter was observed by capturing images on the confocal microscope in two channels. After merging these images, cells were observed for labelling with two markers.

Similarly, observations were made based on the images taken of virally labelled tissue sections in order to determine the direction CSFcCs project along the spinal cord.

2.3.9. Virus

PKD2L1:Cre mice at 8 weeks were injected with the cre-activated adeno-associated virus (AAV) expressed human channel rhodopsin (hChR2) fused to mCherry after activation. Specifically, pAAV-EF1a-double floxed-hChR2(H134R)-mCherry-WPRE-HGHpA (addgene, #20297-AAV1), 2.5×10^9 vg.

2.3.10. Tissue sectioning

The first virally injected spinal cord was sectioned in a transverse plane to check if the injections were successful. Sectioning in this plane meant labelling could be compared with typical CSF_cC spinal cord labelling previously observed. Following this, the second spinal cord was sectioned in the sagittal plane by gelatin embedding as described previously. To maintain the orientation of the cord when mounting the sections, a diagonal cut was made in the top corner of the gelatin at the caudal end of the spinal cord. This would permit tracing of any axons that travelled along multiple spinal cord regions. It also assisted in determining the direction in which axons travelled – rostral or caudal, as well as whether the axons ran along the dorsal horn of the spinal cord or the ventral fissure.

2.4. Results

2.4.1. Different immunohistochemistry methods to label PKD2L1+ CSFcCs

Indirectly conjugated antibody labelling

Using the indirect antibody labelling technique described above, 50 μm transverse sections of spinal cord were incubated in anti-PKD2L1 followed by donkey anti-rabbit-555. This resulted in the labelling of CSFcCs (Figure 10) when observed under a fluorescence microscope. CSFcCs were labelled around the CC region. There is also less clearly defined labelling between the CC and the VF.

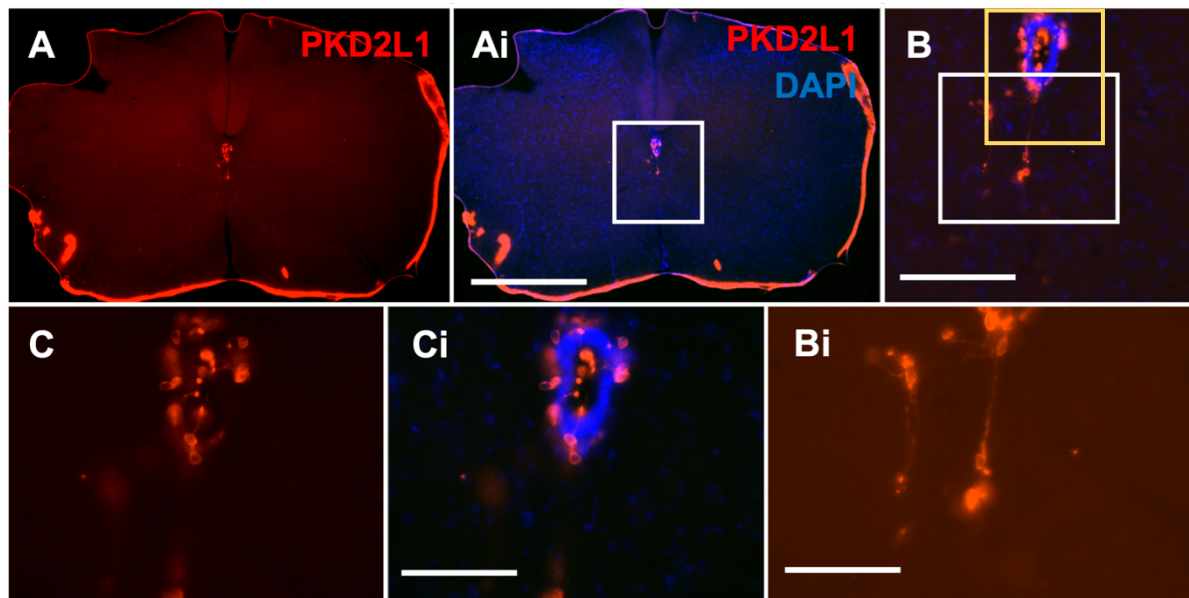


Figure 10: CSFcCs are primarily distributed around the CC. (A) Overview image of a transverse section from the cervical spinal cord, labelled with antibodies to PKD2L1 (red) and dual labelling for PKD2L1 and DAPI (blue) (Ai) showing the typical distribution primarily around the CC. (B) High magnification image of boxed area in (Ai) with some labelling observed towards the VF. (C) and (Ci) Higher magnification image of yellow boxed area in (B), showing PKD2L1+ end bulbs in the CC. (Bi) Higher magnification image of white boxed area in (B), showing PKD2L1+ labelling extending towards the VF. The scale bars are Ai = 500 μm , B = 100 μm , Ci = 80 μm , Bi = 50 μm . DAPI staining of nuclei enhances definition of different regions such as CC. Captured using transmitted light microscopy.

Biotinylated antibodies

Following this, an amplification method of antibody labelling was used aiming to achieve greater labelling in the VF region and increase visualisation of CSFcCs. As above, sections were first incubated in anti-PKD2L1 however an additional biotinylated secondary antibody step was conducted before the binding of a molecule attached to a fluorophore (Figure 7).

The outcome of this was a qualitatively assessed as brighter fluorescent signal around the central canal and some improved labelling of somata around the CC seen at higher magnifications (Figure 11).

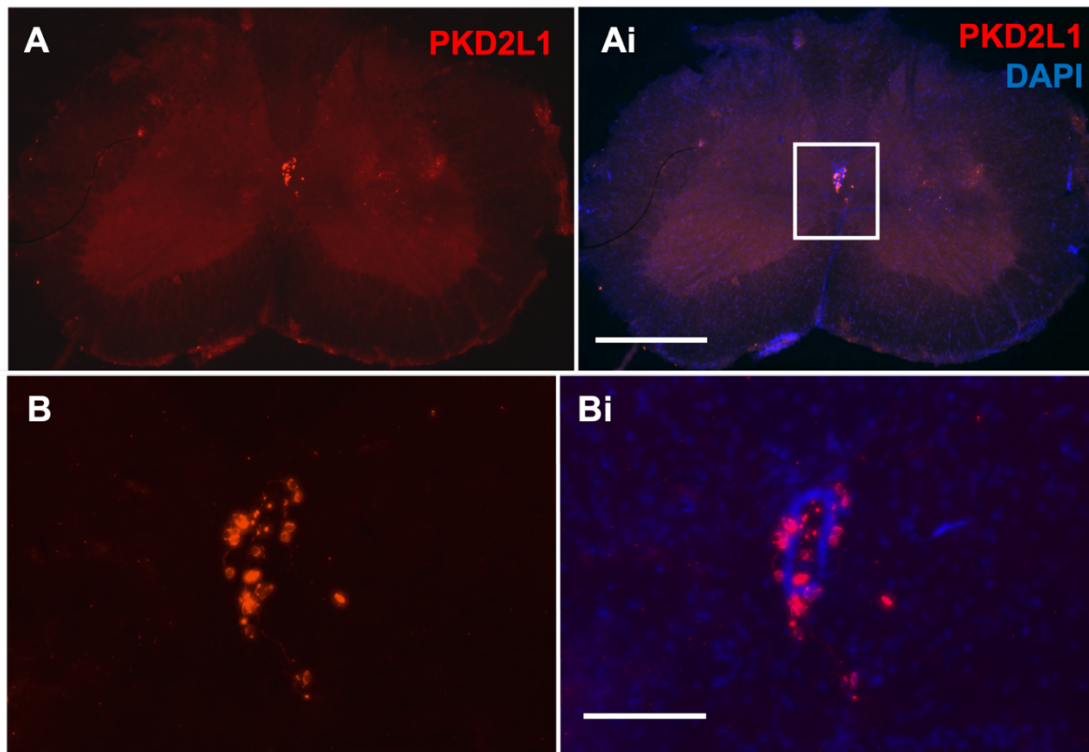


Figure 11: *Biotinylated antibody labelling revealed labelling outside of CC.* Overview image of a lumbar section labelled with PKD2L1 (red) using the biotinylated antibody method to amplify the signal. (A-Ai) Overview initially shows the same CSFcC distribution as with the indirect antibody method with a brighter signal from the CC. (B-Bi) Higher magnification image of the boxed region (Ai) There is greater labelling of the CSFcCs in the CC and some VF labelling similar to what was previously observed. Ai = 500 μ m, Bi = 100 μ m. Captured using transmitted light microscopy.

TSA

When carrying out the labelling of CSFcCs using the TSA method, there was increased axonal labelling between the CC and the VF (Figure 12). At 40 x magnification, boutons can be seen on the extensions extending from CSFcCs, characteristic of axons, highlighted in Figure 12 with arrows.

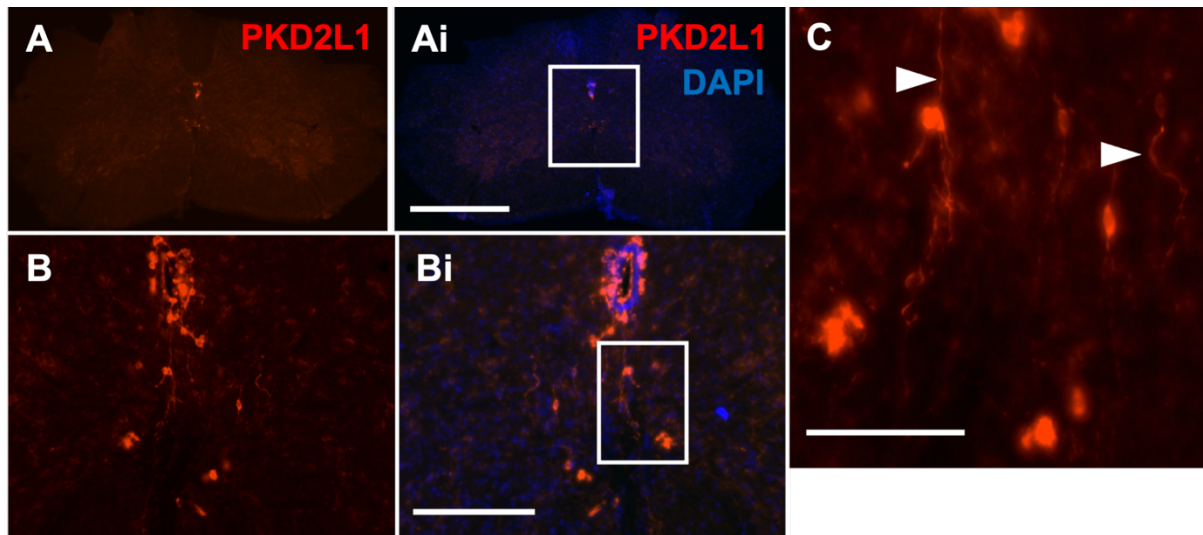


Figure 12: TSA labelling shows extensive axonal labelling in the ventral fissure. (A – Ai) The TSA process initially appears at low magnification to label similarly to previous staining methods with primary labelling in the central canal with some in the ventral fissure region. (B-Bi) Higher magnification images of boxed area (Ai) show more labelling in the VF than previously seen. (C) High magnification image of boxed area (Bi) shows extensive axonal labelling in the VF region (white arrows) with boutons observed. From the soma between the CC and VF, the projections are shown to travel in both directions, dorsally and ventrally. Scale bars as follows, Ai = 500 μm , Bi = 100 μm and C = 50 μm . Captured using transmitted light microscopy.

DAB

DAB differs greatly to the previous fluorescence labelling techniques discussed above. This staining method culminates in the depositing of a brown pigment which contrasts from the background making the cells and axons stand out (Figure 13). Furthermore, the dehydration stages of this protocol help resolve all elements of the section to one focal plane, allowing visualisation of all the elements of the 50 μm section in a single focal plane unlike the previous methods which required variable focus or images captured in multiple planes.

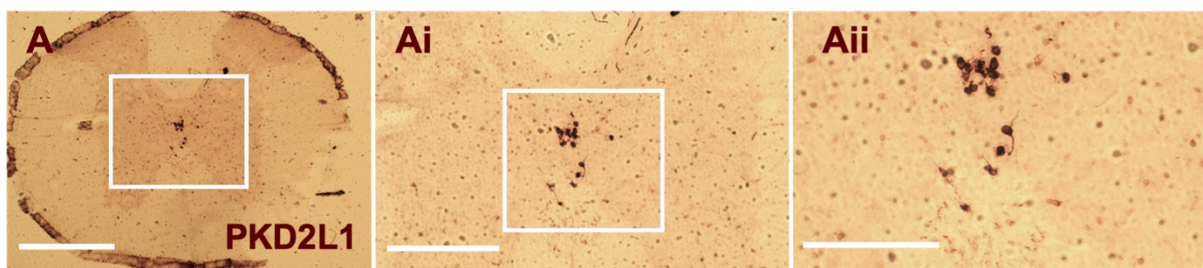


Figure 13: Prominent axons and CSFcc somata outside CC. This shows the vast difference in DAB staining in comparison to the fluorescent labelling techniques previously used. (A) An overview at low magnification, the stained PKD2L1 cells are greatly contrasted from the rest of the tissue. (Ai) Higher magnification of boxed region (A) clearly shows the CSFccs between the CC and the VF. (Aii) When magnified further, the axonal processes from these cells can be seen, to a similar extent seen with TSA. Scale bars; A = 500 μm , Ai = 250 μm , Aii = 150 μm . Captured using transmitted light microscopy.

2.4.2 GCaMP6f expression within PKD2L1+ CSFcCs

Transverse spinal cord sections

To begin assessing GCaMP6f expression within the transgenic PKD2L1:GCaMP6f mouse line, spinal cord tissue was sectioned in a transverse plane and labelled with anti-PKD2L1 alongside anti-GFP to enhance the GCaMP6f signal. First observed was GCaMP6f co-localisation with anti-PKD2L1, Figure 14, verifying the transgenic mouse line. Following this, it was again observed that CSFcCs exist outside of the CC region in which they were previously described (Figure 14 B-Bii, C-Cii). This included labelling of both somata and long spanning axons.

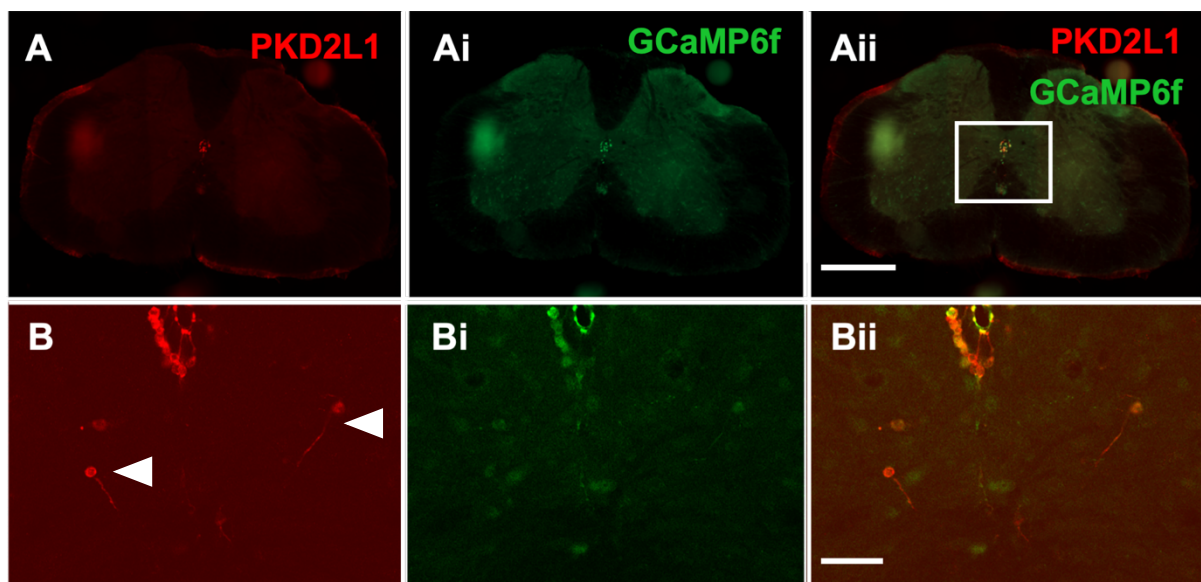


Figure 14: GCaMP6f expression in CC and VF co-localised with PKD2L1. (A- Aii) Typical CSFcC distribution within a 50 µm transverse cervical section. CSFcCs principally surround the central canal. (B-Bii) At higher magnifications, CSFcCs are observed outside of the ependymal zone, located towards the ventral fissure, as indicated with white arrows (B). Focussing on the ventral CC region to the VF showing axons extending from the somata down towards the VF. All cells expressing GCaMP6f co-localise with PKD2L1. Scale bars as follows, Aii = 500 µm, Bii = 75 µm. Captured using transmitted light microscopy.

Sagittal spinal cord sections

When the cord was cut in a sagittal plane, labelling was observed around the CC along the entirety of the rostro-caudal axis. This was consistent with no breaks in the staining at any points. It was also clear to see the group of cells which exist outside of the CC region. (Figure 15A, white arrows). When the cord was cut in this plane, the axonal labelling

previously seen spanning across transverse sections of SC, was now observed running down the VF region, along the length of the spinal cord (Figures 15B-Bii).

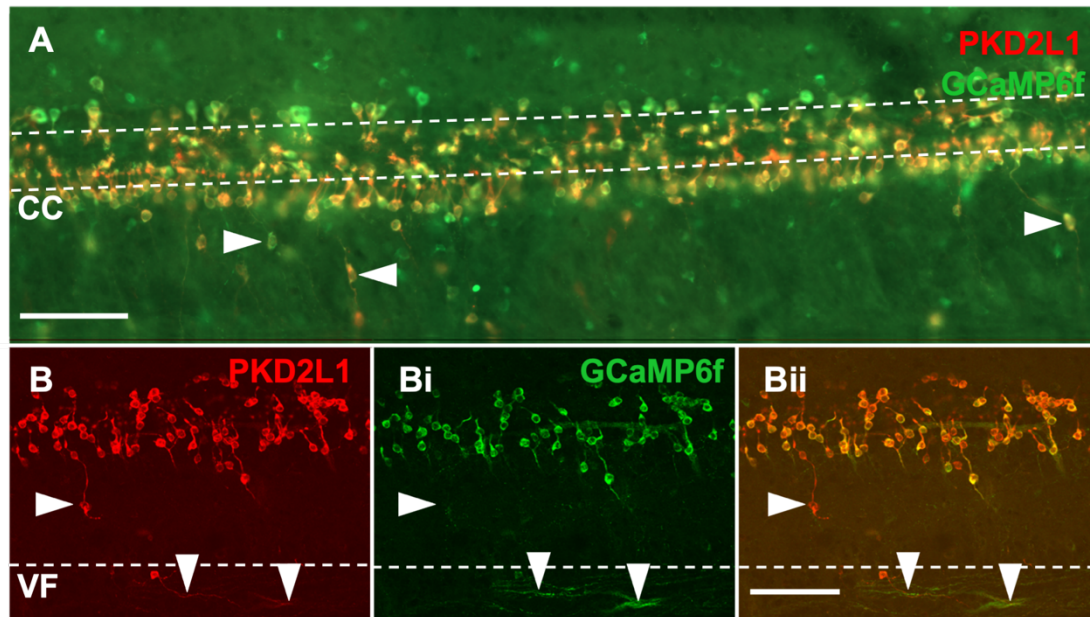


Figure 15: CSFcCs distributed along the entire CC. Shows sagittal sectioned spinal cord from the cervical region labelled with both GCaMP6f (green) and PKD2L1 (red). (A) PKD2L1+ and GCaMP6f+ cells distributed along the length of the CC captured in this image. White arrows indicate some prominent CSFcCs outside of CC region. Due to the sagittal sectioning, the dotted lines provide an indication of where the CC runs, however there are no cell bodies within this region and those seen reflect the angle of cutting and Z stack compiled image which has distorted the CC region. (B-Bii) Higher power confocal images highlighting the even distribution of CSFcCs in the central canal region along the length of the spinal cord and the axons running along the VF region. There is co-localisation between GCaMP6f and PKD2L1. Scale bars; A = 100 μ m, Bii = 100 μ m. Captured using confocal microscopy.

Brain

There was no antibody labelling in either channel when labelling the brain (Figure 16), this was consistent throughout every region, including the forebrain (Figure 16A-Aii), midbrain (Figure 16B-Bii) and hindbrain (Figure 16C-Cii).

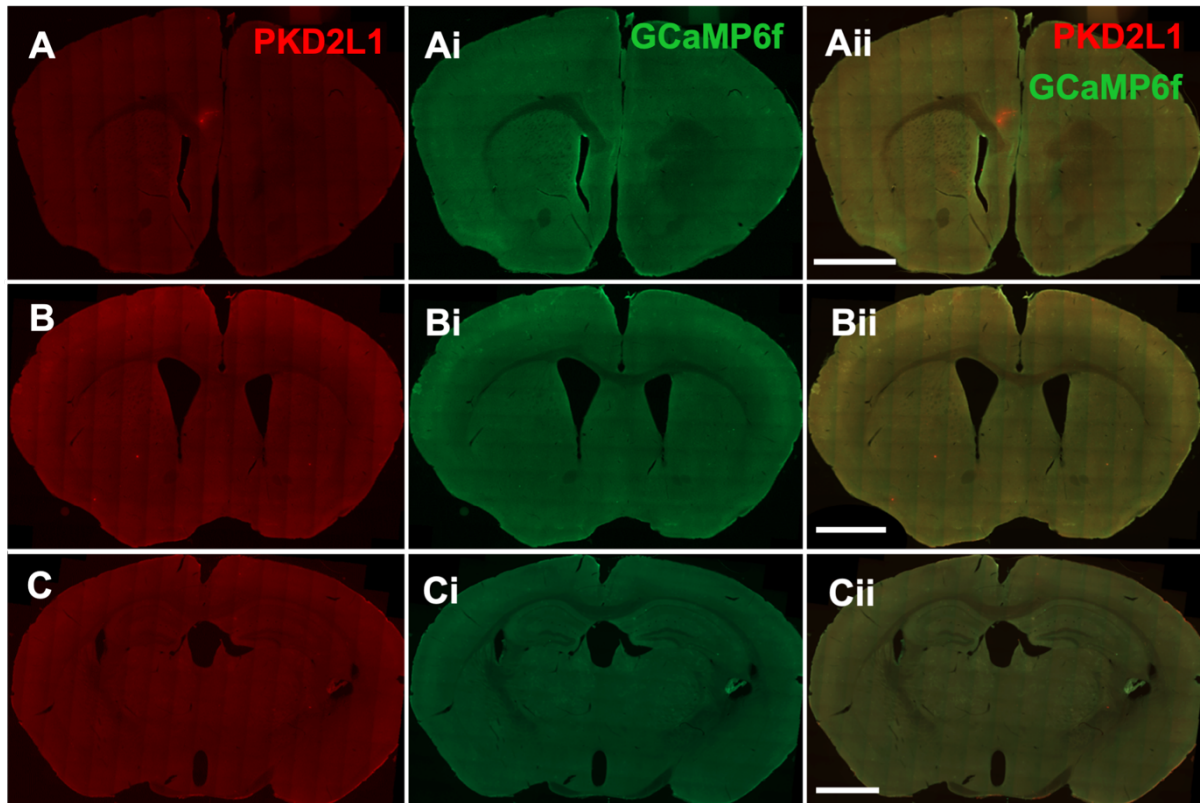


Figure 16: *GCaMP6f* not expressed in the brain. Representative 50 μm sections from the forebrain (A-Aii) midbrain (B-Bii) and hindbrain (C-Cii). None of the images show labelling in any brain region when labelled with PKD2L1 (red) or *GCaMP6f* (green). Scales Aii, Bii, Cii = 1500 μm . Captured using transmitted light microscopy.

Brainstem

The most rostral labelling of CSFcCs within the CNS is in the brainstem. From the caudal brainstem sections (Figure 17), with a distinct CC there is profound labelling seen when staining with both PKD2L1 antibodies and when enhancing the *GCaMP6f* signal. This staining revealed extensive axonal projections and a wide distribution of CSFcCs across the section, terminating in various regions (Figure 18).

The first observation of *GCaMP6f* labelling within the brainstem, was the cells and axons distinctly away from the CC (Figure 17 white arrows) which appear to extend ventrally as far as the nucleus raphe obscurus. Other nuclei identified with either projections from CSFcCs extending towards or CSFcC cell bodies include nucleus raphe obscurus and hypoglossal nucleus (Allen brain atlas, 2008).

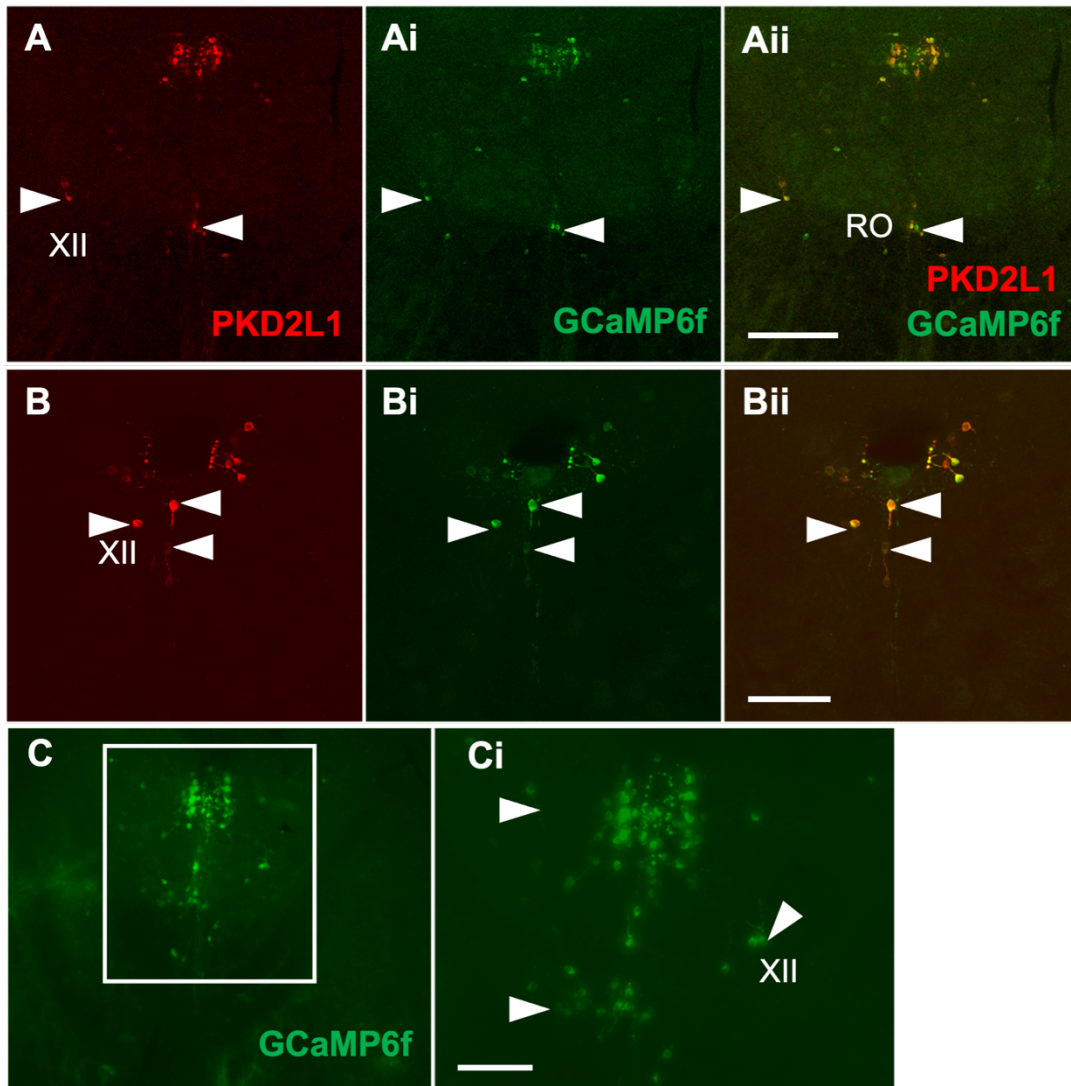


Figure 17: High CSFcC expression within various brainstem nuclei. (A-Aii) GCaMP6f+ (green) and PKD2L1+ (red) labelling overlaps in the brainstem further verifying the transgenic model. Cells and axons observed outside of the CC across different brainstem regions (white arrows) including the nucleus raphe obscurus (RO) and hypoglossal nucleus (XII). (B-Bii) Another representative section showing a GCaMP6f+ cell also PKD2L1+ ventral to the CC with a long process extending ventrally (white arrow). (Cii) Cells again appear within hypoglossal nucleus (XII). Scale bars Aii = 200 μ m, Bii = 100 μ m C = 200 μ m, Ci = 100 μ m. Captured using transmitted light microscopy.

Using a combination of tiled scan images on the confocal of GFP enhanced GCaMP6f as well as lower magnification EVOS images of TSA labelling, we can see the axonal projections in various directions away from the CC (Figure 18). There were projections laterally (Figure 18 A, white arrows). As well as GCaMP6f+ somata along the midline between the hypoglossal nuclei with projections down towards ventral part of the brainstem (Figure 18 Ai-ii). Some sections labelled with GCaMP6f enhanced using the TSA method (Figure 9), which revealed more regions of the brainstem in which GCaMP6f+ cells were located.

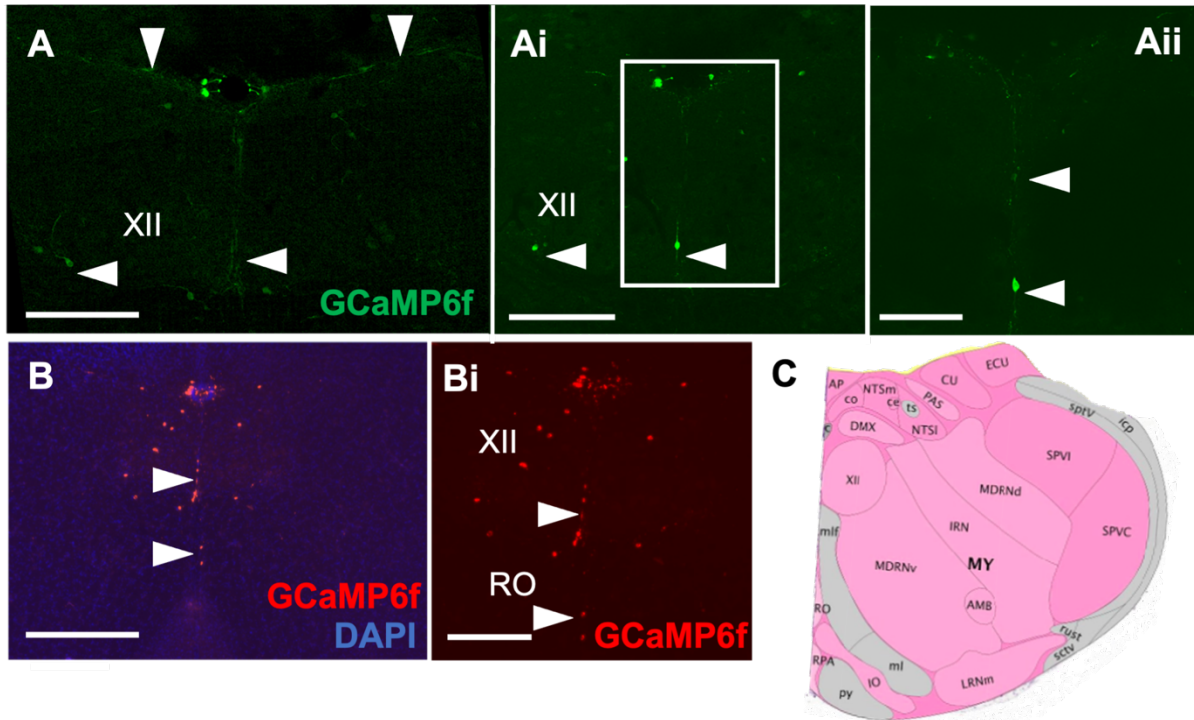


Figure 18: Axonal projections across transverse brainstem sections. (A-Aii) GCaMP6f+ (green) CSFcCs extend laterally away from the CC (white arrows) and ventrally down the midline. (Ai) In a different focal plane a somata is clearly located in the hypoglossal nucleus (XII). (Aii) Magnifying the region boxed (Ai) the axons seem to cluster along the midline of the two XII and the cell body is apparent (white arrow). (B) Lower magnification overview of a transverse section GCaMP6f enhanced using TSA (red) showing cells across various regions of this section, DAPI (blue) included to assist in defining the regions of the section. (Bi) without DAPI to highlight the cells which appear to be within XII and raphe obscurus (RO) (white arrows). (C) Reference atlas used to define regions of the brainstem. Scales; A = 200 μ m, Ai = 100 μ m, Aii = 100 μ m. B = 400 μ m. Captured using transmitted light microscopy.

Following this, the GCaMP6f signal was enhanced with anti-GFP using the DAB staining (Figure 19) method discussed previously, as it improved axonal labelling. This helped define some of the regions CSFcCs appear to project to, including the nucleus of Staderini (Figure 19 Biii).

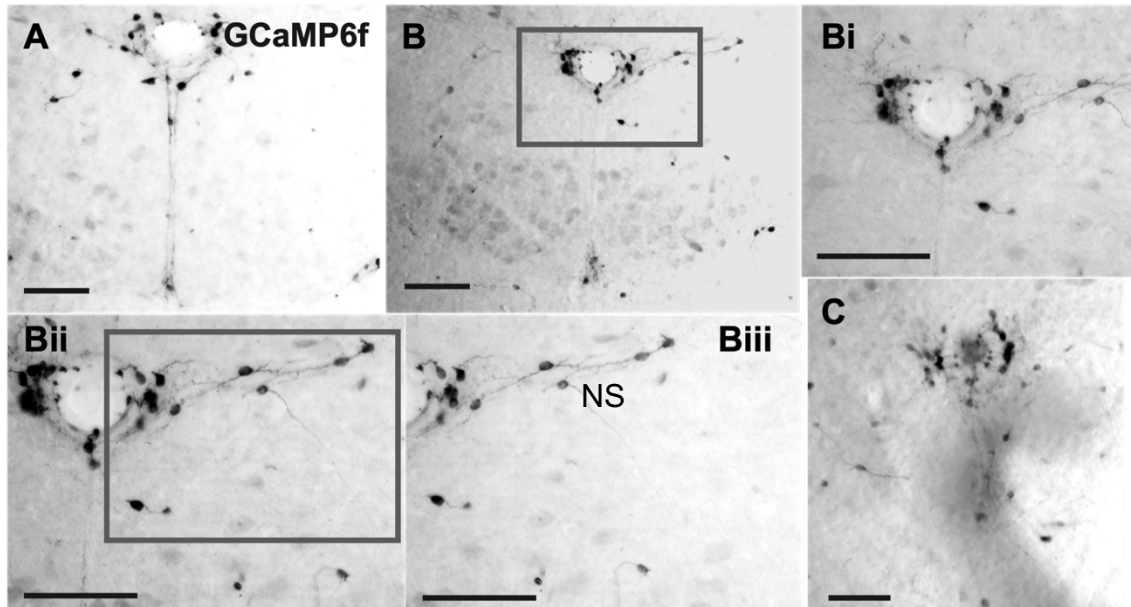


Figure 19: DAB staining of axons in brainstem nuclei. DAB staining to highlight the axonal labelling first observed when characterising GCaMP6f expression in PKD2L1:GCaMP6f mice. (A-B) In the lower magnification images there are extensive axonal projections from CSFcCs in various directions from around the CC region. (Bi) Magnified image of boxed region (B) shows axons and cells ventral and lateral to the CC. (Biii) These projections appear to terminate in different regions of the brainstem including the nucleus of Staderini (NS) shown in a higher magnification image from the boxed region (Bii). (NS). (C) In a more rostral brainstem section there are somata distributed in multiple regions away from the CC. All scale bars = 100 μm . Captured using transmitted light microscopy.

Kidney

Tissue from the kidneys of these transgenic mice was first embedded in gelatin, then sectioned at 50 μm before incubating with both PKD2L1 and GFP antibodies. This was due to high expression of PKD2L1 within the kidneys, a defect in which results in worsened kidney function in mice (Nomura *et al.*, 1998). Immunofluorescent labelling was observed across the entire sections (Figure 20 A, B). At higher magnifications (Figure 20 C-Cii, D-Dii, E-Eii) the labelling was clearly restricted to the outer edges of cells. This reflects PKD2L1 expression within the tubules of the kidney (Berglund *et al.*, 2008, Protein atlas).

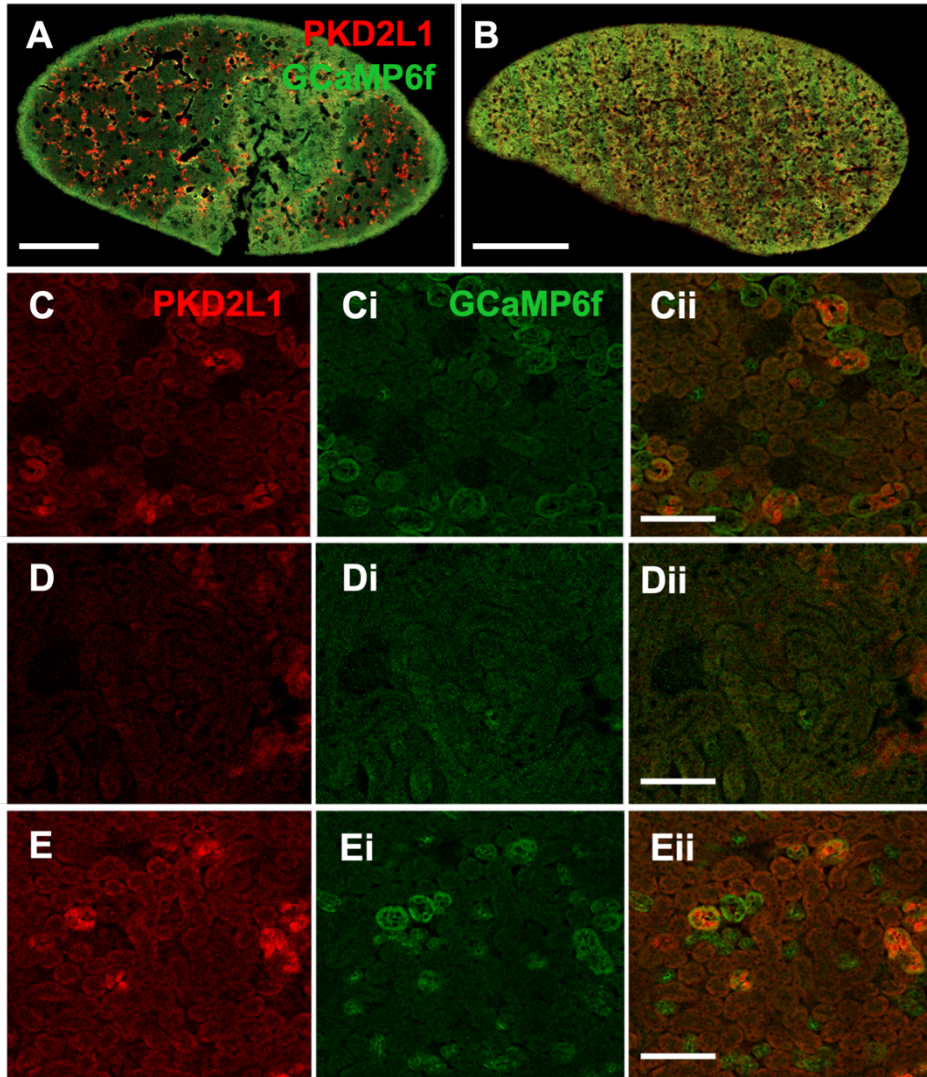


Figure 20: *GCaMP6f* expression in kidney tubules. (A-B) The expression varied between sections and is diffuse across the entirety of the section, notably expression appears at the edges of the cells (E-Eii) reflecting expression in the tubules. Scale bars, A = 1000 μ m, B = 1500 μ m, Cii, Dii, Eii = 100 μ m. Captured using transmitted light microscopy.

2.4.3. Double labelling of CSFcCs infers novel properties

Most PKD2L1+ CSFcCs express VGAT

From VGAT:GCaMP6f mice, tissue was sectioned in a transverse plane and incubated with anti-PKD2L1 and anti-GFP (Table 3). This revealed labelling of CSFcCs with both antibodies (Figure 21 A-Aii, white arrows) in the somata of CSFcCs and the bulbs terminating in the CSF. This supports previous suggestions that CSFcCs are GABAergic (Stoeckel *et al.*, 2003, Fidelin *et al.*, 2015) as they express VGAT, a protein implicated in the transport of GABA into vesicles, although this doesn't show CSFcCs release GABA from their terminals. As expected, GCaMP6f, which is not fused to the VGAT protein but expressed only under control of its promoter, was significantly localised to the cell cytoplasm.

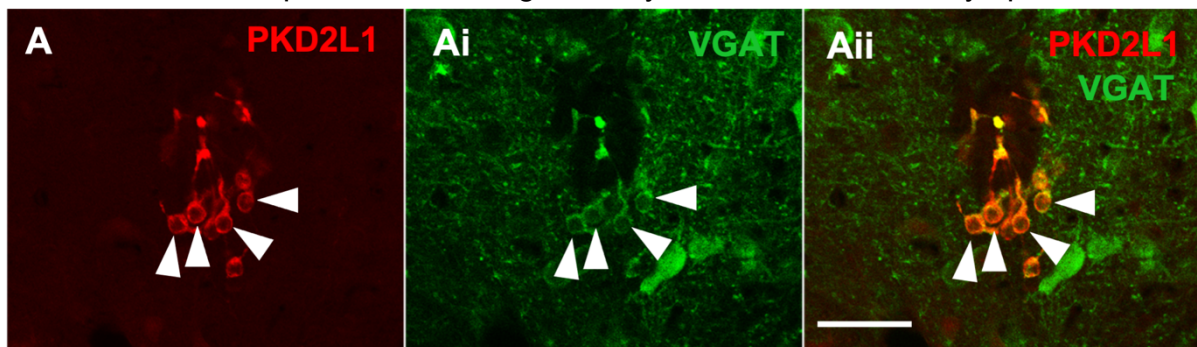


Figure 21: PKD2L1 co-localises with VGAT:GCaMP6f+ CSFcCs. (A-Aii) Around the CC, a large proportion of the PKD2L1+ (red) CSFcCs are also VGAT:GCaMP6f+ (green). There is also extensive GCaMP6f expression outside of the CC region. Scale bar Aii = 50 μ m. Captured using confocal microscopy.

CSFcCs express protein required for exocytosis

When labelling transverse sections from VGAT:GCaMP6f mice with PKD2L1 and SV2, the terminals of CSFcCs within the CSF were immunopositive for both antibodies (Figure 22 A-Aii). This shows CSFcCs have some of the apparatus required for the release of vesicles from their terminals, supporting their previously discussed neuronal-like properties.

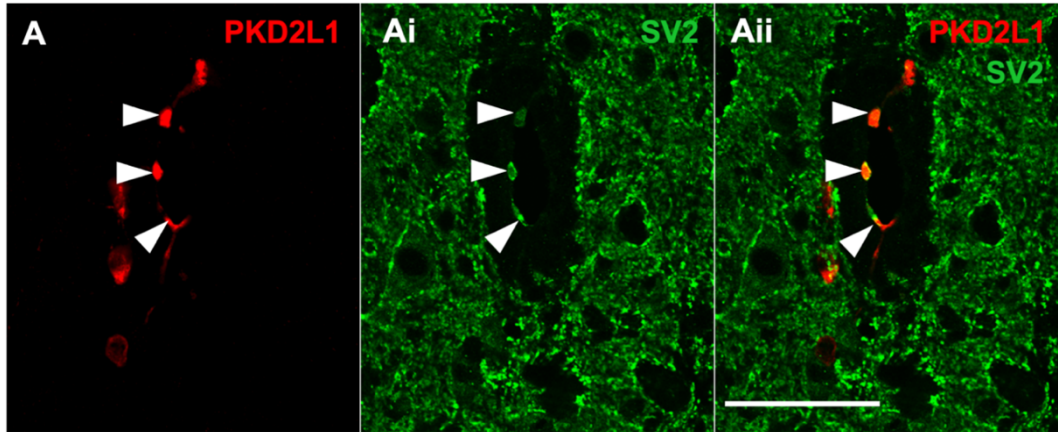


Figure 22: CSFfC terminals express SV2. (A) PKD2L1+ (red) bulbs of CSFfCs seen in the CC region co-localise with SV2 (green) (Ai) as highlighted with arrows. SV2 is a protein involved in the release of vesicles from synapses. Scale bar = 50 μm . Captured using confocal microscopy.

CSFfCs express GLP1R

If CSFfCs are behaving as neurones, they likely require inputs. One receptor possibly expressed on these cells is the GLP1R (Figure 2). This was demonstrated using antibody labelling in PKD2L1:GCaMP6f spinal cord sections. Figure 23 Aii shows CSFfCs were immunopositive for GLP1R and PKD2L1 (white arrows) with all of the CSFfCs in this focal plane double labelled, confirming the expression of GLP1Rs on CSFfCs.

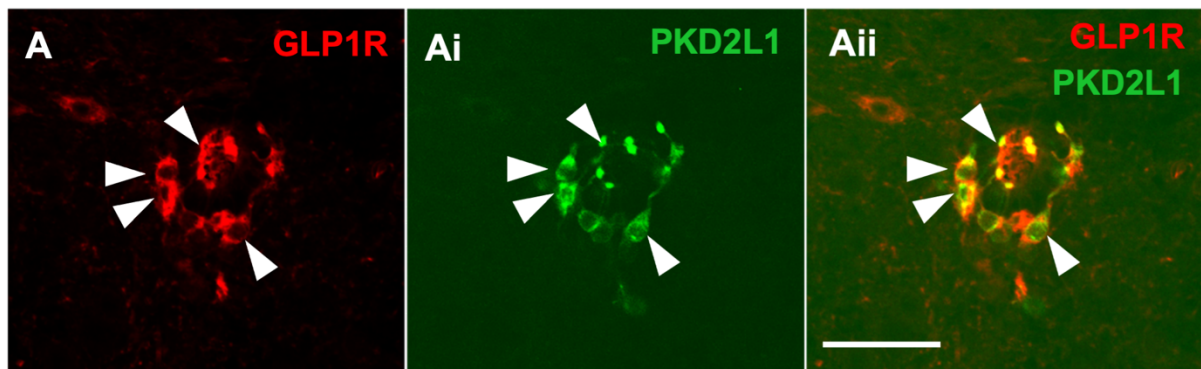


Figure 23: CSFfCs express the GLP1R. (Ai) The CSFfC cell bodies within the CC region labelled with PKD2L1 (green) co-localise with GLP1R (red) (A). This is also seen within the terminals in the CC. Scale Aii = 50 μm . Captured using confocal microscopy.

In other sections from PKD2L1:GCaMP6f tissue, the GFP fluorescence was enhanced in sections also labelled with GLP1R (Figure 24 A-Bii). This also showed CSFfCs to express GLP1R (Figure 24 Aii and 24 Bii, white arrows). This overlapping staining was seen in the somata distributed around the CC and within the bulbs observed in the CSF. To quantify the proportion of CSFfCs expressing GLP1Rs, counts were conducted of the number of PKD2L1+ CSFfCs, then the proportion of which were GLP1R+. This was then compared in comparative sections with the proportion of GCaMP6f+ CSFfCs that were GLP1R+ (Figure

24 C). The counts revealed over 80% of CSFcCs labelled with GCaMP6f also stained with GLP1R. Counts in GCaMP6f tissue, mean of N = 3 mice, 20, 15, 14 sections counted from each animal respectively from all regions of the cord. Mean calculated from counts using PKD2L1 and GLP1R N = 2 mice, 15 and 24 sections counted from each with sections from every region which showed around 65% of CSFcCs were GLP1R+. This difference is likely to be due to the level of the labelling with each antibody within the tissue, the stains label the same cells in different focal planes. With GCaMP6f and GLP1R it was easier to define double labelled cells, reflected in the greater proportion of cells double labelled.

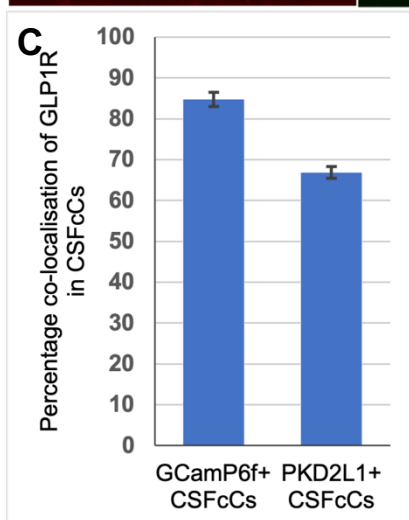
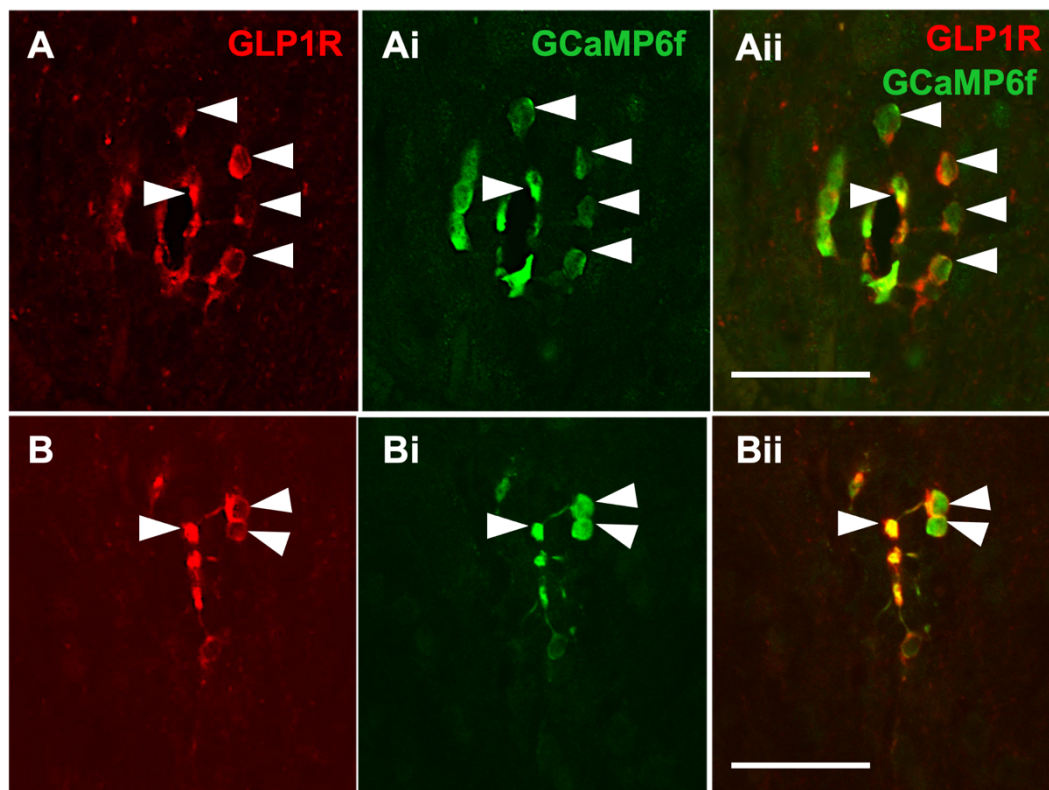


Figure 24: High GLP1R expression in CSFcCs. (A-Aii) Cervical spinal cord section shows CSFcCs labelled with GCaMP6f and GLP1R (white arrows). (B-Bii) Transverse section from the thoracic region with CSFcC somata and bulbs immunopositive for GLP1R and GCaMP6f. (C) Graph displaying the percentage of CSFcCs GLP1R+. These counts are from 50 μ m transverse sections PKD2L1:GCaMP6f tissue where the CSFcCs were visualised in two distinct ways; with anti-GFP and anti-PKD2L1. Bars represent standard error of the mean (SEM). All scale bars 50 μ m. Captured using confocal microscopy.

Early neuronal marker in CSFcCs

In PKD2L1:GCaMP6f tissue, Hu C/D was used to label neurones at an early stage of maturation (Akamatsu *et al.*, 2005) (Figure 25 A) labelling lots of cells across the grey matter. These sections were also incubated with anti-GFP to enhance the signal from GCaMP6f within CSFcCs (Figure 25 Aii) This shows the GCaMP6f+ CSFcCs also express Hu C/D (Figure 25 Bii, white arrows). This image was captured in a single optical section resulting in fewer CSFcCs imaged than seen in previous transverse sections which were images taking in multiple planes of focus.

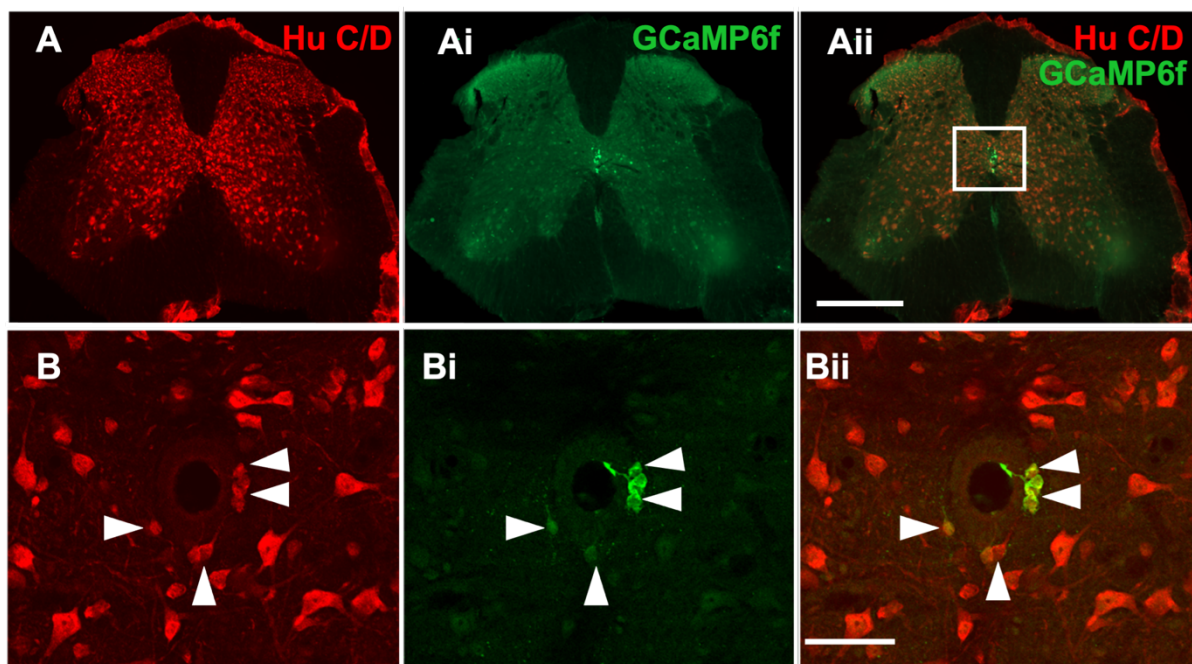


Figure 25: CSFcCs express neuronal marker Hu C/D. (A) Hu C/D+ neurones exist across the grey matter of the transverse lumbar section. (Ai) This shows the GCaMP6f+ (green) CSFcCs around the CC region. (B-Bii) Higher magnification confocal image of the boxed region (Aii) CSFcCs are double labelled with Hu C/D and GCaMP6f (white arrows). Aii = 500 μ m, Bii = 50 μ m. Captured using confocal microscopy.

EpCs and CSFcCs around the CC

To demonstrate the close apposition of EpCs with CSFcCs PKD2L1:GCaMP6f tissue was labelled with SOX2 (Figure 26 A, B), a marker of pluripotent stem cells found in EpCs (Zhang *et al.*, 2014). This shows there is no overlap between SOX2+ cells in the CC and GCaMP6f+ CSFcCs (Figure 26 Aii, Bii). However, CSFcCs are closely located to EpCs which does suggests these cells may be able to influence the environment around such cells.

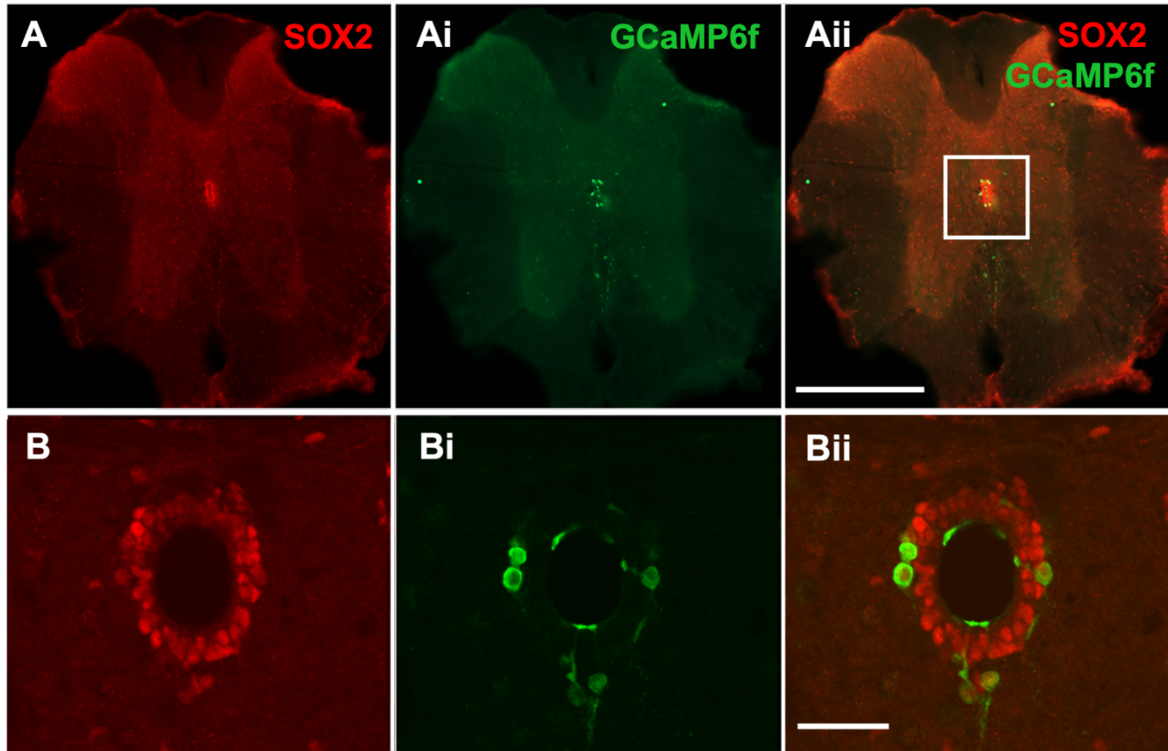


Figure 26: *Distribution of CSFcCs within ependymal zone.* (A) This shows a thoracic transverse section labelled with SOX2 (red) (B) GCaMP6f positive CSFcCs (Ai and Bi) (green). The ependymal cell layer contains many EpCs expressing SOX2, interlaced with CSFcCs (Bii), however there is no co-localisation between these. Scales Aii = 500 μ m, Bii = 50 μ m. Captured using confocal microscopy.

2.4.4. Viral tracing of CSFcC projections along ventral fissure

mCherry labelled CSFcC somata around CC and axons in VF

A floxed virus was injected into the lumbar region of the spinal cord. The virus expressed a fused Chr2-mCherry protein which permitted visualisation of where the axons projected to using anti-mCherry. In the lumbar transverse sections of cord taken from the injection site (Figure 27 A) it was only CSFcC cell bodies labelled. In lumbar sections adjacent to this region (Figure 27 B, C) there were still CSFcCs labelled around the CC, however there was additional labelling in the VF, indicative of axons from the cells at the injection site. When transverse sections from the thoracic region, rostral to the injection site, were stained there was no longer mCherry labelled cells around the CC, only VF labelling (Figure 27 D-E). This suggests CSFcCs in the lumbar region project rostrally, up the cord sending axons along the VF.

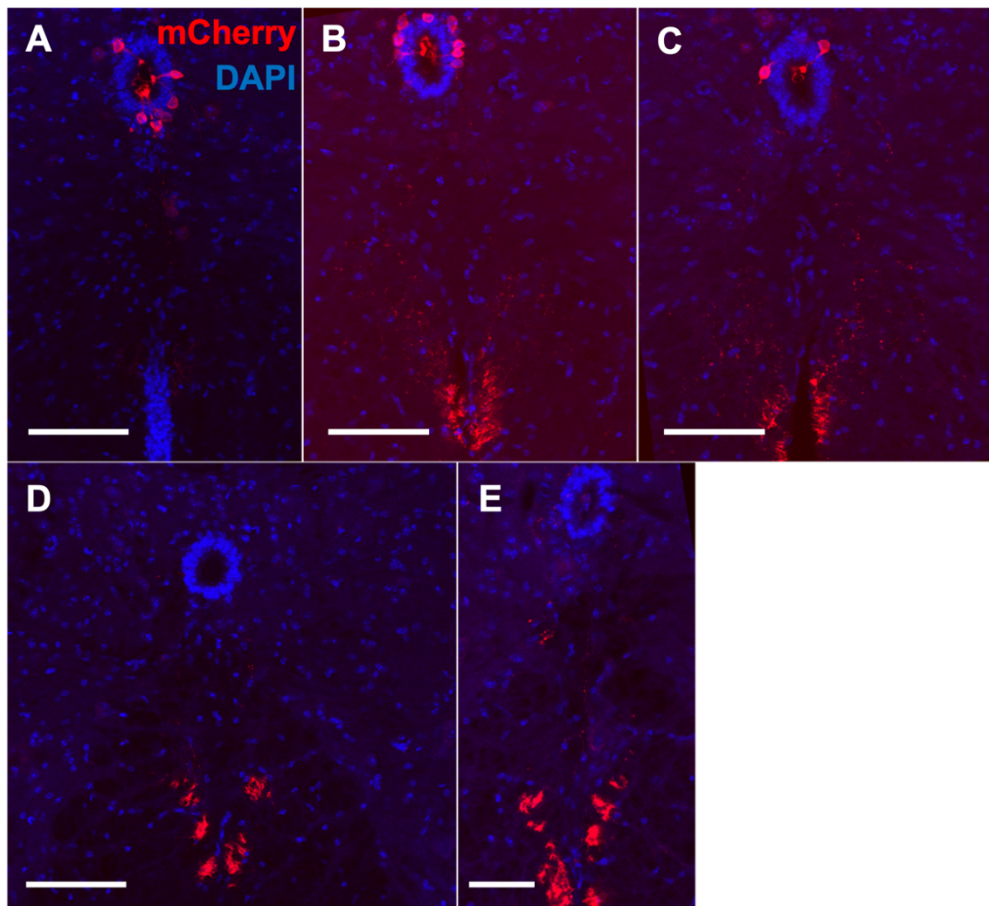


Figure 27: *mCherry expression reveals rostral axon projections from CSFcCs.* (A) At the injection site mCherry expression was limited to the cell bodies of CSFcCs, whereas in sections adjacent to the lesion site (B-C) mCherry is expressed both in CSFcC cell bodies around the CC, as well as in the ventral fissure (VF). (D-E) expression of mCherry in thoracic sections restricted to the VF. It is only the axons and no longer cell bodies, which suggests these are processes from the somata labelled in the lumbar sections. Scale bars, A-D = 100 μ m, E = 50 μ m. Captured using transmitted light microscopy.

Sections from another spinal cord injected as above, were cut in a sagittal plane after gelatin embedding. Figure 28 shows sections from the injection site within the lumbar region in which CSFcCs were labelled in around the CC. In the VF there are axons running along the spinal cord (white arrows) which have boutons, characteristic of axons. There are also cells between the CC and VF (white arrows) resembling what was previously seen with CSFcC labelling.

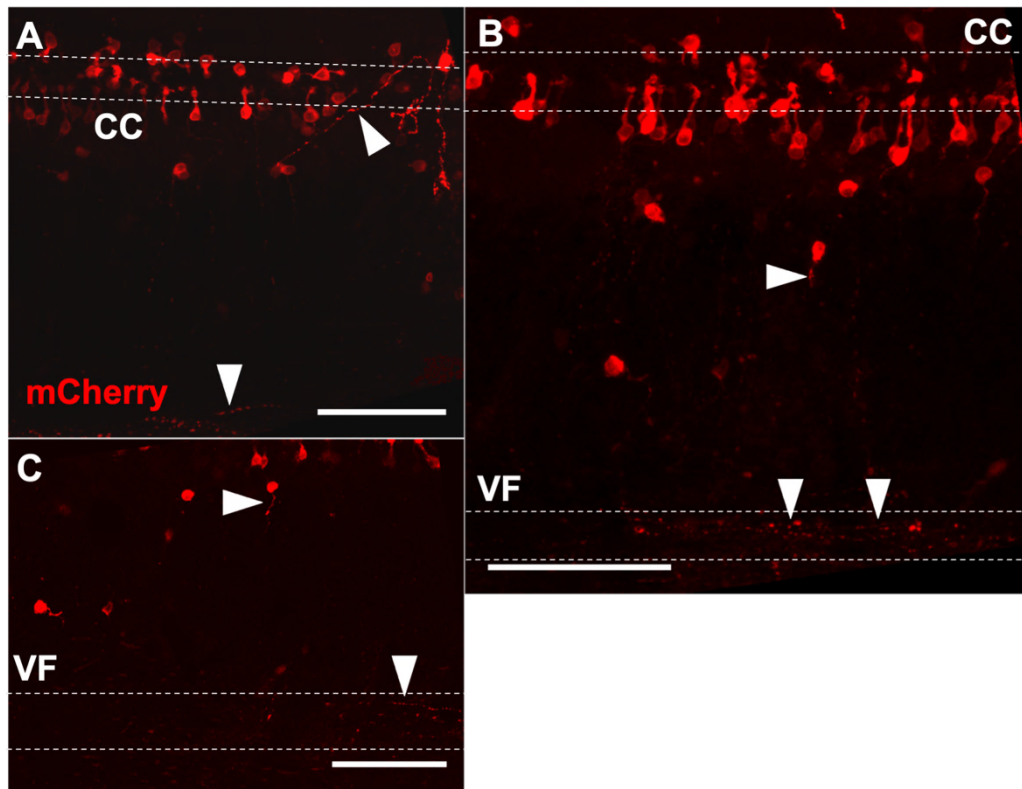


Figure 28: *mCherry* expression within CC and VF immediately below injection site. (A, B) sagittal sections representative of the injection site. At the injection site, cell bodies are labelled resembling CSFcCs. (C), the regions adjacent to the injection site are not labelled with CSFcCs. In the VF there are clear axonal projections with boutons, characteristic of axons highlighted with arrows. Scales A-C = 100 μ m. Captured using confocal microscopy. Due to the sagittal sectioning, the dotted lines provide an indication of where the CC runs, however there are no cell bodies within this region and those seen reflect the angle of cutting and Z stack compiled image which has distorted the CC region.

In the sagittal plane, sections away from the injection site in other spinal cord regions were checked for any mCherry+ labelling. This was seen in the sacral region, caudal to the lumbar injection site. Figure 29 A shows a long axon running along a sacral section, originating from a CSFcC in the lumbar region with distinctive boutons. Other sacral sections had labelling which appeared punctate (Figure 29 Bi, white arrows), as though axons are terminating onto cells. This mCherry+ labelling is less clearly defined, Figure 19 B is the same section labelled with DAPI to rule out autofluorescence as the source of the punctate labelling.

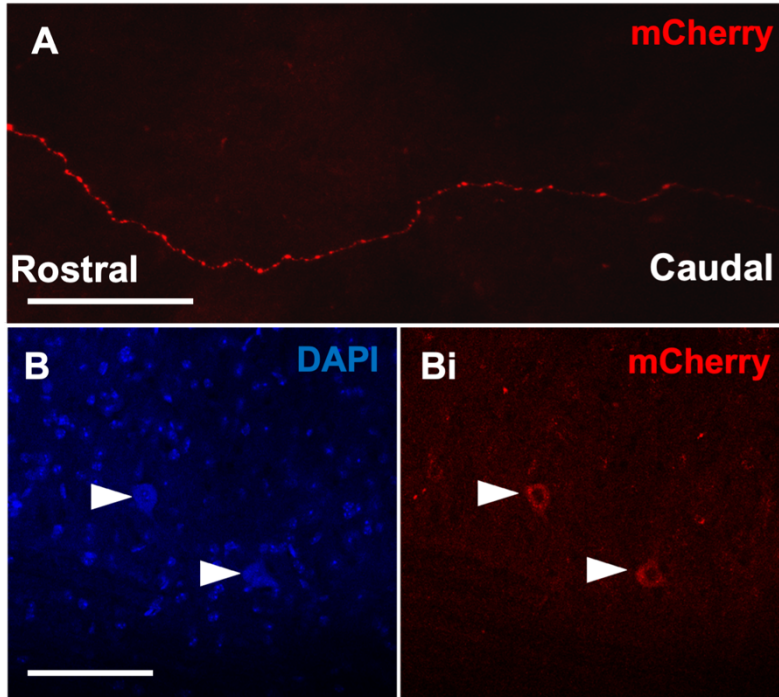


Figure 29: Axonal projections are observed in sacral sections, caudal to injection. (A) In the sections taken from the sacral region of cord, caudal to the sagittal lumbar sections, large axons were observed indicative of lumbar CSFcCs communicating with cells in regions lower down the cord. (B-Bi) There were also numerous circular areas of staining which appears punctate as if it may be terminals onto another cell within the sacral region. Scale A and B = 100 μ m. Captured using confocal microscopy.

2.5. Discussion

2.5.1. CSFcCs can be clearly and selectively visualised using antibodies for PKD2L1

The indirect antibody method first used to visualise CSFcCs revealed their typical morphology and distribution. PKD2L1+ CSFcCs were consistently detected around the CC with each staining technique used. There is also some less clearly defined labelling in the VF however it was the latter staining methods, amplifying the signal, which showed axonal projections between the CC and the VF. Notably, there are cells from around the CC extending axons in the direction of the VF as well as cells located in the VF itself. These cells also extend axons in multiple different directions, best shown with the TSA enhanced antibody staining. This suggests that CSFcCs send information and project within at least one spinal cord level and are communicating with other cells. In line with the literature discussed (Strachan *et al.*, 2004, Fahimi and Herzog, 1973, Faget and Hnasko, 2015, Hunyady *et al.*, 1996, Chao *et al.*, 1996), using qualitative analysis, CARD and enzyme linked signal amplification methods increased the overall fluorescent signal detected which is apparent at lower magnifications. Significantly, the axon labelling was greatly enhanced using TSA and DAB labelling, which are best for labelling molecules expressed at low abundance, suggesting there is less PKD2L1 expressed in the axons of CSFcCs compared to expression in the soma, therefore the signal from the primary antibody binding in these regions required amplification. The axonal labelling and VF staining observed here is underreported in previous studies of these cells (Stoeckel *et al.*, 2003) potentially offering greater insight into functional roles.

Another region with consistently high fluorescence is the bulbs of the apical extensions projecting from CSFcCs around the CC into the CSF. This suggests high PKD2L1 expression in this region of the cells. These terminals are ciliated, which was the initial indicator of these cells having sensory functions (Kolmer, 1921, Agdhur, 1922, Dale *et al.*, 1987). Nauli *et al.* (2016) report the localisation of PKD2L channel subtypes to primary cilia. Similarly, DeCaen *et al.* (2013) show cilia to be specialised calcium compartments regulated by PKD2L1 channels with a measurable outward current when expressed in HEK-293 cells. This supports the observation of high PKD2L1 antibody labelling within the ciliated region of the CSFcC.

2.5.2. CSFcC distribution in PKD2L1:GCaMP6f mice

Firstly, when labelling the tissue from the PKD2L1:GCaMP6f mice, it was essential to verify the phenotype was such that GCaMP6f was solely expressed in PKD2L1+ cells. The tissue was incubated with anti-PKD2L1 to label CSFcCs, alongside anti-GFP to enhance the GCaMP6f fluorescence signal. This resulted in clear co-localisation between these two antibodies within CSFcCs, verifying the transgenic mouse line in which GCaMP6f is exclusively expressed in PKD2L1+ cells, thus CSFcCs.

Following this, GCaMP6f expression within these mice was used to describe CSFcC distribution along the rostral caudal axis and in the brain and brainstem. Labelling was also observed in the kidneys as a control region in which high expression of the receptor was expected (Nomura *et al.*, 1998).

In transverse spinal cord sections, expression of GCaMP6f in cells was representative of the typical morphology and distribution of CSFcCs. All GCaMP6f+ cells around the CC were also PKD2L1+. This labelling was observed at all levels of the spinal cord – cervical, thoracic, lumbar and sacral. As seen within the previous immunohistochemistry staining methods, there are apparent CSFcCs and axonal processes outside of the CC towards the VF region, once again raising the question as to their function here. Within this region they are likely no longer sensing CSF flow (Orts-Del'Immagine *et al.*, 2020), changes in pH (Huang *et al.*, 2006, Orts-Del'Immagine *et al.*, 2012, Jalalvand *et al.*, 2016) or osmolarity, their previously defined functions. This subsequently requires further investigations continued in later chapters.

Sectioning tissue in a sagittal plane permitted visualisation of the axons running along the VF. There are numerous cell bodies outside of the CC region positioned between the CC and the VF, along the midline, with axons running along the VF – rostral or caudal, as seen in sagittal sections, and across the cord – dorsal and ventral, seen in a singular transverse plane. This suggests CSFcCs have widespread circuitry and heterogeneous functions, raising the question of where the axons project to and what cells they terminate on. Sectioning in this plane also reiterates the consistency of CSFcC expression throughout the whole cord, indeed in long sections of cord there are no breaks in CSFcC expression around the CC, emphasising the importance of their role throughout the whole spinal cord.

GCaMP6f expression in the brainstem revealed profound and extensive CSFcC labelling around the CC with axonal projections extending across the brainstem sections. The extensive labelling and fine axons observed in this region through fluorescence labelling led to the use of TSA and DAB staining methods, in order to increase the visualisation, as seen previously. When comparing representative sections labelled with GCaMP6f, with the reference atlas (Allen brain atlas, 2008) projections appear to extend towards the nucleus raphe obscurus and hypoglossal nucleus. The hypoglossal nucleus is involved in control of the tongue and patency of upper airways and so participates in control of breathing and swallowing, the raphe obscurus contains serotonergic neurones with widespread projections and is implicated in many modulatory functions, including influencing motor and sensory function (Basinger and Hogg, 2021). It also appears that projections extend to the nucleus of Staderini, indicating possible novel functional roles. The nucleus of Staderini refers to neurones within the medulla oblongata (Cascella, 2016) a region first described by Staderini in 1984. This region has a suggested role in nystagmus, involuntary eye movements and the movement of the eyes in relation to body movements. This may link to movements of the upper cervical region within the neck being relayed to the brain, similar to their previously discussed roles in detecting and responding to spinal movements (Wyart *et al.* 2009, Bohm *et al.*, 2016, Fidelin *et al.*, 2015).

There were no CSFcCs located within any brain regions, from the opening of the CC into the 4th ventricle to the very front of the brain in the olfactory bulb. This concluded that CSFcCs within the CNS have restricted expression around the CC of the whole CNS from the brainstem to the most caudal, sacral spinal cord. Furthermore, the labelling of cells and axons outside of this region towards the VF suggests novel circuitry running along the length of the cord.

The kidneys were sectioned as a control region of tissue in which high GCaMP6f expression was expected due to the important role of PKD2L1 receptors in this region (Nomura *et al.*, 1998). GCaMP6f+ cells were seen across the entirety of sagittal kidney sections. At higher magnifications it was apparent that staining lined the edges of cells, reflecting the expression of this receptor in kidney tubules (Berglund *et al.*, 2008, Protein atlas).

2.5.3. Antibody labelling for other markers in PKD2L1+ CSFcCs

The markers expressed in CSFcCs, overlapping with PKD2L1+ cells, suggests further properties that may contribute to their function. There was clear labelling of PKD2L1+

CSFccs with GCaMP6f around the CC, reflecting VGAT expression. VGAT is a neurotransmitter transporter responsible for the movement of GABA from the cytoplasm, post synthesis, to the terminal (McIntire *et al.*, 1997). Although this doesn't show that CSFccs release GABA, this evidence coupled with previous evidence that such cells are GABAergic (Marichal *et al.* 2009, Orts-Del'Imagine *et al.*, 2012) indicates CSFccs may have the ability to release GABA. This contributes to the hypothesis in which CSFccs secrete both GABA and peptides that may influence surrounding cells such as EpCs, since these are shown using RNA-seq to possess GABA receptors (Rosenberg *et al.*, 2016) and respond to GABA applications in slices (Corns *et al.*, 2013). It also suggests they may be able to communicate with other cells when coupled with their extensive axonal network seen previously.

CSFcc terminal projections into the CSF labelled with both PKD2L1 and SV2. This reveals that CSFccs possess some components required for the release of vesicles from the synapse (Feany *et al.*, 1992), including the release of GABA (Marichal *et al.* 2009, Orts-Del'Imagine *et al.*, 2012, Stoeckel *et al.*, 2003). This also supports the suggestion by Prendergast *et al.* (2019) that CSFccs contain peptides that may be released during an immune response. Anything released from these terminals into the CSF would affect the microenvironment, which is essential in maintaining the proliferative state of EpCs.

In line with findings by Marichal *et al.* (2009), CSFccs co-localise with Hu C/D, an early neuronal marker, however not all GCaMP6f expressing CSFccs around the CC were labelled with Hu C/D supporting previous findings (Jalalvand *et al.*, 2014) that they are a heterogeneous cell population with some neuronal properties (Marichal *et al.*, 2008, Jalalvand *et al.*, 2014, Fidelin *et al.*, 2015). Neurones require a means of transmitting signals, which links to the presence of SV2, a synaptic vesicle protein, in their terminals.

From the labelling of EpCs with SOX2 and labelling of CSFccs with GCaMP6f in the transgenic mice, the primary cell types in the CC, EpCs and CSFccs are clearly two distinct, non-overlapping cell populations within the spinal cord. However, they very closely appose each other and thus, we can hypothesise that they may influence the functions of one another.

As discussed in the introduction, there is preliminary evidence that CSFccs express the GLP1R (Allen brain atlas, 2008, Ghazale *et al.*, 2019) and these data also suggests this with GLP1R+ labelling in the majority of PKD2L1+ CSFccs. This is also shown with double

labelling of CSFcCs with GCaMP6f and GLP1R. To quantify the proportion of GLP1R CSFcCs, counts of the number of CSFcCs around the CC of a 50 μm transverse section were conducted followed by counts of the number of CSFcCs that were also GLP1R+. This was carried out with both PKD2L1 antibody staining and GCaMP6f labelling of CSFcCs. The outcome is that the majority of CSFcCs possess GLP1Rs, with over 80% of CSFcCs labelled with GCaMP6f also labelled with GLP1R, supporting the preliminary evidence. The slightly lower proportion of CSFcCs labelled with PKD2L1 colocalised with GLP1R is likely due to differences in the level to which each antibody reaches within the tissue. Demonstrating the presence of these receptors on such a large proportion of CSFcCs, provides a possible target for stimulating CSFcCs. The complex second messenger cascades associated with GLP1R activation (Carlessi *et al.*, 2017) may affect CSFcC activity and provide a means of manipulating CSFcCs.

2.5.4. Projections from PKD2L1+ CSFcCs along ventral fissure

After verifying the transgenic mouse line and characterising CSFcCs, viral tracing methods were used to examine their projection patterns. After locating the injection site within transverse lumbar sections mCherry+ staining was observed in the VF. This aligns with the previous observations of PKD2L1+ staining in this region, affirming the idea that there are axons travelling along the VF from CSFcCs around the CC. In the transverse sections, labelling was observed of somas and VF axons in the lumbar regions, and VF labelling in thoracic sections. This suggests projections from caudal to rostral spinal cord regions. Axonal labelling was observed in lumbar regions adjacent to the injection site in both directions.

The sagittal sections clearly displayed axons, containing varicosities, running along the VF region below the injection site. There are also apparent cell bodies in the region between the CC and the VF. Since the virus was injected into the CC, this indicates these cells have projections into the CC and out into the VF. The sacral sections cut in a sagittal plane from this spinal cord show long axons spanning the length of the sections. This differs from the observations of the transverse sections, showing projections from the lumbar spinal cord in a caudal direction. Thus, there may be different cells projecting in opposing directions and the extent of the projections for CSFcCs is running the length of the cord. In the sacral cord there is also punctate staining that appears to surround cell bodies. These cells are likely to be the projection targets of CSFcCs. Morphologically, they resemble CSFcCs however this would need to be defined with double labelling. Due to freeze-thawing of the cold room in

which the tissue was stored, I was unable to double stain the third spinal cord virally injected to confirm this.

There was no mCherry labelling seen in the brain or brainstem of these animals. This suggests that CSFcCs in the lumbar region do not project the entire length of the cord, it is perhaps the CSFcCs higher up the cord communicating with these regions. Further experiments including viral injections into various other spinal cord regions and labelling with other cell markers to define where CSFcCs project to are required to investigate further the CSFcC circuitry. Based on literature in zebrafish, and the similar morphology observed within these experiments, it may be that CSFcCs project onto motor neurones (Hubbard *et al.*, 2016), or interneurones (Fidelin *et al.*, 2015) in response to different types of movement. This relates to their ability to sense CSF flow (Orts-Del'Immagine *et al.*, 2020) and relay information regarding the direction of spinal curvature. All of which would implicate CSFcCs in sensory motor circuits. This may be related to the tracts shown to run close to the VF region, rostral reticulospinal tract and lateral vestibulospinal tract (Watson and Harrison, 2012), which control posture, sensory circuits and motor activity in preparation for movement (Peterson *et al.*, 1975, Iwamoto and Sasaki, 1990, Drew *et al.*, 2004) and motor functions and eye movements (Cullen, 2016) respectively.

2.5.5. Conclusions

In conclusion, the experiments conducted within this chapter verified the expression of GCaMP6f within PKD2L1+ CSFcCs in the newly produced transgenic mouse line and revealed some possible properties of CSFcCs inferred from antibody labelling of markers associated with vesicular loading and release of vesicles. The expression of GLP1Rs within CSFcCs may provide a novel input which could be targeted to manipulate these cells, something which will be explored in the next chapter.

Expression of PKD2L1+ CSFcCs in various brainstem nuclei was also observed suggesting further possible properties relating to the control of neck and eye movements.

Viral tracing methods revealed some CSFcCs within the lumbar regions project at least one region along the spinal cord in either direction – rostral and caudal. This suggests they are part of a wider circuit, potentially motor and sensory circuits similarly to what is reported in zebrafish larvae.

Chapter 3: Does manipulation of CSFcCs influence EpC proliferation?

3.1. Introduction

CSFcCs have been repeatedly described as neurones (Marichal *et al.*, 2009, Stoeckel *et al.*, 2003, Orts-Del'Imagine *et al.*, 2012, 2016, Fidelin *et al.*, 2015) displaying electrophysiological responses to neurotransmitters (Marichal *et al.*, 2009, Orts-Del'Imagine *et al.*, 2012, Corns *et al.*, 2015) and labelling with markers of neurones at different stages of maturation (Marichal *et al.*, 2009).

Neurones output signals to transmit information, following an input, which stimulates such a response. The presence of GLP1Rs on CSFcCs offers a novel input to these cells which may be utilised to elicit a response. GLP1Rs are G-Protein coupled receptors with complex second messenger cascades resulting in a significant intracellular response upon activation. GLP1R agonists have been shown to increase levels of intracellular cAMP (Thorens *et al.*, 1993) as well as other signalling pathways including phospholipase C activation and increased levels of intracellular calcium (Wheeler *et al.*, 1993). These intracellular changes will influence the activity of the cell that could subsequently influence surrounding cells.

GLP1R activation has been shown to control exocytosis via the release of vesicles containing signalling peptides from chromaffin cells of the adrenal gland (González-Santana *et al.*, 2021). Exendin-4, a GLP1 analogue caused a significant increase in the expression of adrenal catecholamines and the enzyme responsible for their synthesis, tyrosine hydroxylase, within cultured chromaffin cells after 24-hour exposure. This effect resulted from increases in protein kinase A and cAMP following GLP1R activation.

Considering CSFcCs exhibit neuronal behaviours, they may output signals in order to transmit information within a circuit. The evidence so far regarding peptides released by CSFcCs includes the labelling of CSFcCs with GAD, the enzyme responsible for production of GABA (Fidelin *et al.*, 2015), immunocytochemical localisation of GABA within P2X2+ CSFcCs (Stoeckel *et al.*, 2003) and the presence of mRNA for various anti-inflammatory peptides within CSFcCs linking to their possible role in response to infection of the spinal cord (Prendergaast *et al.*, 2019). Additionally, I have shown CSFcCs express SV2 in their terminals, a protein involved in the release of vesicles from the synapse, and VGAT, a protein implicated in loading of GABA into vesicles, further indicating their possible ability to release signalling molecules from the synapse. Attempts to harness these properties of CSFcCs will be explored in this chapter.

Local cell types surrounding the CC may be influenced by the outputs of CSFcCs. CSFcCs are interlaced among EpCs. EpCs extensively proliferate *in vitro* when isolated from the spinal cord and cultured (Weiss *et al.*, 1996, Johansson *et al.*, 1999, Martens *et al.*, 2002). They also express markers of NSCs (Alfaro-Cervello *et al.*, 2012), and have been shown to proliferate at baseline within the spinal cord (Johansson *et al.*, 1999, Horner *et al.*, 2000, Hamilton *et al.*, 2009), despite this occurring at a quiescent rate. They have also been suggested to differentiate into each primary cell type present within the spinal cord; astrocytes, oligodendrocytes and neurones *in vitro* from cell cultures (Weiss *et al.*, 1996). EpC activity is significantly influenced by environmental changes. An example of this is the increase in EpC proliferation in response to SCI (Meletis *et al.*, 2008, Moreno-Manzano *et al.*, 2009, Ren *et al.*, 2017). In these instances there are catastrophic changes to the environment EpCs reside within; physical stress (Dumont *et al.*, 2001), vascular damage, neurotoxicity, ionic changes, inflammation and many other mechanisms contributing to the secondary insult (Alizadeh *et al.*, 2019) which may all contribute to the increased proliferative capacity of EpCs.

EpCs express GABA receptors (Rosenberg *et al.*, 2018) and in spinal cord slices depolarise in response to bath applied GABA (Corns *et al.*, 2013). Since GABA is present in CSFcCs (Stoeckel *et al.*, 2003) this offers a possible mechanism by which CSFcCs can influence the activity of EpCs. Liu *et al.* (2005) show activation of GABA_A receptors on neural stem cells within the SVZ limited progression through the cell cycle and reduced the number of BrdU cells in hemisected brain slices, highlighting that GABA is able to influence the proliferation of neural stem cells. This effect may be seen in EpCs. Based on this information, this chapter will aim to activate or damage CSFcCs to determine if this can influence the proliferation of EpCs.

As previously discussed, tissue or cell specific expression of proteins is possible within transgenic mice where cre is expressed under the promoter of a specific gene. In the previous chapter, the PKD2L1:GCaMP6f mouse line was validated. In this chapter, this is utilised in the specific targeting of PKD2L1+ cells. Here an adenoassociated virus (AAV) was used to terminally injure CSFcCs. This AAV is taken up by all cells surrounding the injection site and expresses mCherry in all non-cre expressing cells. When cre recombinase is present in cells (in this case PKD2L1+ CSFcCs) the virus stops expressing mCherry and instead expresses diphtheria toxin A subunit.

Diphtheria toxin subunit A (DTA) causes apoptosis of the cell target of pathogenic strains of *Corynebacterium diphtheriae* (reviewed by Collier, 1975), therefore viruses modified to express DTA can be used to kill cells of interest.

3.2. Hypothesis and Aims

The exogenous activation of GLP1Rs within the spinal cord through the drug treatment with a GLP1 analogue, Liraglutide, will influence EpC proliferation via CSFcCs. This results from activation of the second messenger cascade associated with GLP1R. A subsequent change in the microenvironment around the CC and of the CSF composition may alter the rate of EpC proliferation, since their proliferative rate is influenced by their environment (Meletis *et al.*, 2008, Moore *et al.*, 2016). They have also been shown to express GABA receptors (Rosenberg *et al.*, 2018), which could respond to GABA released from CSFcCs (Stoeckel *et al.*, 2003, Fidelin *et al.*, 2015, Jalalvand *et al.*, 2016). GABA dampens the proliferation of NSCs within the SVZ, hence a similar effect is anticipated here from proliferating EpCs. This will be assessed by injecting Liraglutide intraperitoneally into mice, simultaneously with 5-ethynyl-2'-deoxyuridine (EdU) a thymidine analogue which is incorporated into the DNA of proliferating cells, similarly to BrdU. Counts of the number of EdU labelled proliferating cells around the CC and in other spinal cord regions in both control and test groups will indicate whether the GLP1 agonist has an effect.

If the CSFcCs influence EpC proliferation, then removal of them should affect EdU labelling. Injection of a virus which expresses diphtheria toxin (DTA) selectively in cre expressing cells, within a PKD2L1-IRES-Cre mouse, will injure or kill PKD2L1+ CSFcCs. If CSFcCs release peptides or neurotransmitters from their terminal, death of these cells is likely to influence the microenvironment of the CC. In turn this could affect EpC proliferation, survival or activity. Additionally, if they release GABA from their bulbs into the CSF, close to EpCs, there is likely to be an increase in proliferation in the absence of GABA. The opposite effect to what is expected upon stimulation of GLP1R receptors on CSFcCs causing an increase in GABA. As above, these mice will be injected with EdU which can be counted indicating the number of cells proliferating in the CC of a 50 µm section. This tissue will also be labelled with antibody markers of cell death and CSFcCs in order to analyse the success of DTA in killing cells and to observe any changes in CSFcC morphology or distribution.

3.3. Methods

3.3.1. Animals

Three phenotypes of mice were used in the following experiments. Wildtype (WT) C57Bl/6 female mice were used for the Liraglutide experiments. PKD2L1-IRES-Cre mice were used for preliminary viral injections to review injection site and regions of viral expression.

PKD2L1:GCaMP6f mice, validated in the previous chapter were used for the viral injections to target CSFcCs and as controls.

3.3.2. Liraglutide and EdU Injections

10 WT mice at 9 weeks of age were intraperitoneally injected every 24 hours for 5 days in the evening, between 4-6pm (Figure 30). 5 were injected with 10 mM EdU in 0.1 mL saline, as control. 5 animals were injected with 10 mM EdU and 1 μ g/kg Liraglutide (Novo Nordisk, UK) in 0.1 mL saline, test. After the final injections, the mice were left for 3 days before they were perfused as described previously (1.8.4.).

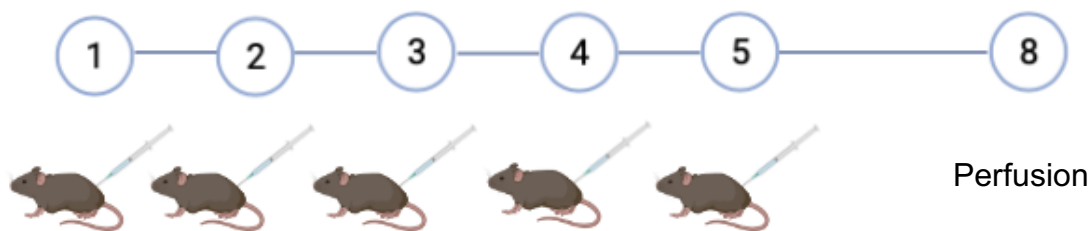


Figure 30: Liraglutide and/or EdU injection schedule. All mice were injected with EdU on days 1-5. They were left for 3 days before perfusion. 5 of the mice were simultaneously injected with Liraglutide.

3.3.3. Virus and Injections

AAV-EF1a-mCherry-flex-dtA - AAV2/retro (Canadian neurophotonics, #construct-387-aav2-retro), titre of $2E11$ vg, was used in this experiment. This virus expresses mCherry when taken up at the terminals of cells not expressing cre. However, when taken up by cre expressing cells, expression is switched to DTA, which has been shown to damage cells (Wu *et al.*, 2014). In the preliminary round of injections to review injection site and regions of viral expression, PKD2L1-IRES-Cre animals were used. In the second group, viral injections were conducted in PKD2L1:GCaMP6f mice (Table 6). In both groups, 3 test mice, at 6-weeks-old were given intraspinal injections (Figure 4) into the upper lumbar region. These

mice were left for 2 weeks, after which they were injected with EdU on 3 out of 8 days, followed by perfusion on day 8 (Figure 31). N = 3 control mice received no viral injections, but EdU injections were given at the same time as virally injected mice.

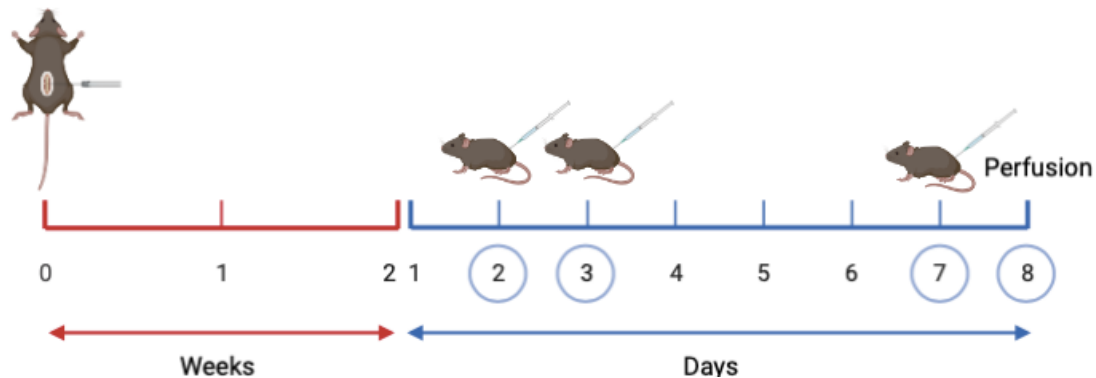


Figure 31: Virus and EdU injection timeline. 3 mice from preliminary group, 3 mice from experimental group injected with virus, detailed above, at 3 weeks. 2 weeks post viral injection, EdU injections began. EdU was administered on days 2, 3 and 7. Animals were perfused on day 8.

Tissue was also obtained from another experiment in which pAAV.hSyn-FLEX.iGABASnFR.F102G (addgene, 112164-AAV1) was injected as previously described (Figure 4) and left for 3 weeks before perfusion, referred to as GABASnfr throughout. This tissue was used as a control to assess any cell death caused by the injection of a virus.

3.3.4. Immunohistochemistry

To visualise the protein expressed in all non-cre expressing cells that had taken up the virus, sections were incubated with anti-mCherry (Table 3). Although 3 mice were injected with the virus, after mCherry+ labelling was observed, it was apparent in one cord that the injection didn't reach the CC and therefore would not have been taken up by CSFcs so it wasn't used in this experiment.

To visualise EdU expression a click chemistry method was used. Tissue sections were first permeabilised by incubating in PBST 0.2% for 20 minutes. This was followed by two 10-minute washes in Tris buffer pH 7.6 0.1 M. This buffer was removed, each well was filled with 500 μ L of solution; 35.53 M dH₂O, 0.5 mM Cu(III)SO₄, 0.1 M Tris pH 8.5, 0.01 mM biotinylated azide, 0.1 M ascorbic acid. The ascorbic acid was added last as it activated the reaction. The azide forms a bond with the EdU incorporated into the DNA permitting later visualisation. This solution was left for 15 minutes and covered to shield from light. This was washed off with two 10-minute Tris buffer pH 7.6 0.1 M and one 10-minute PBS wash. The sections were then incubated with Streptavidin-555 (Table 4) to visualise the biotinylated azide bound to EdU.

3.3.5. Tissue used

Phenotype	N	Age (weeks)	Antibody	Spinal cord sections per animal				Other tissue
				C	T	L	S	
C57Bl/6	10	10	Biotinylated azide (EdU)	-	3	3	-	-
PKD2L1-Cre	2	9	mCherry	8	8	8	3	Brain and brainstem
			PKD2L1	8	8	8	3	
PKD2L1:GCaMP6f	6	9	mCherry	2	2	2	2	Brain and brainstem Caspase3 (brain) mCherry/EdU (brain) mCherry/GFP (brainstem) Caspase3/EdU (brainstem)
			GFP/caspase-3/EdU	5	5	5	5	
			Caspase3/EdU	5	5	5	5	
			GFP/EdU	5	5	5	5	

Table 6: Tissue used for Liraglutide and DTA counts and analysis. Detail of the tissue obtained from mice in Liraglutide and DTA experiments. Shows the number of sections labelled with each antibody, from which counts and analysis were conducted. C = cervical, T = thoracic, L = lumbar and S = sacral.

3.3.6. Imaging

A combination of the imaging techniques discussed in 1.8.9. were repeated the analyse the results from these experiments including the laser confocal microscope and the automated slide scanner.

To assess general morphological changes within CSFCs high power Z-stack images taken in multiple planes were required but of multiple sections. To achieve this an Olympus IX83 Fluorescent / Deconvolution microscope was used. After capturing images in multiple planes of each section, cellSens software was used to apply the deconvolution step which eliminated lots of the background fluorescence, enhancing the signal from antibody+ cells.

3.3.7. Counts and analysis

For analysis of the tissue obtained from the Liraglutide experiments, mounted slides were imaged using an automated slide scanner (Zeiss Axioscan Z.1) which took a Z stack image

in Alexa-555 and DAPI channels. This generated compressed images which showed clearly, the EdU positive (EdU+) cells, each bright signal on the 555-channel, thought to be an EdU+ cell, was verified by checking co-localisation with DAPI to verify the signal was from a cell. 3 sections from each of thoracic and lumbar regions of the spinal cord were counted from every mouse; N = 5 control (EdU only), N = 5 test (Liraglutide and EdU injected). In the spinal cord, total counts were recorded as well as regional counts within CC, dorsal horn/column, white matter and grey matter. Resulting in n = 30 sections counted from each group. These were initially averaged per mouse, then averaged per group. This was followed by two tailed, independent, Student T-tested for significance ($p < 0.05$).

Similarly, in the DTA virus experiments, counts were conducted of proliferating cells. EdU+ cells within the CC from 5 animals, N = 2 DTA virus injected, N = 3 control (EdU only) were counted using a Leica DMRE microscope. At least n = 12 sections from each spinal cord region from each animal were counted for EdU+ cells (cervical, thoracic, lumbar), n= 6 sacral and subsequently averaged per mouse. These values were then averaged within each group, test group refers to N = 2 mice injected with the DTA virus, the control group refers to N = 3 mice not injected with anything before EdU. Sections from every region were labelled with mCherry to verify viral expression at all levels of the spinal cord and to validate the injection site. 2 sections from each region of every mouse were observed for native GCaMP6f fluorescence as an indicator of CSFcc health, dead or compromised cells are likely to have an influx of calcium (Orrenius and Nicotera, 1994) and therefore have higher fluorescence from the GCaMP6f protein, a genetically encoded calcium indicator. Sections from every spinal cord region were labelled with caspase-3 as a marker of cell death (Table 3).

Before any counts began, all animal numbers were blinded by an independent lab member to ensure there was no bias influencing the counts. For image files produced by the slide scanner, the mice were organised into blind folders before counting. For counts obtained from slides on the microscope, the slide label was covered with masking tape and assigned a new number.

3.4. Results

3.4.1. Liraglutide decreased proliferation within the spinal cord

From EdU+ counts within the thoracic and lumbar regions of mice injected with liraglutide, compared to control groups not injected with Liraglutide, there was an apparent decrease in the number of EdU+ cells. This was consistent throughout each region of the spinal cord but was only significant in the CC, white matter (WM) and total EdU+ within a 50 μm transverse section (Figure 32 B). In representative map of EdU+ cells within a lumbar section from a control (Figure 32 C) and a test (Figure 32 D) animal this recorded decrease is apparent. These maps indicate how the counts were conducted and divided into different spinal cord regions (Figure 31 A). In the CC the mean number of EdU+ cells per section \pm SEM decreased from 1.65 ± 0.239 in the control group to 0.97 ± 0.175 in the test group, this decrease was significant with a p value of 0.0271. The EdU+ cells in the white matter decreased from 40.4 ± 2.1 to 29.2 ± 2.58 , this was also significant, $p = 0.00128$. Finally, the total number of EdU+ cells in the control group was 58.6 ± 3.35 whereas the test group had an average of 45.2 ± 4.12 , $p = 0.0138$. Means were calculated from counts $n = 3$ thoracic sections, $n = 3$ lumbar sections, averaged per mouse. The graph displays averages per group, $N = 5$ control mice, $N = 5$ test mice. Total number of sections counted and averaged within each group was $n = 30$. The lumbar region was damaged from one test mouse during dissection therefore these averages reflect 27 sections counted.

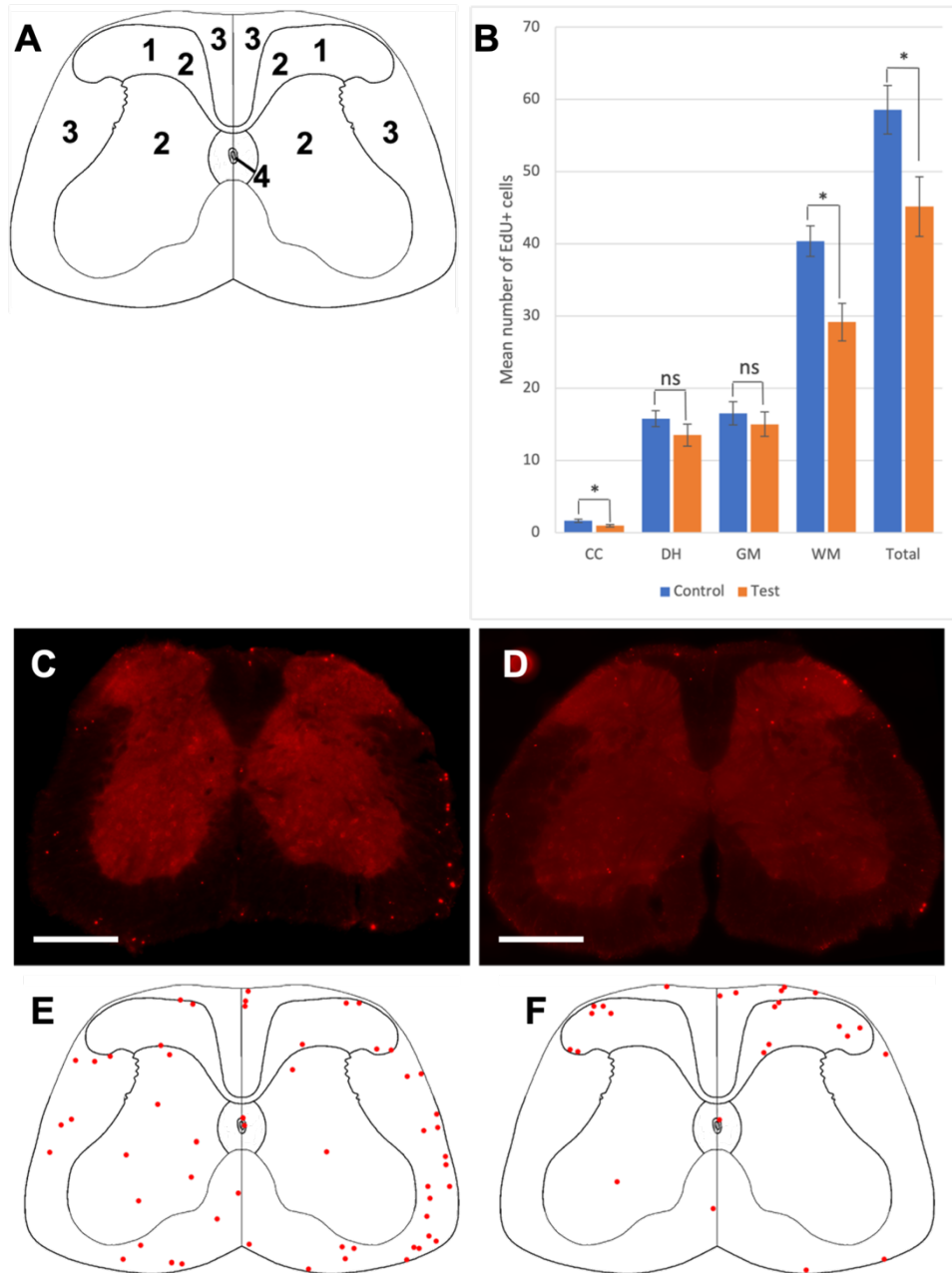


Figure 32: Significant decrease in the number of EdU+ cells after Liraglutide treatment. (A) Map of a transverse spinal cord section showing how counts were defined by region, 1 = dorsal horn/column (DH), 2 = white matter (WM), 3 = grey matter (GM), 4 = central canal (CC). (B) Graph showing a decrease in EdU+ cells in all regions of the spinal cord; CC, DH, GM, WM and total within a 50 μ m transverse section. Bars represent SEM. Student independent t-tests, * = $p < 0.05$, ** = $p < 0.01$, not significant (ns) = $p > 0.05$. (C) Tile scan transmitted light microscopy image of control lumbar section EdU+ bright cells red, mapped in (E). (D) Tile scan image of lumbar section from control mouse, EdU+ bright cells red as mapped in (F). (E) Representative map of EdU+ cells within the lumbar spinal cord from a control animal. (F) A comparable representative section from the lumbar region of a test animal with significantly fewer EdU+ cells. Scale bars 300 μ m.

3.4.2. Viral expression of DTA in CSFcCs increased EpC proliferation

mCherry expressed at all levels of virally injected mice

The DTA expressing virus was of a serotype that is transported retrogradely in neurones, therefore mCherry labelling would be expected to occur at the injection site and regions projecting to it. DTA mouse 1 displayed broad mCherry+ labelling throughout all regions of the spinal cord. In cervical regions there is labelling of cells and axons in the dorsal horn and around the CC (Figure 33 A). In thoracic sections there is labelling in the centre of the transverse section (Figure 33 B). All sections from the injection site revealed a broad spread of mCherry+ labelling axons and cells across all regions of the white matter (Figure 33 C-E) indicating the injection successfully reached the CC. In lumbar sections there is also broad labelling along the midline of the section from the dorsal edge down to the ventral fissure (Figure 33 F). The sacral region had a few cells labelled (Figure 33 G).

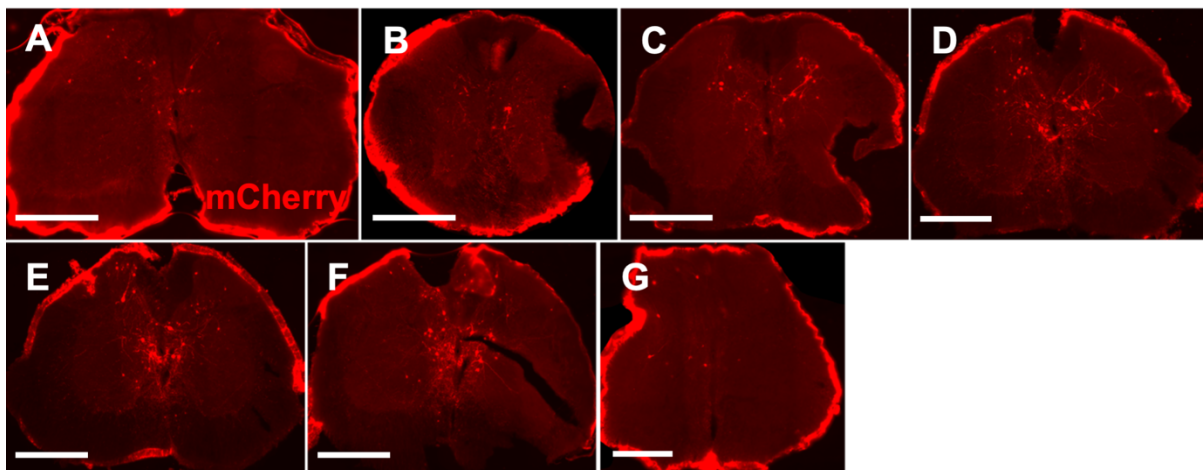


Figure 33: Viral expression of mCherry across whole spinal cord at injection site in DTA mouse 1. (A) Cervical section with sparse mCherry+ axons and cells in the dorsal horn and along the midline up to the CC. (B) Similar distribution of mCherry in the thoracic region. (C) mCherry+ axons and cells within dorsal white matter reached the CC. (D and E) Sections from the injection site with the majority of mCherry+ labelling in the central region of the sections closely surrounding the CC. (F) Lumbar section with considerable mCherry+ along the midline of the section with labelling from the dorsal edge down to the ventral boundary of the white matter. (G) Sacral section with a few mCherry+ cells. A-F = 500 μ m, E = 300 μ m. Captured using transmitted light microscopy.

In DTA cord 2 there is mCherry+ in the corticospinal tract in the cervical region (Figure 34 A). Some mCherry+ cells around the middle of the white matter of the thoracic section from the injection site (Figure 34 B). In the lumbar section from the injection site there is mCherry+ labelling in the dorsal white matter and lateral to the CC (Figure 34 C) indicating this injection did penetrate to the CC. The lumbar region had labelling around the midline and CC (Figure 34 D).

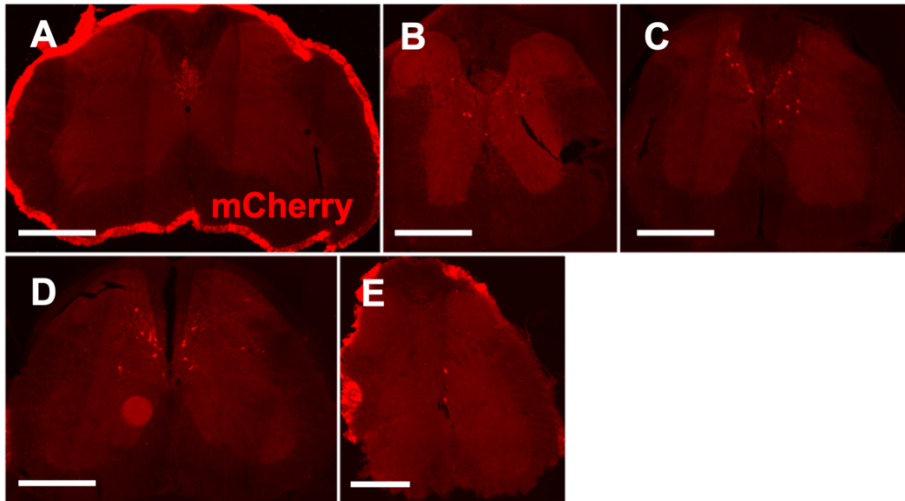


Figure 34: Viral expression of mCherry reaching CC at the injection site in DTA mouse 2. (A) Corticospinal tract mCherry+ in the cervical region. (B-D) Sections from around the injection site with labelling in the dorsal horn and along the midline up to the CC. (D) mCherry+ in the lumbar region in dorsal white matter up to the CC. (E) Few mCherry+ cells in the sacral region. Scales; A-D = 500 μ m, E = 300 μ m. Captured using transmitted light microscopy.

Increased EpC proliferation after viral injection

Injections into the spinal cord of the virus expressing DTA when cre recombinase was present were given to selectively damage or kill cre expressing CSFcCs. After verifying mCherry+ expression within the spinal cords, any changes in proliferation within the spinal cord were assessed using counts of EdU+ cells around the CC from sections at each level of the cord – cervical (C), thoracic (T), injection site (I), lumbar (L) and sacral (S) – from 2 virally injected mice (DTA mice) and 3 control mice (no injection before EdU). This revealed an increase in proliferation around the CC within all regions of the spinal cord (Figure 35), this change was significant in counts from the thoracic ($p = 0.0278$), injection site ($p = 0.264 \times 10^{-5}$), lumbar ($p = 0.661 \times 10^{-5}$) and sacral region ($p = 0.0017$). The counts from cervical sections follow the same trend but were not statistically significant ($p = 0.205$). The counts from the CC of each section were averaged per region for each animal, before calculating the mean within each group. EdU+ cells around the CC of the control group remained fairly consistent between spinal cord regions ranging from an average of 2.8 ± 0.254 in the lumbar region to 1.56 ± 0.297 in the sacral region. The increase shown in the cervical region was from 2.13 ± 0.26 in control to 2.67 ± 0.308 in the test group. In sections counted from the thoracic region it is from 1.56 ± 0.211 to 2.65 ± 0.399 . Mean EdU+ within the CC of sections from the injection site were 2.31 ± 0.257 in the control group whereas there was a much higher mean of 5.60 ± 0.590 within the test group. The largest change was seen within the lumbar region with a mean of 2.80 ± 0.254 within the control group increasing to 6.12 ± 0.655 in the DTA group. Finally, in the sacral region the number of EdU+ cells in the CC

increased from 1.56 ± 0.297 to 4.35 ± 0.641 . Then these values were combined to provide an overall average of EdU+ cells within the CC per group, N = 2 test, N = 3 control, within each region.

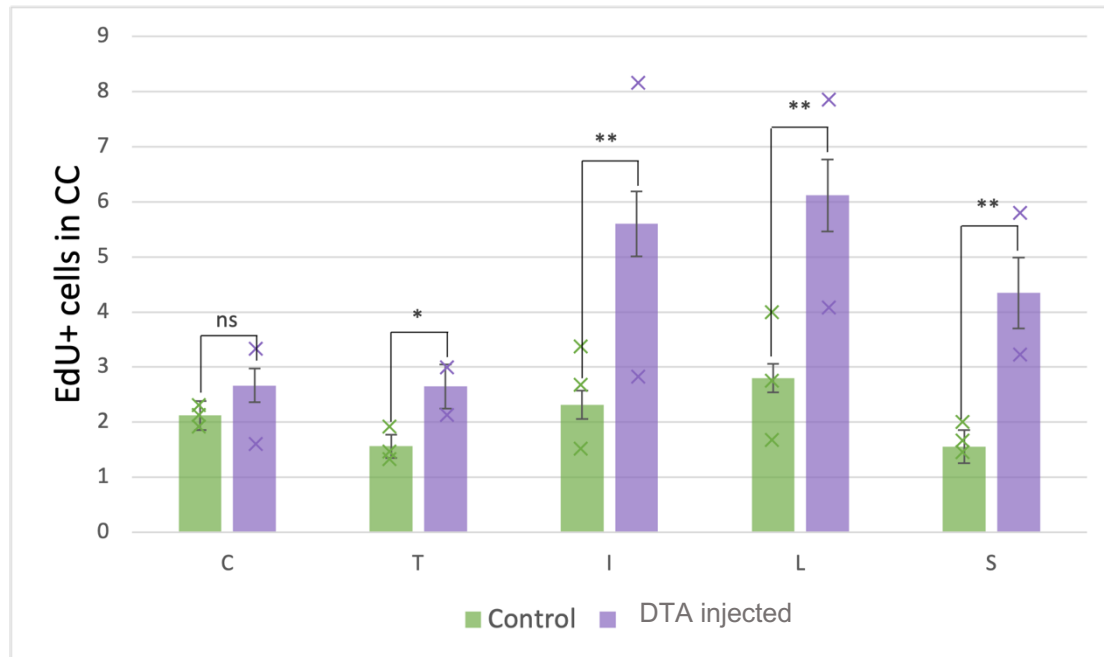
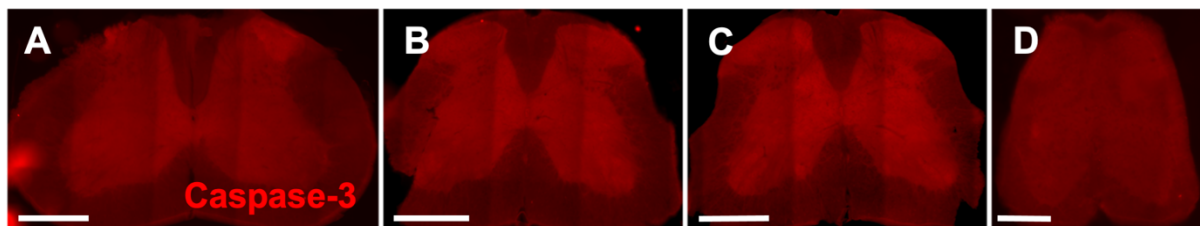


Figure 35: Significant increase in the number of proliferating EdU+ cells around the CC after viral injection. This graph shows the consistent increase in the number of EdU+ cells around the CC of 50 μ m transverse sections in the DTA mice (test) compared with the control mice within each region of the spinal cord. This increase was significant in counts from the thoracic, injection site, lumbar and sacral cord however the changes seen in the cervical cord were not statistically significant. Statistical analysis using t-tests, * = $p < 0.05$, ** = $p < 0.01$, ns = not significant. Bars represent SEM. Data points plotted represent the average calculated from each mouse, combined to provide the averages represented in the bars.

Immunohistochemistry indicates phenotypic changes including cell death

To account for the increase in proliferation, regional changes in EdU+ were compared with caspase-3 labelling between the DTA and control mice. Caspase-3 was used as an indicator of cell death as it is a marker of apoptosis (Table 3). As a negative control, caspase-3 was incubated with sections from control mouse 1 which revealed no caspase-3+ at any spinal cord level (Figure 36).



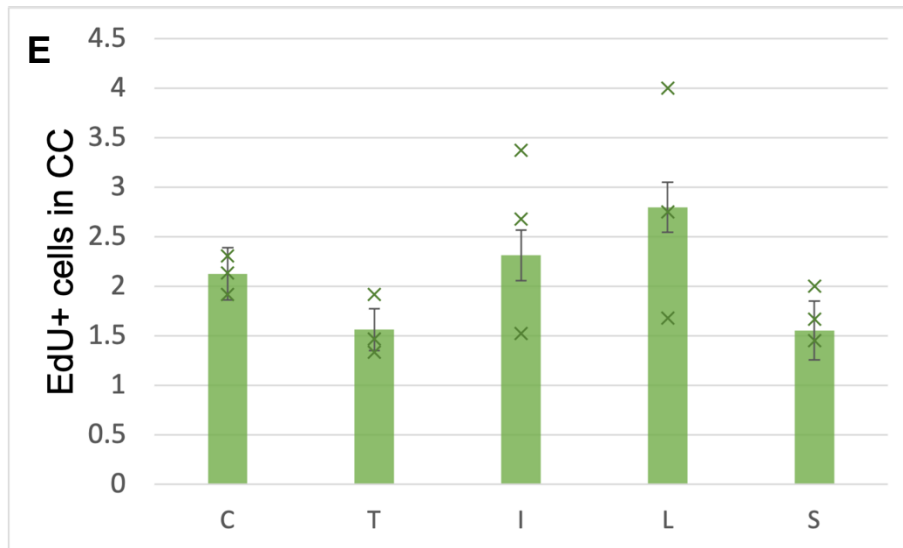


Figure 36: No caspase-3+ in any region of control mouse 1, little variation in EdU+ between regions. (A-D) Representative 50 μ m section from the cervical, lower thoracic injection site region, lumbar and sacral region respectively, all show no caspase-3+. Scale bars A-C = 500 μ m. D = 200 μ m. (E) Graph shows the little variation between regions of the spinal cord in the average number of EdU+ cells.

Since these control mice had not received any injections, it was important to assess whether the injection caused an increase in caspase-3, and subsequently caspase-3+ labelling. Tissue from a different experiment, in which a GABA_Asnr virus was injected to the same region of PKD2L1-IRES-cre mice, expressing a fluorescent protein in PKD2L1+ CSFCs but not killing them, was incubated with the antibody for caspase-3. This showed no caspase-3+ labelling (Figure 37), verifying that any caspase-3+ labelling within the DTA cords was a result of the DTA expression and not the injection of a virus itself.

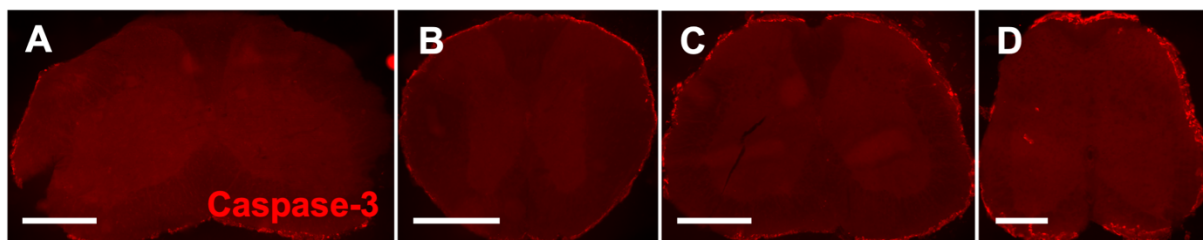


Figure 37: Viral injection into the spinal cord doesn't cause caspase-3 expression. (A-D) Representative sections from each spinal cord region of a virally injected mouse show no caspase-3+ labelling. Scales, A-C = 500 μ m, D = 200 μ m. Captured using transmitted light microscopy.

Having observed significant changes in the proportion of EdU+ cells following injection of a virus expressing DTA, it was important to assess any phenotypic changes that may indicate what influenced changes in EdU+ cells within the ependymal layer. Caspase-3+ was used to indicate cell death (Table 3).

mCherry+ was seen throughout sections from DTA mouse 1, dorsal to ventral, confirming the injection reached the CC. In this mouse, the changes in EdU+ counts were calculated within each region (Figure 38). The mean EdU+ cell counts within the CC of each region

were as follows; cervical 1.60 ± 0.406 (n = 18), thoracic 2.133 ± 0.561 (n = 19), injection site 2.83 ± 0.412 (n = 26), lumbar 4.083 ± 0.554 (n = 24), sacral 3.23 ± 0.567 (n = 13).

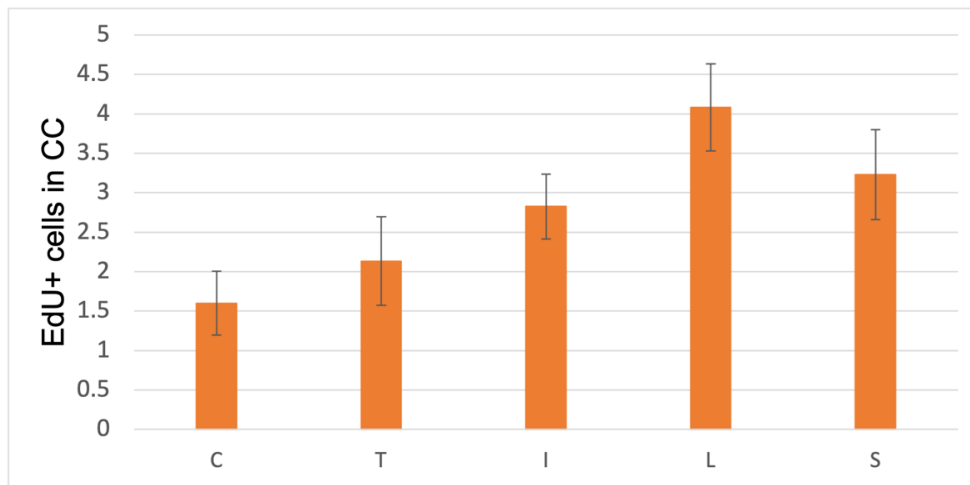


Figure 38: Regional changes in EdU+ around CC of DTA mouse 1. EdU+ counts within the CC with highest numbers seen in the lumbar region.

Sections were incubated with caspase-3 to label cells undergoing apoptosis alongside anti-GFP to enhance the GCaMP6f signal and observe CSFcC morphology. In DTA mouse 1 caspase-3+ labelling in a cervical section was observed alongside aberrant GCaMP6f+ CSFcCs. Notably, there were bent axons seen (Figure 39 Fi, white arrows), indicative of a change in the state of CSFcC. Caspase-3+ around the CC was seen in cervical (Figure 39 A and F), thoracic (Figure 39 G), injection site (Figure 39 H) and sacral (Figure 39 E and I) sections. There was no caspase-3 seen in any sections taken from the lumbar region.

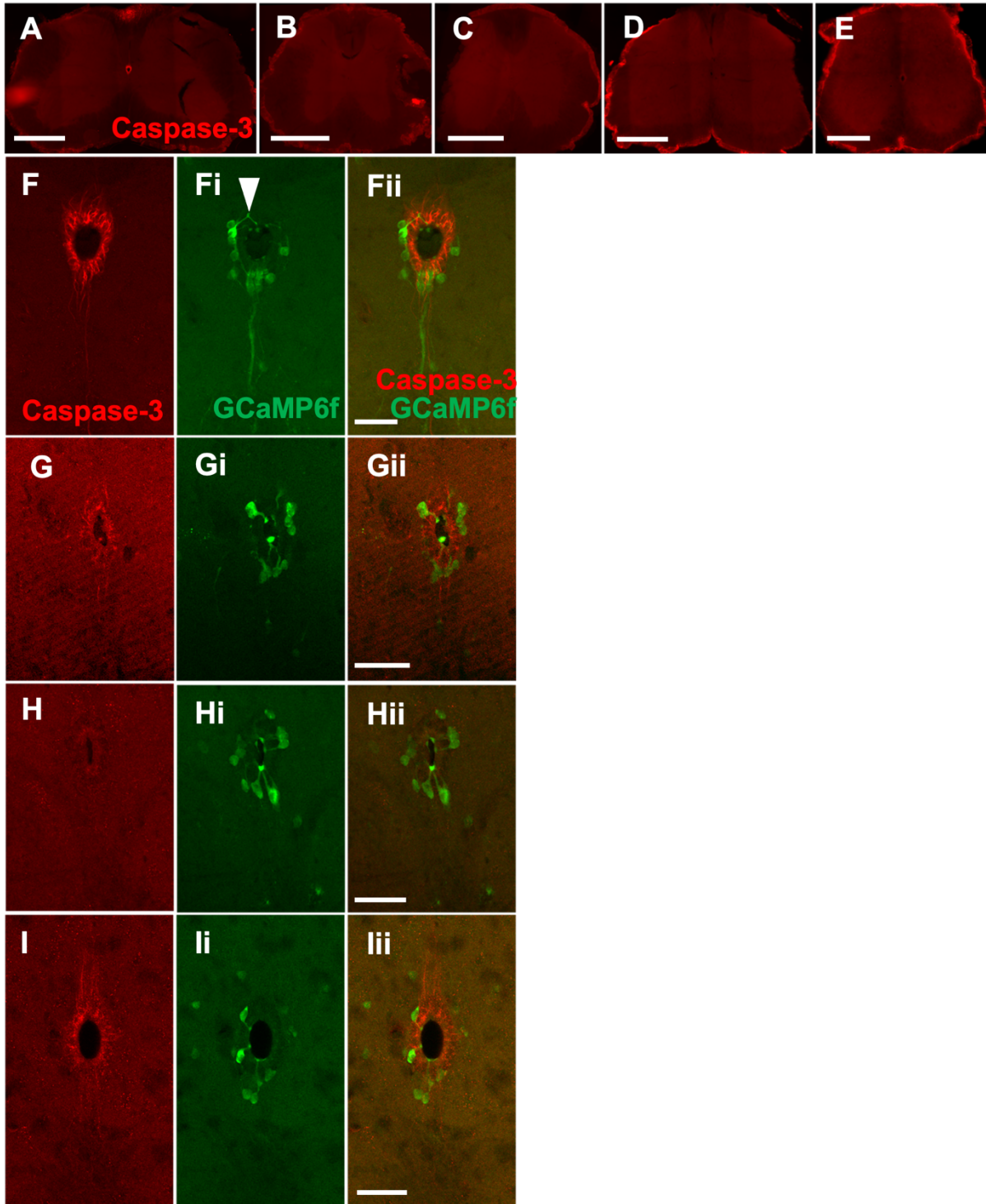


Figure 39: Caspase-3+ CC and changes in CSFcC morphology in DTA cord 1. (A-D) Overview of caspase-3+ sections from cervical, thoracic, injection site and sacral spinal cord regions. A-F = 500 μ m, E = 300 μ m. (F-Fii) CC from a cervical section caspase-3+ (red) around CC, GCaMP6f+ CSFcCs (green), unusual morphology of a bent axon in dorsal CC (white arrow). (G-Gii) Thoracic section with subtle caspase-3+ around CC. (H-Hii) Faint caspase-3+ around CC of section from the injection site. (I-iii) Sacral section caspase-3+. Fii, Gii, Hii = 50 μ m, iii = 75 μ m. Overview images captured using transmitted light microscopy, high power CC captured using confocal microscopy.

EdU+ cells around the CC were highest in DTA cord 2 within the test group (Figure 40). Bars represent averages calculated from the sections counted from each region of the spinal

cord, cervical 3.33 ± 0.387 (n = 26), thoracic 3.00 ± 0.556 (n = 24), injection site 8.16 ± 0.814 (n = 27), lumbar 7.86 ± 1.02 (n = 2), sacral 5.8 ± 1.14 (n = 11).

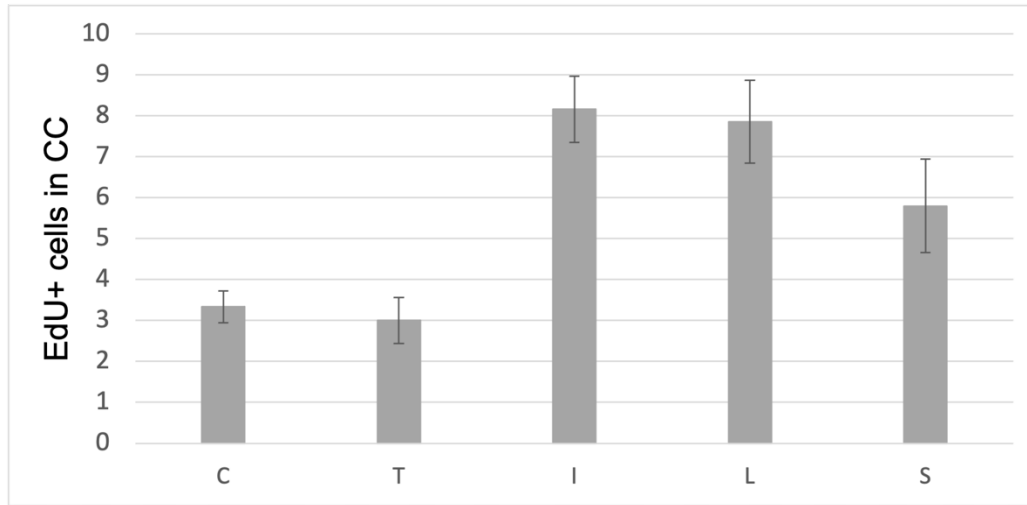


Figure 40: High number of EdU+ cells around CC DTA mouse 2. EdU+ counts from the CC of sections taken from each spinal cord region. Much greater EdU+ CC in the injection site and lumbar region. Bars represent SEM.

These observations seen within DTA mouse 2 correlate with bright caspase-3+ labelling around the CC (Figure 41 A-D). Caspase-3+ was apparent in cervical (Figure 41 A, F and G), thoracic (Figure 41 D and H) and sacral sections (Figure 41 I). In the cervical sections imaged, there were some differences in GCaMP6f+ CSFcC morphology, such as exhibiting uncharacteristically bent axons (Figure 41 Fi and Gi, white arrows).

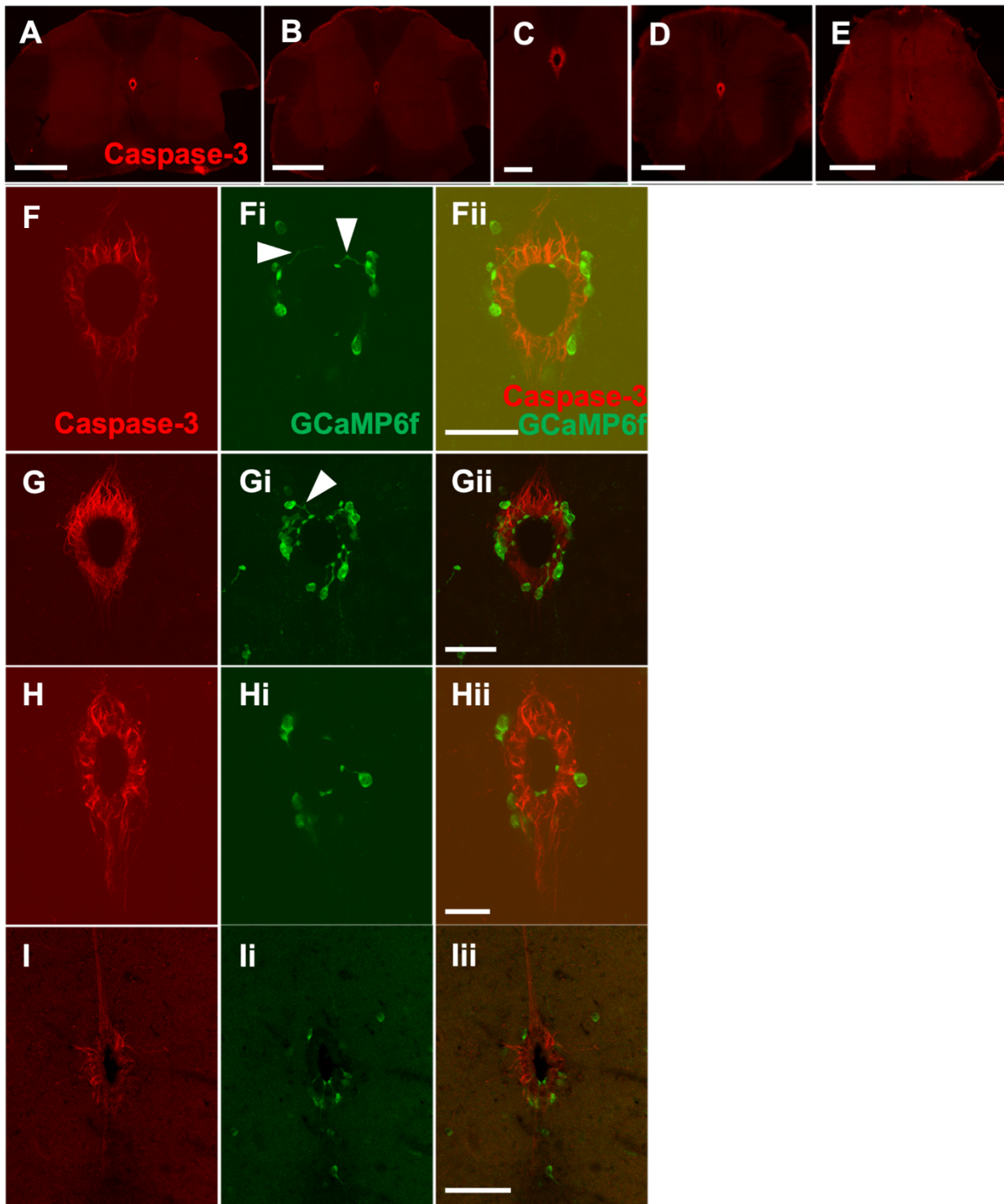


Figure 41: Caspase-3+ around CC of many regions from DTA mouse 2 and unusual morphology of CSFcCs. (A-E) Overviews of transverse sections from each region of DTA mouse 3. A, B = 500 μm , C = 100 μm , D, E = 300 μm . (F-Fii) CC from cervical section with caspase-3 (red) around CC and GCaMP6f+ CSFcCs (green), some bent axons around dorsal CC (Fi, white arrows). (G-Gii) Another cervical section with caspase-3+ around the CC and GCaMP6f+ bent axons around the dorsal CC. (H-Hii) Caspase-3+ in thoracic section. (I-Iii) Sacral section caspase-3+ CC. Fii, Gii = 50 μm , Hii = 30 μm , Iii = 75 μm . Overview images captured using transmitted light microscopy, high power CC captured using confocal microscopy.

Morphological differences in CSFcCs indicating cell death

After caspase-3 was observed in the DTA mice and none of the control mice, it was important to assess whether these changes correlated with any morphological changes within the population of PKD2L1+ CSFcCs expressing GCaMP6f around the CC. This was anticipated since it is evident that the viral injection reached the CC, shown with mCherry+ labelling, and there was caspase-+ labelling around the CC, indicating cell death within this region. The virus only expressed DTA in cre-expressing cells therefore defining what happened in the GCaMP6f+ CSFcCs was important.

Initially, when sections were mounted after sectioning, without incubation with any antibodies, they were observed under the fluorescent microscope to look for any differences between the endogenous fluorescence of GCaMP6f between each group. It was apparent that in sections from DTA mice, it was possible to see some GCaMP6f+ CSFcCs around the CC, however in the control sections there was no fluorescence seen. In attempt to quantify this difference in fluorescence signal, sections were imaged on the confocal microscope maintaining the capture settings and gain just changing the focus between each section. Unfortunately, due to not having enough sections imaged from every animal, it wasn't possible to analyse these changes in fluorescence intensity.

Another way to assess changes in CSFcCs after DTA viral injection was by making observations of sections in which the GCaMP6f signal was enhanced with anti-GFP. These observations were made blind and notes were made in a simplified format, commenting on any aberrant CSFcCs based on morphology and position. High power CC images were then captured to exemplify these comments (Figures 42, 43 and 44), with images from DTA mice 1 and 2 and compared with control mouse 1. The primary observations seen in the DTA cords differing from the control were bent axons extending from CSFcCs around the CC in various directions (Figure 43 A, D and E, Figure 44 A, B and F), some larger somata and abnormal shapes (Figure 43 G, white arrow, Figure 44 F) with more somata ventral of the CC. There were also some CCs with considerably less CSFcCs around the CC upon first observation.

In the control animal, typical GCaMP6f+ CSFcC distribution around the CC and towards the VF was seen (Figure 42). In some sections there are fewer CSFcCs (Figure 42 A) than in others. Overall, there tends to be an even spread of CSFcCs around the CC and a few cells between this region and the VF (Figure 42 B, C and D, white arrows).

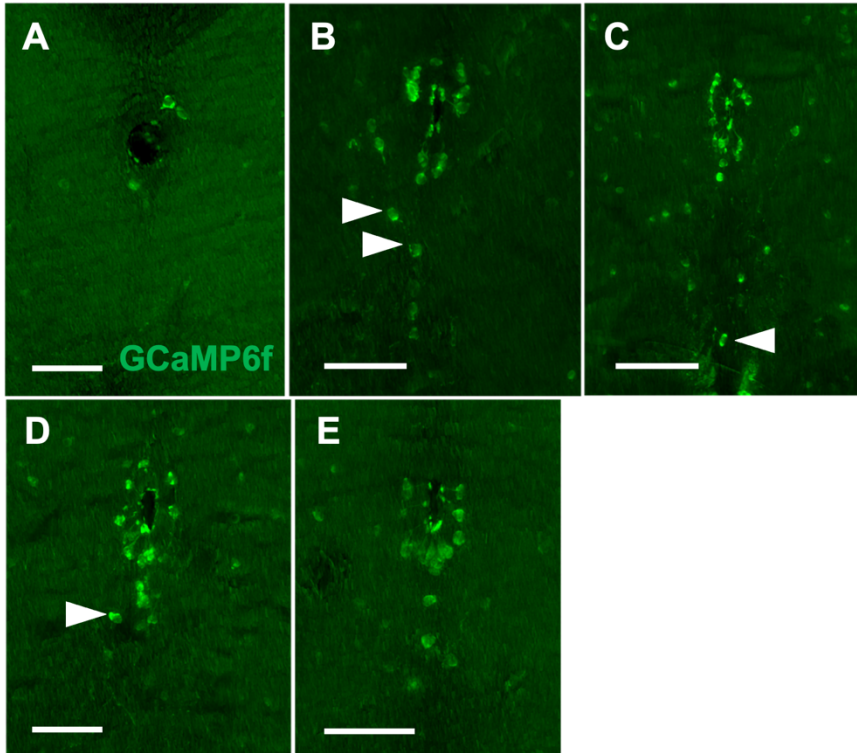


Figure 42: *GCaMP6f*+ CSFcCs in a control animal with typical morphology. (A) Cervical transverse section with few CSFcCs around the CC (B-C) Thoracic sections with typical consistent *GCaMP6f*+ CSFcCs around the entire CC and some in the VF. (D-E) Lumbar sections with *GCaMP6f*+ CSFcCs, white arrow highlights a cell away from the VF midline reiterating the subtle differences seen between slices with this cell's distribution. A, B, D and E = 75 μ m, C = 100 μ m. Captured using transmitted light microscopy after deconvolution

In sections from DTA mouse 1, there were some apparent differences in the morphology of the CSFcCs however this wasn't quantified. Notably, throughout the spinal cord there was a repeated observation of axons that appear bent (Figure 43 A). This was discussed previously in the higher power confocal images of the CC. In the dorsal region of the CC axons appear to extend in one direction, then at a sharp angle, to another. This is not something observed in any of the tissue from the control spinal cords (Figure 42).

Additionally, more sections appear to have CSFcCs laterally, away from the midline running ventrally from the CC (Figure 43 D and E), with long axons laterally crossing the section (Figure 43 D and E, white arrows). Some cells appear to be larger than what is typical for CSFcCs or misshapen (Figure 43 G, white arrow). Some sections appear have very few *GCaMP6f*+ around the CC (Figure 43 B, F and G), in spite of these images reflecting Z-stacks, with an image taken from multiple planes within each section reflecting all of the visible cells within each 50 μ m section.

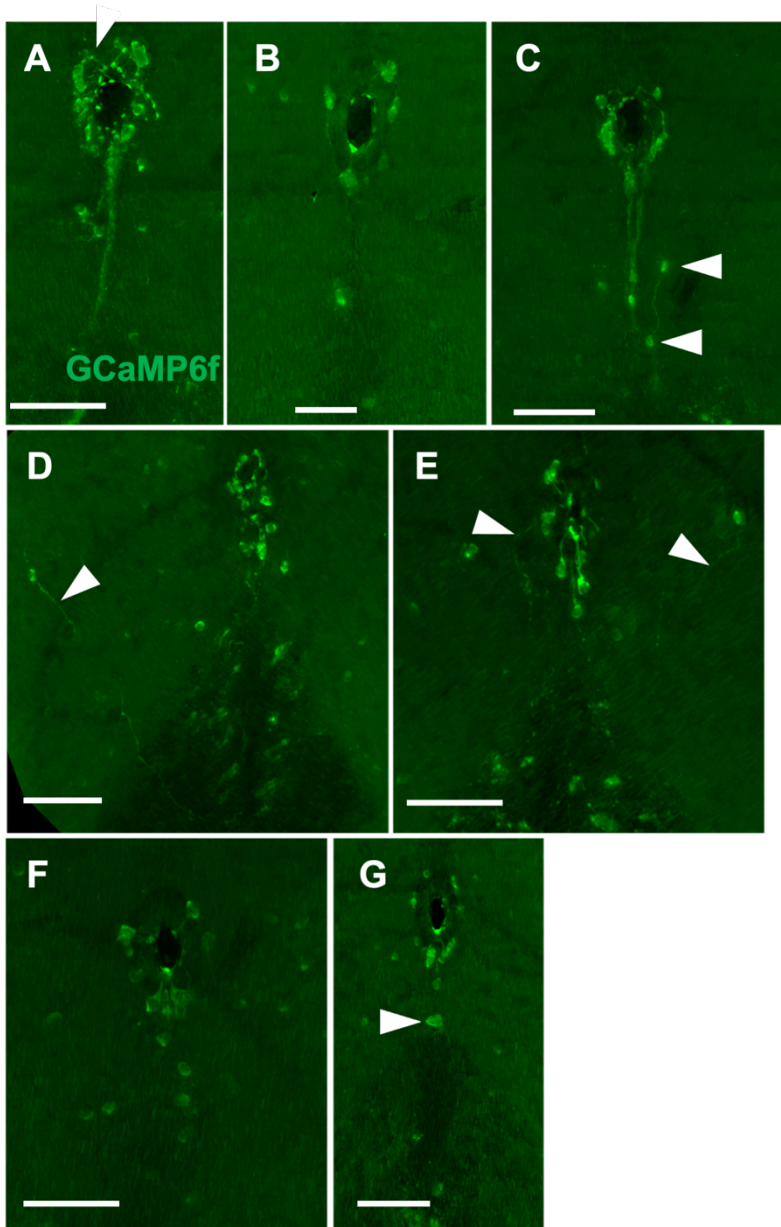


Figure 43: GCaMP6f+ CSFccs in DTA mouse 1 with notable morphological changes in GCaMP6f+ CSFccs. (A-C) Cervical sections GCaMP6f+ CSFccs (green) around the CC and in the VF region. (A) Axons in the dorsal CC with an aberrant morphology, directing away from the CC and then bending towards it. (B) Few CSFccs around the CC. (C) Trail of GCaMP6f+ CSFccs towards the VF (white arrows), (D-E) Thoracic sections with axons laterally in the white matter away from the CC (white arrows), (F-G) Lumbar sections also with few CSFccs around the CC. (G) One aberrant cell larger somata than those around the CC and less regular in shape. A = 100 μ m, B-G = 75 μ m. Captured using transmitted light microscopy after deconvolution.

Similarly, observations of GCaMP6f+ CSFccs morphology in DTA mouse 2 suggest an effect of the DTA virus on these cells. There are long axons in various locations around the CC region (Figure 44 A and B, white arrows). A section from the injection site displayed a GCaMP+ CSFcc dorsal to the CC (Figure 44 F, white arrow) which is also larger than the cells around the CC. Sections from the cervical, thoracic and lumbar region with few CSFccs around the CC, Figures 44 C, D and G respectively.

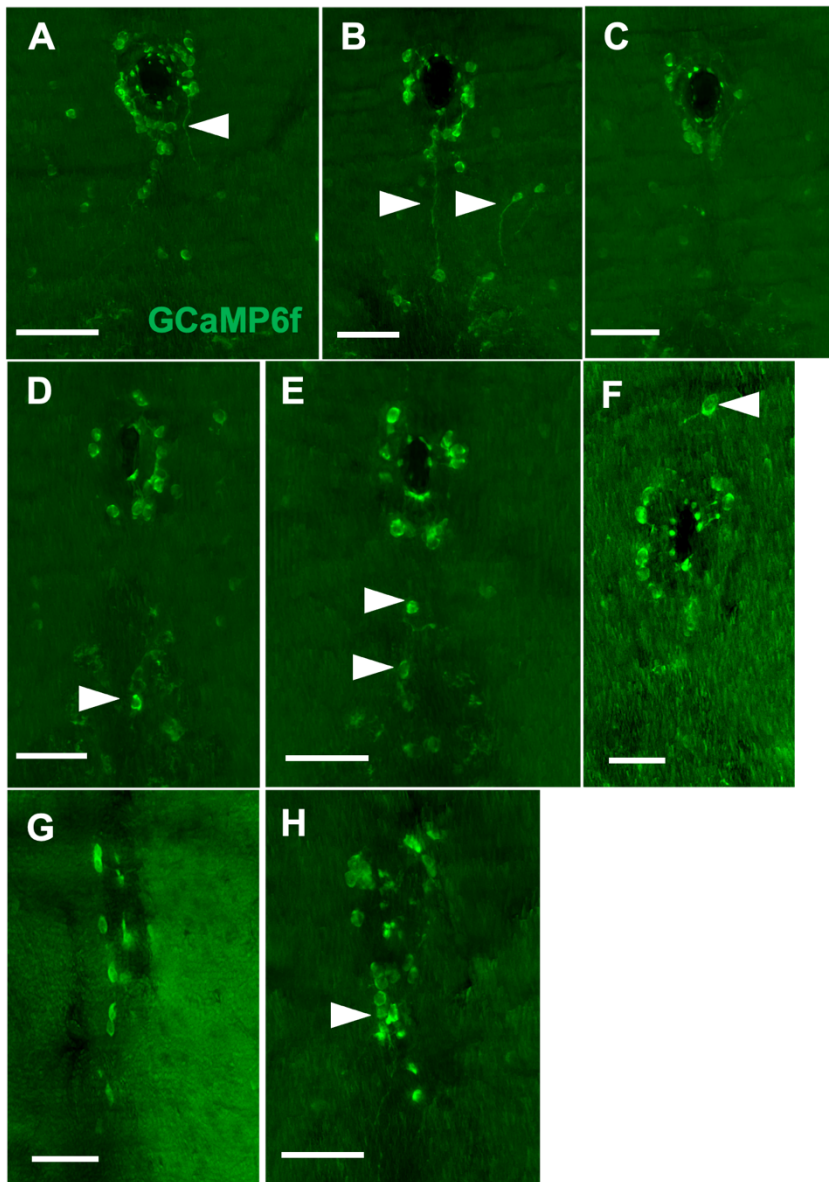
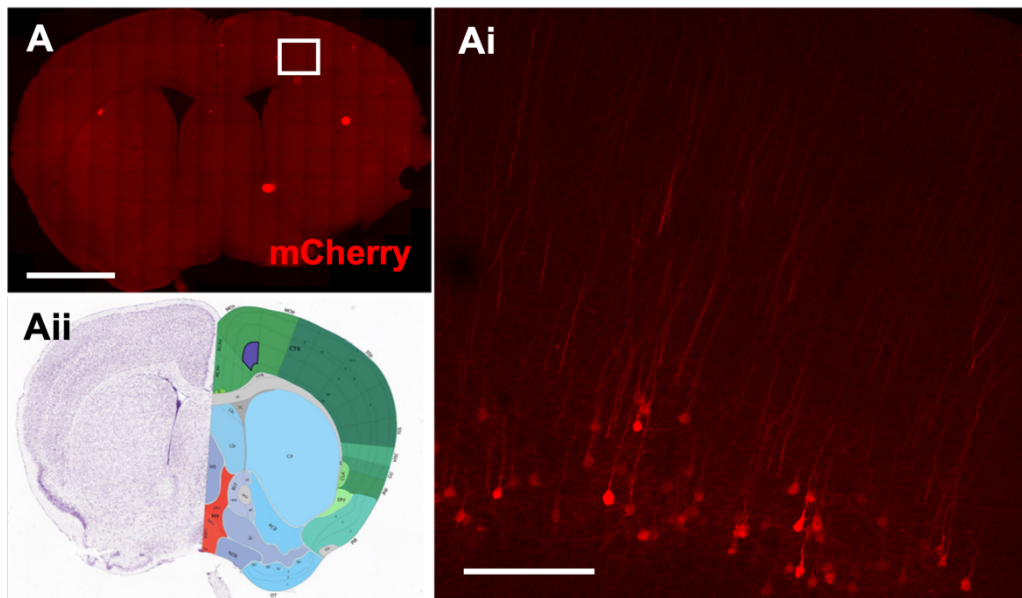


Figure 44: *GCaMP6f+ CSFcCs in DTA mouse 2 with some unusual morphological features.* (A-C) Cervical sections. (A-B) Axons from GCaMP6f+ CSFcCs (green) lateral to the CC within the white matter and heading ventrally. (C) A section with few cells around the CC. (D-E) Thoracic sections with ventral cells (white arrows). (F) Section from the injection site with a notable GCaMP6f+ cells dorsal to the CC, larger than those located in the CC. (G-H) Lumbar sections. (G) Few CSFcCs around the CC. A-E, G-H = 75 μ m, F = 50 μ m. Captured using transmitted light microscopy after deconvolution

Virus travelled retrogradely from the injection site labelling regions of the brain and brainstem that project to the spinal cord

The AAV used was a retrograde virus that travelled along axons after it was taken up by terminals in the opposite direction to neural signals. This resulted in mCherry+ labelling of cells and axons throughout the CNS, rostral to the injection site. To confirm that this was the case in the spinal cord, the pattern of labelling within the brain and brainstem of DTA mouse 1 was assessed. As a negative control, the mCherry and caspase-3 antibodies were also incubated with the tissue from the brain and brainstem of a control mouse to verify there was no background or auto fluorescence labelling. There was no labelling observed in these sections.

Representative sections from the forebrain (Figure 45 A) midbrain (Figure 45 B, C and D) and hindbrain (Figure 45 E) incubated with anti-mCherry to assess viral expression within DTA mouse 1. This revealed mCherry+ cells and axons in regions of the forebrain and midbrain known to project to the spinal cord. This includes the sensory motor area (Figure 45 Aii, purple) and the primary somatosensory area (Figure 45 Bii, Ci and Di, purple), defined using representative reference brain atlas images (Allen brain atlas, 2008).



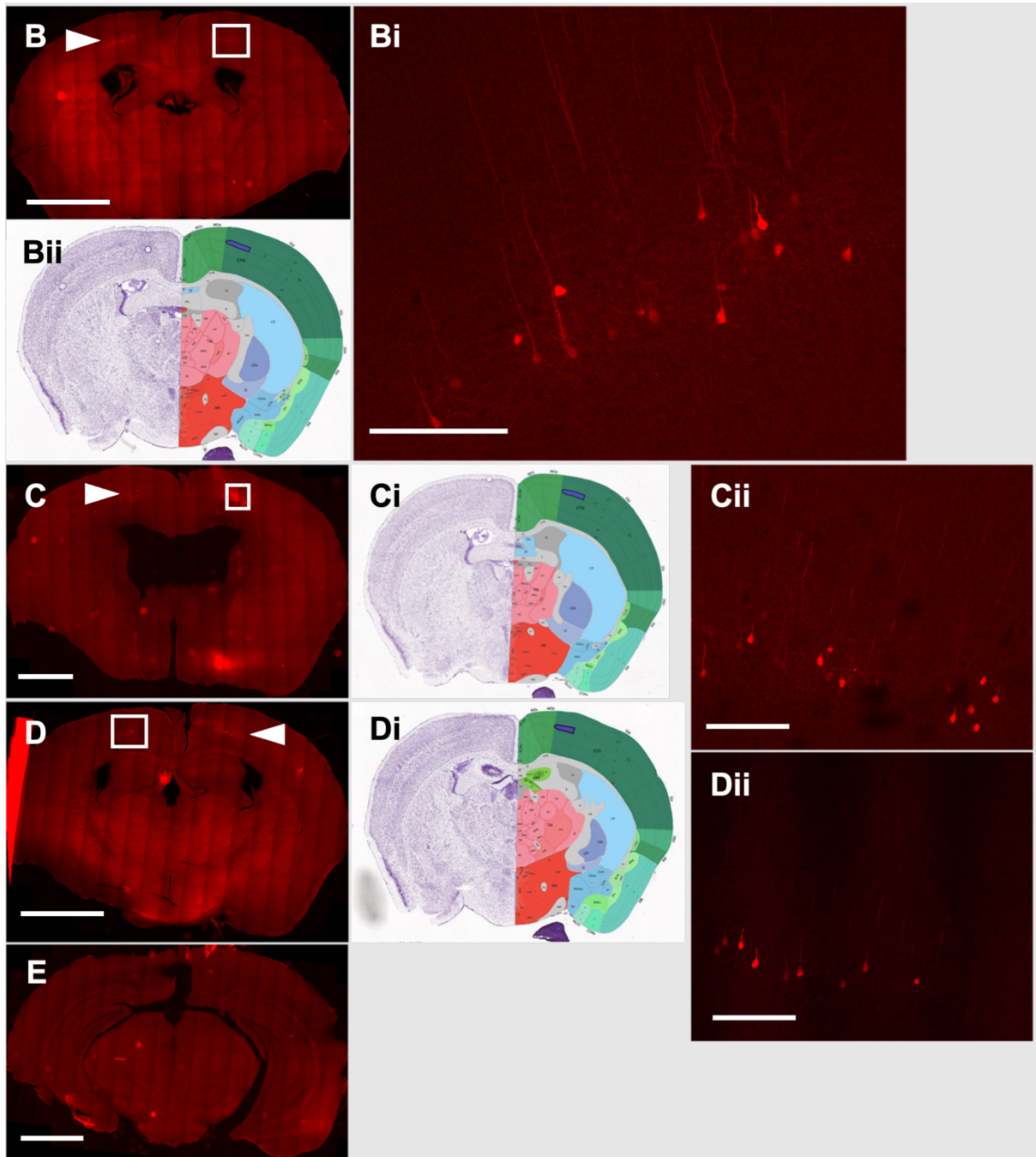


Figure 45: *mCherry+* within motor and somatosensory areas of the brain. (A) Section from the forebrain with labelling seen in the sensory motor area as shown in purple on the reference atlas image (Aii). (Ai) Higher magnification of boxed area (A) showing *mCherry+* cells and dendrites indicating cells that project to the spinal cord. (B) Section from the midbrain, cells on either side of the midline labelled (white arrow and boxed region). (Bi) Higher magnification of boxed region (B). (Bii) Labelling within somatosensory area as indicated in purple (C) Labelling seen either side of midline (boxed region and white arrow). Representative atlas shows the labelling to be within somatosensory area (Ci, purple). (C) Higher power image of boxed region. (D) Further caudal midbrain section including the hippocampus with *mCherry+* in the primary somatosensory area (white arrow). (Dii) Boxed region (D) at a higher magnification to visualise cells and axons. (Di) Reference atlas with labelling shown in somatosensory area (purple). (E) Hindbrain section with no *mCherry+* labelling. Scale bars A, B, and D = 2000 μm , C and E = 1500 μm , Ai, Bi, Cii, Dii = 200 μm , E = 1500 μm . Overview images captured using transmitted light microscopy, high power CC captured using confocal microscopy.

Brain regions from a DTA injected mouse were also incubated with the antibody for caspase-3 to check for any cell death. None of the brain sections were caspase-3+ (Figure 46). This relates to the findings in chapter 2, there are no PKD2L1+ CSFcCs within the brain, therefore no cells expressing cre driving expression of DTA.

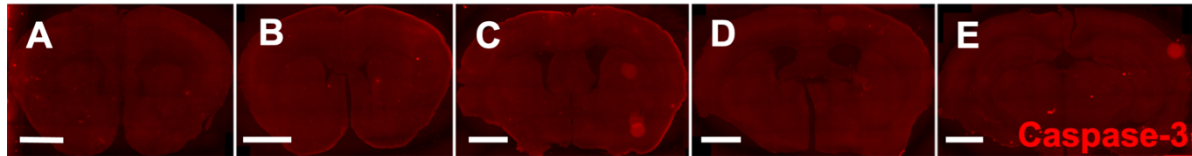


Figure 46: Brain sections were not caspase-3+. (A-E) Representative sections from each brain region, rostral to caudal, no mCherry+ observed. Scales, A-E = 1500 μ m. Captured using transmitted light microscopy.

In the brainstem, mCherry and GCaMP6f labelling were imaged in the same sections to assess overlap between spinal cord projections and CSFcCs within the brainstem. As above, mCherry+ labelling in the brainstem was representative of regions known to project to the spinal cord including the NTS (Figure 47 B). In some sections there appear to be mCherry labelled axons close to GCaMP6F+ CSFcCs (Figure 47 C-Ci and D-Dii, white arrows). Indicating that these cells may be part of circuitry projecting from the brainstem to the spinal cord.

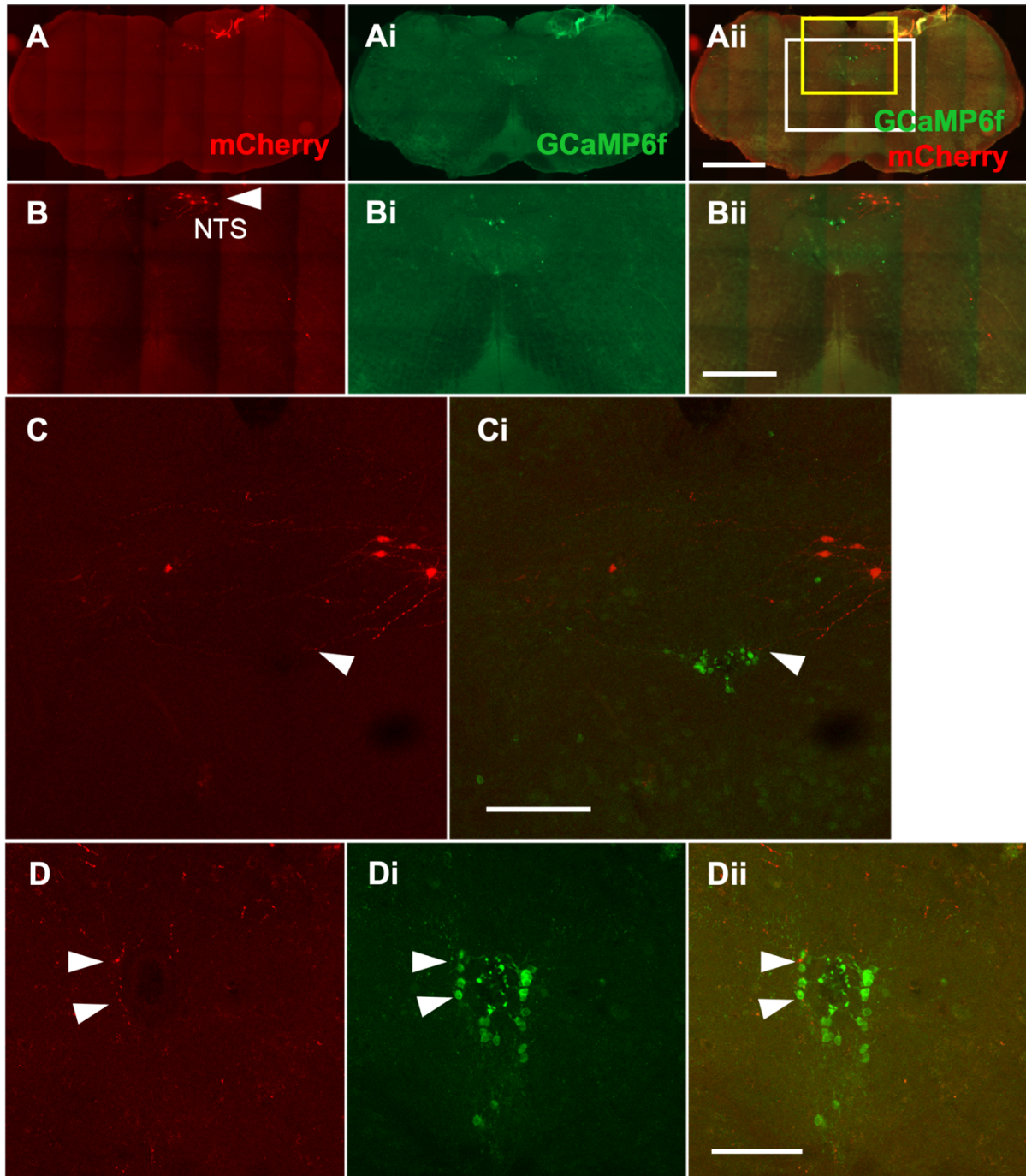


Figure 47: *mCherry*⁺ cells and axons in the NTS. (A-Aii) *mCherry*⁺ labelling in the dorsal brainstem (red) above *GCaMP6f*⁺ CSFccs (green). (B-Bii) Higher magnification image of white boxed region (Aii) showing cell bodies located within the NTS (white arrow). (C-Ci) Higher resolution image of yellow boxed region (Aii) shows *mCherry*⁺ axon terminating on *GCaMP6f*⁺ CSFcc (white arrow). (D-Dii) Another brainstem sections with punctate boutons surrounding somata of CSFccs (white arrows). Scale bars Aii = 1000 μ m, Bii = 500 μ m, Ci = 200 μ m, Dii = 100 μ m. Overview images captured using transmitted light microscopy, high power CC captured using confocal microscopy.

Similar labelling was seen in DTA mouse 2 with different representative sections from the brainstem (Figure 48). *mCherry*⁺ cells were located in the NTS (Figure 48 A). There were also *mCherry*⁺ axons terminating on *GCaMP6f*⁺ CSFccs in various sections (Figure 48 C-Cii, F-Fii and H-Hii, white arrows).

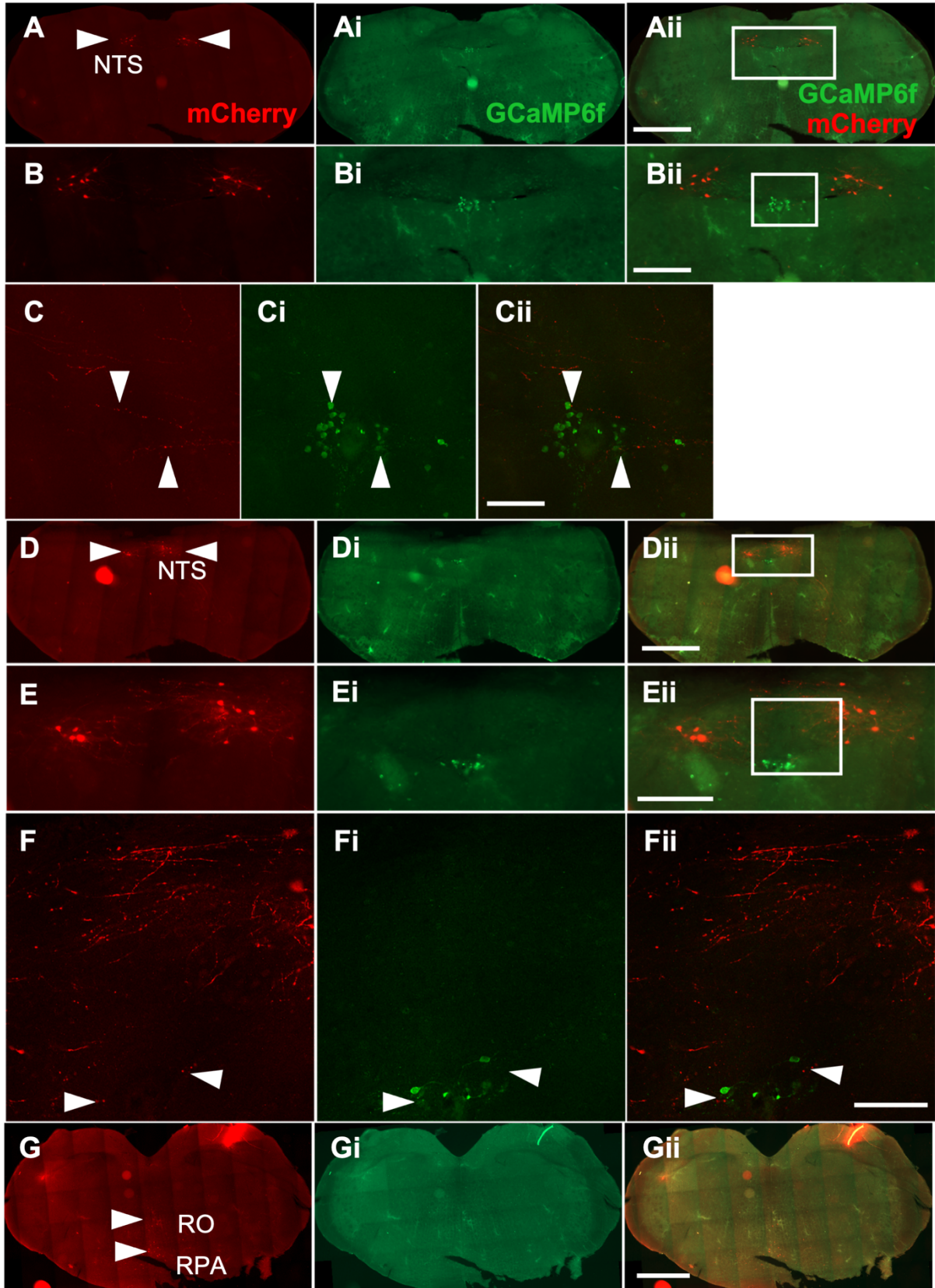


Figure 48: *mCherry+* projections in the region of *GCaMP6f+* CSFcCs in brainstem and within raphe nuclei. (A-Aii) *mCherry+* (red) cells and axons either side of CC within NTS. (B-Bii) Higher magnification image of boxed region (Aii). (C-Cii) Another section showing *mCherry+* projections reaching *GCaMP6f+* (green) CSFcCs. (D-Dii) Section with lots of *mCherry+* within NTS. (E-Eii) Magnification of boxed region (Dii). (F-Fii) Higher power image of boxed region (Eii) showing *mCherry+* projections surrounding *GCaMP6f+* CSFcCs. (G) More rostral brainstem section showing *mCherry* labelling in the RO and nucleus raphe pallidus (RPA). (Gii) No *GCaMP6f+* as the more rostral regions of the brainstem do not have a CC. Scales in μm ; Aii = 1000, Bii = 400, Cii = 100, Dii = 1000, Eii = 300, Fii = 100, Gii = 1000. Overview images captured using transmitted light microscopy, high power CC captured using confocal microscopy.

3.5. Discussion

These experiments attempted to manipulate CSFcCs to determine if this influenced EpC proliferation. Injections of the GLP1R agonist liraglutide aimed at increasing CSFcC activity reduced EpC proliferation. In contrast, selective expression of a toxin within CSFcCs enhanced EpC proliferation.

3.5.1. Liraglutide injections dampened EpC proliferation in the spinal cord

Liraglutide caused a significant decrease in the total number of proliferating cells within the SC. When counts were analysed within each region of the spinal cord, the decrease in EdU+ cells in the CC and WM within the test group, compared to the control, were significant. Although there were also decreases seen in the DH and GM, these were not significant. The decrease in number of proliferating cells within the CC region, supports the hypothesis that EpC proliferation would decrease upon CSFcC activation. This is potentially due to GLP1R activation stimulating the release of GABA (Stoeckel *et al.*, 2003, Fidelin *et al.*, 2015) from CSFcCs which dampens the baseline rate of EpC proliferation, a similar effect to GABA in the SVZ on neural stem cells of the SVZ (Liu *et al.*, 2015) compared with the number of proliferating cells at baseline as seen in the control group. This relates to the ability of GLP1R to stimulate exocytosis (González-Santana *et al.*, 2021).

The decrease in EdU cells in the WM was not anticipated as this does not relate to activation of the CSFcCs. This may reflect the expression of GLP1Rs observed outside of the CC within the spinal cord (Chen *et al.*, 2017). Activation of these cells may also cause the release of factors able to influence surrounding proliferating EdU+ cells. Alternatively, this may reflect peripheral effects of Liraglutide. Since Liraglutide was administered intraperitoneally, it cannot be ruled out that these changes in proliferation result from peripheral effects of the drug. Something which also applies to the changes seen within the CC region. Andersen *et al.* (2021) used a transgenic mouse line expressing tdT under the promoter GLP1R resulting in the expression of an RFP in GLP1R+ cells. GLP1R expression was mapped using a combination of GLP1R mRNA in situ hybridisation and immunohistochemistry of the GLP1R. They reported GLP1R expression within the stomach, Brunner's gland and enteroendocrine cells of the gut, various cell types within the pancreas, smooth muscle walls of renal arteries, liver, lungs and cells of the thyroid. This diverse GLP1R expression across different systems within the animal indicate a range of peripheral effects IP Liraglutide could have initiated. These may have influenced the changes seen in

the SC. Particularly, the anti-inflammatory effect of Liraglutide (Que *et al.*, 2019, Zobel *et al.*, 2021). This is the opposite of what happens after SCI, in which there is an inflammatory response with lots of inflammatory markers released causing an increase in EpC proliferation. This may relate to the dampening of EpCs observed in this experiment.

Contributing to the possibility that the changes observed did not result from central effects of Liraglutide acting on receptors within the spinal cord is the conflicting evidence of whether Liraglutide can cross the blood brain barrier. Hunter and Hölsher (2012) measured the kinetics of Liraglutide crossing the blood brain barrier by snap freezing brains immediately after perfusion 30 minutes after IP injection of Liraglutide. They used a GLP1 ELISA assay which showed significantly higher Liraglutide levels compared with saline IP injected controls. This correlated with an increase in cAMP. However, Christensen *et al.* (2015) sampled blood and CSF, obtained via lumbar puncture, from type 2 diabetes patients the day after subcutaneous Liraglutide injections. They found Liraglutide in the CSF had no correlation with Liraglutide concentration in the blood. Patients with the highest blood Liraglutide level showed no Liraglutide in the CSF. Therefore, we cannot be sure the effects seen in this experiment result from the activity of this drug within the spinal cord.

Further experiments could be carried out to verify whether Liraglutide is able to cross the blood brain barrier. One of which would be administering Liraglutide conjugated to a fluorescent molecule intraperitoneally. Following this, the mice would be perfused, and spinal cord sectioned to look for the fluorescence within the spinal cord. Alternatively, different *ex vivo* experimental set ups could be used in order to assess the effect of this drug directly onto the spinal cord, overcoming any problems with crossing the blood brain barrier. This includes acute slice experiments in which slices are cut from the spinal cord immediately after decapitation and bathed in oxygenated artificial CSF. If Liraglutide was applied to these slices along with EdU, changes in proliferation could be observed over a short period. Alternatively, slice cultures could be generated from the spinal cord and similarly incubated with Liraglutide and EdU chronically, to assess any changes in proliferation over a longer period. This also eliminates peripheral effects of Liraglutide influencing the cells within the spinal cord. Although these experiments will provide information regarding the effect of Liraglutide on the spinal cord, they do not reflect changes that may occur in a whole physiological system.

3.5.2. Viral expression of DTA influenced CSFcCs, increasing EpC proliferation

Initially, tissue from the DTA virally injected mice was incubated with anti-mCherry to enhance the fluorescence from the mCherry expressed by the virus when taken up into non cre expressing cells. This revealed whether the virus had spread throughout the whole spinal cord and whether it had reached the central canal. This was essential as the CSFcCs around the CC had to take up the virus in order to initiate DTA expression. At this stage there was clear mCherry labelling throughout all levels of both virally injected animals.

The primary indicator of changes within this experiment was the number of EdU+ cells within the CC of each region of the spinal cord. When comparing the averages calculated from N = 3 control mice and N = 2 DTA injected mice, there was an increase in the number of EdU+ cells in the CC within all regions of the cord in the DTA mice. This increase was significant in sections from the thoracic, injection site, lumbar and sacral regions. It did not reach significance in the cervical regions. This may be due to the time in which the animals were perfused after viral injection. The virus was injected into the upper lumbar region of the cord therefore it had to retrogradely move along axons to these more rostral regions of the spinal cord before expressing DTA. The cervical region was furthest from the injection site therefore it may not have had time to cause the same effect here. Additionally, at the site of injection, an injury is caused to the spinal cord, the needle may have pierced through the central canal region, thus the ependymal layer. Ren *et al.* (2017) show that direct injury to the ependymal layer causes an increase in EpC proliferation. The region of highest number of EdU+ cells in the CC was in the lumbar region, below the injection site, which was not the site of injection therefore this effect was independent of the injection itself and likely an effect of the virus.

There is literature suggesting the incorporation of EdU into a cell doesn't just occur when cells are dividing. BrdU, a similar analogue used to mark cell division has been used to pulse-label cells exposed to agents that damaged the DNA (Kalle *et al.*, 1993, Selden *et al.*, 1993). In these studies BrdU indicated DNA repair therefore we cannot be certain as to whether EdU+ cells in this experiment reflect cell division or DNA repair.

There are two possible reasons for the observed increases in EdU+ cells within the virally injected group. The first of which is the hypothesised idea that when CSFcCs are killed or injured, the GABA released by these cells at baseline maintains a low rate of proliferation, subsequently in the absence of this GABA, there was an increase in EpC proliferation. This

effect is consistent with previous work from the laboratory where GABA signalling increased EdU+ labelling (L New, PhD thesis, unpublished).

Alternatively, a concept introduced earlier is that CSFcCs have the capacity to respond to changes in the pH of CSF as well as to neurotransmitters and mechanical stimuli. All of which may cause a response or output from CSFcCs, which could be contributing to the maintenance of the microenvironment around the CC. Therefore it may be the case, that in the absence of CSFcCs, EpCs can no longer survive, therefore they also die, reflecting the caspase-3 expression around the entire CC. If EpC were dying in this way, the increased in proliferation would be to restore the EpC population.

Using caspase-3 as the marker of apoptosis within these cords, it was apparent that there was apoptosis in most regions of the cord following viral expression of DTA. Therefore, we assume the effects seen do reflect cell death. However there was no overlap between caspase-3+ and GCaMP6f+ suggesting the CSFcCs are not the cells that died. This was unexpected so observations were made of CSFcC morphology that may indicate an effect of DTA.

When observing CSFcC morphology and distribution between control and test mice there were some apparent differences. This was assessed qualitatively, looking first at the GCaMP6f labelled CSFcCs in control sections, then comparing the appearance of the somata and axons within the test sections. The unusual appearance of the axons extending from the apical surface of CSFcCs was striking when compared to the control mice. Consistently in control animals, the axons that extend towards the CC are straight and short. In the test mice, there were long, bent axons extending in various directions around the CC. There were also occasionally cells dorsal or ventral of the CC with larger somata compared with the somata around the CC and irregular morphologies appearing less circular than typical CSFcCs. Numerous sections had very few CSFcCs around the CC. Collectively, these observations support the indications of caspase-3+ labelling that DTA has had some effect on these cells. However, further quantitative analysis would be required to verify these changes.

A quantitative measure of the GCaMP6f CSFcC health, was the fluorescence intensity from the signal of the GCaMP6f protein. As a calcium indicator, high fluorescence from this protein before enhanced for visualisation, can indicate the health of the cells since an influx of calcium occurs after cells undergo apoptosis (Orrenius and Nicotera, 1994). When transverse sections were first observed down the microscope, without the addition of any antibodies, the GCaMP6f signal from CSFcCs around the CC was visible in sections from

DTA virus injected mice but not control. This suggests a change in the calcium levels of the cell caused by the virus, suggesting that injured CSFcCs were unable to appropriately regulate calcium levels

3.5.3. Conclusions

The experiments conducted show a possible influence of manipulating CSFcCs resulting in changes to EpC proliferation. There was a decrease in proliferation after injections of Liraglutide. This differed from the increase in proliferation of EpCs seen when CSFcCs were targeted with the selective expression of a toxin. These findings are summarised in Figure 49. Overall, this suggests there may be some relationship between these neighbouring cell types within the spinal cord however further experiments are required to verify the effects resulted from changes in CSFcC activity and not other influences.

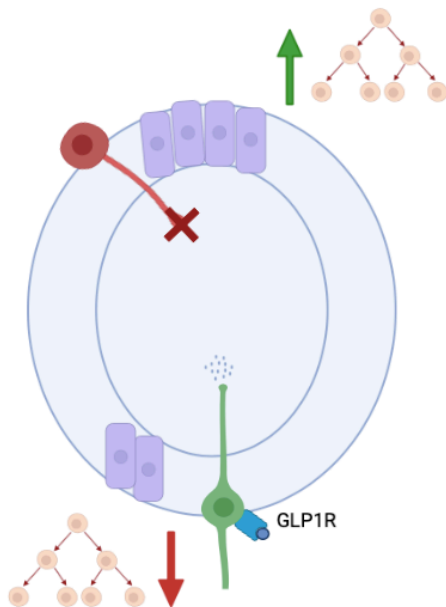


Figure 49: Manipulation of CSFcCs can result in increased or decreased EpC proliferation. Summary of findings within a representative CC simplified with just CSFcCs and EpCs. When CSFcCs were targeted with DTA virus, possibly causing changes to their health (red), there was a significant increase in EdU+ incorporation into cells within the CC which may have resulted from the removal of signals released by CSFcCs. Opposing this, when Liraglutide was given intraperitoneally, EdU+ within cells around the CC decreased which may have resulted from the release of substances such as GABA from the terminal within the CSF.

4. Future Experiments

Having shown the PKD2L1-IRES-Cre mouse line has resulted in animals with cre expressed in PKD2L1+ CSFcCs, this can be utilised to produce various other transgenic animals and manipulate CSFcCs in various ways.

Firstly, if crossed with a floxed ChR mouse line, the animals could be used in optogenetic experiments to selectively activate CSFcCs and assess behavioural or phenotypic changes. In slices, in the presence of a GABA indicator such as GABA_{snfr} it may be possible to determine if CSFcCs are able to release GABA in response to stimuli.

Similarly, if a floxed chemogenetic virus is injected into the spinal cord of PKD2L1-IRES-cre animals, it would be possible to selectively activate PKD2L1+ CSFcCs by injecting clozapine-N-oxide (CNO) a specific activator of the receptors genetically expressed in CSFcCs. This may also indicate the functional role of CSFcCs by assessing any behavioural or movement changes. Similarly, the tissue could be assessed for changes in EdU+ cells, providing a counter experiment to the DTA targeted killing of CSFcCs attempted in this project.

The DTA experiment showed some significant changes in EdU+ cells which require further investigations. Firstly, another suitable control would be injection of the same virus into WT mice in order to look at any effects of the virus when it is not in the presence of cre cells and assess any changes caused by the injection or the virus independent of the effect on cre expressing CSFcCs. Additionally, the use of an antibody to label the DTA toxin should be used to verify the virus did express this toxin in the desired cells, CSFcCs. As the marker of cell death, caspase-3 isn't present within CSFcCs but the region around them. The effect seen throughout the cord or an increase in EdU+ cells around the CC wasn't present in the cervical region. This suggests the virus may not have had time to express the toxin in this region, or the CSFcCs here did not take up the virus, as it was the furthest from the injection site. Next time these animals should be left for longer to assess changes within this region.

Having seen changes in EpC proliferation after injection of Liraglutide, it is important to determine whether this drug can cross the blood brain barrier since current literature is conflicting. This will offer insight as to whether the effects seen could result from activity within the spinal cord or whether this resulted from peripheral effects. This could be done by intraperitoneal injections of Liraglutide conjugated to a fluorescent marker followed by perfusion and dissection to look for the fluorescence within the spinal cord.

Another way in which the activity of liraglutide could be assessed specifically within the spinal cord would be using slice cultures, with no blood brain barrier. In slice cultures, Liraglutide could be applied directly to the CC. In PKD2L1:GCaMP6f tissue any changes in CSFcC electrophysiology could be observed. By changes in the fluorescence intensity of these cells reflecting changes in calcium activity which occur during firing, depolarising or hyperpolarising events.

The viral tracing experiments revealed a small part of some CSFcC axonal projections along the spinal cord. These experiments could be continued by injecting in different regions along the cord to assess the direction and length of projections from different regions. To better understand CSFcC circuitry, it would also be important to label this tissue with other cell markers to determine what cell types they project onto.

Similarly the effect of a DTA injection higher into the cord would offer the chance to look at the effect of this within other regions including the cervical cord and the brainstem. These experiments would offer some further knowledge regarding the functional role of CSFcCs in rodents and the relationship between CSFcCs and EpCs.

5. Conclusions

Overall, from the experiments carried out in this thesis, I have established some novel information regarding CSFcC distribution and properties within rodents. Firstly, there is a clear population of these cells that exist outside of the CC region, between the CC and the VF. There are axons projecting towards the CC and towards the VF. The current defined functions for CSFcCs don't account for cells in this region.

Secondly, I validated the PKD2L1:GCaMP6f transgenic mouse line which can be used to generate further transgenic lines used to manipulate CSFcCs. When assessing the distribution of CSFcCs within tissue from these animals I also established the vast and extensive CSFcC cell population within brainstem nuclei. This indicates various novel functions for these cells.

The evidence that CSFcCs label with markers of both VGAT and SV2 indicate they have the apparatus required to load GABA into vesicles and release vesicles from the synapse. This gives another possible insight into how these cells function within a circuit and relay information to other cells. CSFcCs project between spinal cord levels, which also indicates they are part of a wider circuit, yet to be defined.

The changes in EdU+ cells within the ependymal cell layer suggest a possible interrelationship between CSFcCs and EpCs around the CC. The decrease in EdU+ labelling after Liraglutide injections may have resulted in activation of GLP1Rs present on CSFcCs, although this may have resulted from activation of these receptors present on other cells or via peripheral effects. The presence of GLP1Rs on CSFcCs within the spinal cord does however provide a novel input by which these cells may be able to be manipulated.

The apparent increase in EdU+ cells around the CC following DTA viral injections into the spinal cord also suggest a relationship between CSFcCs and EpCs since the toxin expression was targeted to the cre expressing CSFcCs.

The experiments conducted and the conclusions drawn begin to unveil just part of the phenotype of these unusual cells within the spinal cord of rodents. Further experiments are required to define their circuitry and function as well as exploring whether they are able to influence EpC proliferation. This would have tremendous therapeutic benefit since increase cell proliferation within the spinal cord is desirable in many disease and injury contexts.

6. References

- Allen Institute for Cell Science. 2008. Allen spinal cord atlas. [Online]. [Accessed 1 April 2020]. Available from: <http://mousespinal.brain-map.org/imageseries/show.html?id=100031731>.
- Agduhr, E. 1922. Über ein zentrales Sinnesorgan (?) bei den Vertebraten. *Zeitschrift für Anatomie und Entwicklungsgeschichte*. **66**(3), pp.223-360.
- Akamatsu, W., Fujihara, H., Mitsuhashi, T., Yano, M., Shibata, S., Hayakawa, Y., Okano, H.J., Sakakibara, S.-i., Takano, H., Takano, T., Takahashi, T., Noda, T. and Okano, H. 2005. The RNA-binding protein HuD regulates neuronal cell identity and maturation. *Proceedings of the National Academy of Sciences of the United States of America*. **102**(12), pp.4625-4630.
- Alfaro-Cervello, C., Soriano-Navarro, M., Mirzadeh, Z., Alvarez-Buylla, A. and Garcia-Verdugo, J.M. 2012. Biciliated ependymal cell proliferation contributes to spinal cord growth. *Journal of Comparative Neurology*. **520**(15), pp.3528-3552.
- Alizadeh, A., Dyck, S.M. and Karimi-Abdolrezaee, S. 2019. Traumatic Spinal Cord Injury: An Overview of Pathophysiology, Models and Acute Injury Mechanisms. *Front Neurol*. **10**, p282.
- Andersen, D.B., Grunddal, K.V., Pedersen, J., Kuhre, R.E., Lund, M.L., Holst, J.J. and Ørskov, C. 2021. Using a Reporter Mouse to Map Known and Novel Sites of GLP-1 Receptor Expression in Peripheral Tissues of Male Mice. *Endocrinology*. **162**(3).
- Basinger, H. and Hogg, J.P. 2021. Neuroanatomy, Brainstem. *StatPearls*. Treasure Island (FL): StatPearls Publishing Copyright © 2021, StatPearls Publishing LLC.
- Berglund, L., Björling, E., Oksvold, P., Fagerberg, L., Asplund, A., Szigartyo, C.A., Persson, A., Ottosson, J., Wernérus, H., Nilsson, P., Lundberg, E., Sivertsson, A., Navani, S., Wester, K., Kampf, C., Hober, S., Pontén, F. and Uhlén, M. 2008. A gene-centric Human Protein Atlas for expression profiles based on antibodies. *Mol Cell Proteomics*. **7**(10), pp.2019-2027.
- Bican, O., Minagar, A. and Pruitt, A.A. 2013. The spinal cord: a review of functional neuroanatomy. *Neurol Clin*. **31**(1), pp.1-18.
- Biorender. 2017. [Online]. [Accessed 15 January 2021]. Available from: <https://app.biorender.com>
- Böhm, U.L., Prendergast, A., Djenoune, L., Nunes Figueiredo, S., Gomez, J., Stokes, C., Kaiser, S., Suster, M., Kawakami, K., Charpentier, M., Concordet, J.-P., Rio, J.-P., Del Bene,

F. and Wyart, C. 2016. CSF-contacting neurons regulate locomotion by relaying mechanical stimuli to spinal circuits. *Nature Communications*. **7**(1), p10866.

Boyden, E.S., Zhang, F., Bamberg, E., Nagel, G. and Deisseroth, K. 2005. Millisecond-timescale, genetically targeted optical control of neural activity. *Nature Neuroscience*. **8**(9), pp.1263-1268.

Bussolati, G. and Radulescu, R.T. 2011. Blocking Endogenous Peroxidases in Immunohistochemistry: A Mandatory, Yet Also Subtle Measure. *Applied Immunohistochemistry & Molecular Morphology*. **19**(5), p484.

Carlessi, R., Chen, Y., Rowlands, J., Cruzat, V.F., Keane, K.N., Egan, L., Mamotte, C., Stokes, R., Gunton, J.E., Bittencourt, P.I.H.d. and Newsholme, P. 2017. GLP-1 receptor signalling promotes β -cell glucose metabolism via mTOR-dependent HIF-1 α activation. *Scientific Reports*. **7**(1), p2661.

Cascella, M. 2016. The intercalatus nucleus of Staderini. *J Hist Neurosci*. **25**(4), pp.408-419.

Chao, J., DeBiasio, R., Zhu, Z., Giuliano, K.A. and Schmidt, B.F. 1996. Immunofluorescence signal amplification by the enzyme-catalyzed deposition of a fluorescent reporter substrate (CARD). *Cytometry*. **23**(1), pp.48-53.

Chen, J., Wang, Z., Mao, Y., Zheng, Z., Chen, Y., Khor, S., Shi, K., He, Z., Li, J., Gong, F., Liu, Y., Hu, A., Xiao, J. and Wang, X. 2017. Liraglutide activates autophagy via GLP-1R to improve functional recovery after spinal cord injury. *Oncotarget*. **8**(49), pp.85949-85968.

Christensen, M., Sparre-Ulrich, A.H., Hartmann, B., Grevstad, U., Rosenkilde, M.M., Holst, J.J., Vilsbøll, T. and Knop, F.K. 2015. Transfer of liraglutide from blood to cerebrospinal fluid is minimal in patients with type 2 diabetes. *Int J Obes (Lond)*. **39**(11), pp.1651-1654.

Collier, R.J. 1975. Diphtheria toxin: mode of action and structure. *Bacteriol Rev*. **39**(1), pp.54-85.

Corns, L.F., Atkinson, L., Daniel, J., Edwards, I.J., New, L., Deuchars, J. and Deuchars, S.A. 2015. Cholinergic Enhancement of Cell Proliferation in the Postnatal Neurogenic Niche of the Mammalian Spinal Cord. *Stem Cells*. **33**(9), pp.2864-2876.

Corns, L.F., Deuchars, J. and Deuchars, S.A. 2013. GABAergic responses of mammalian ependymal cells in the central canal neurogenic niche of the postnatal spinal cord. *Neurosci Lett*. **553**, pp.57-62.

Cozzari, C. and Hartman, B.K. 1980. Preparation of antibodies specific to choline acetyltransferase from bovine caudate nucleus and immunohistochemical localization of the enzyme. *Proc Natl Acad Sci U S A*. **77**(12), pp.7453-7457.

Cullen, K.E. 2016. Physiology of central pathways. *Handb Clin Neurol.* **137**, pp.17-40.

Dale, N., Roberts, A., Ottersen, O.P. and Storm-Mathisen, J. 1987. The morphology and distribution of 'Kolmer-Agduhr cells', a class of cerebrospinal-fluid-contacting neurons revealed in the frog embryo spinal cord by GABA immunocytochemistry. *Proc R Soc Lond B Biol Sci.* **232**(1267), pp.193-203.

DeCaen, P.G., Dellinger, M., Vien, T.N. and Clapham, D.E. 2013. Direct recording and molecular identification of the calcium channel of primary cilia. *Nature.* **504**(7479), pp.315-318.

Di Terlizzi, R. and Platt, S. 2006. The function, composition and analysis of cerebrospinal fluid in companion animals: Part I – Function and composition. *The Veterinary Journal.* **172**(3), pp.422-431.

Djenoune, L., Khabou, H., Joubert, F., Quan, F.B., Nunes Figueiredo, S., Bodineau, L., Del Bene, F., Burckle, C., Tostivint, H. and Wyart, C. 2014. Investigation of spinal cerebrospinal fluid-contacting neurons expressing PKD2L1: evidence for a conserved system from fish to primates. *Front Neuroanat.* **8**, p26.

Drew, T., Prentice, S. and Schepens, B. 2004. Cortical and brainstem control of locomotion. *Prog Brain Res.* **143**, pp.251-261.

Dumont, R.J., Okonkwo, D.O., Verma, S., Hurlbert, R.J., Boulos, P.T., Ellegala, D.B. and Dumont, A.S. 2001. Acute spinal cord injury, part I: pathophysiologic mechanisms. *Clin Neuropharmacol.* **24**(5), pp.254-264.

Faget, L. and Hnasko, T.S. 2015. Tyramide Signal Amplification for Immunofluorescent Enhancement. *Methods Mol Biol.* **1318**, pp.161-172.

Fahimi, H.D. and Herzog, V. 1973. A colorimetric method for measurement of the (peroxidase-mediated) oxidation of 3,3'-diaminobenzidine. *J Histochem Cytochem.* **21**(5), pp.499-502.

Feany, M.B., Lee, S., Edwards, R.H. and Buckley, K.M. 1992. The synaptic vesicle protein SV2 is a novel type of transmembrane transporter. *Cell.* **70**(5), pp.861-867.

Fidelin, K., Djenoune, L., Stokes, C., Prendergast, A., Gomez, J., Baradel, A., Del Bene, F. and Wyart, C. 2015. State-dependent modulation of locomotion by GABAergic spinal sensory neurons. *Current Biology.* **25**(23), pp.3035-3047.

Ganapathy, M.K., Reddy, V. and Tadi, P. 2021. Neuroanatomy, Spinal Cord Morphology. *StatPearls.* Treasure Island (FL): StatPearls Publishing

Copyright © 2021, StatPearls Publishing LLC.

- Gerdes, J., Schwab, U., Lemke, H. and Stein, H. 1983. Production of a mouse monoclonal antibody reactive with a human nuclear antigen associated with cell proliferation. *Int J Cancer*. **31**(1), pp.13-20.
- Ghazale, H., Ripoll, C., Leventoux, N., Jacob, L., Azar, S., Mamaeva, D., Glasson, Y., Calvo, C.-F., Thomas, J.-L., Meneceur, S., Lallemand, Y., Rigau, V., Perrin, F.E., Noristani, H.N., Rocamonde, B., Huillard, E., Bauchet, L. and Hugnot, J.-P. 2019. RNA Profiling of the Human and Mouse Spinal Cord Stem Cell Niches Reveals an Embryonic-like Regionalization with MSX1+ Roof-Plate-Derived Cells. *Stem Cell Reports*. **12**(5), pp.1159-1177.
- González-Santana, A., Estévez-Herrera, J., Seward, E.P., Borges, R. and Machado, J.D. 2021. Glucagon-like peptide-1 receptor controls exocytosis in chromaffin cells by increasing full-fusion events. *Cell Reports*. **36**(8), p109609.
- Gordon, J.W., Scangos, G.A., Plotkin, D.J., Barbosa, J.A. and Ruddle, F.H. 1980. Genetic transformation of mouse embryos by microinjection of purified DNA. *Proc Natl Acad Sci U S A*. **77**(12), pp.7380-7384.
- Haddon, C. and Lewis, J. 1996. Early ear development in the embryo of the zebrafish, *Danio rerio*. *J Comp Neurol*. **365**(1), pp.113-128.
- Hamilton, L.K., Truong, M.K.V., Bednarczyk, M.R., Aumont, A. and Fernandes, K.J.L. 2009. Cellular organization of the central canal ependymal zone, a niche of latent neural stem cells in the adult mammalian spinal cord. *Neuroscience*. **164**(3), pp.1044-1056.
- Heppner, K.M., Kirigiti, M., Secher, A., Paulsen, S.J., Buckingham, R., Pyke, C., Knudsen, L.B., Vrang, N. and Grove, K.L. 2015. Expression and distribution of glucagon-like peptide-1 receptor mRNA, protein and binding in the male nonhuman primate (*Macaca mulatta*) brain. *Endocrinology*. **156**(1), pp.255-267.
- Horner, P.J., Power, A.E., Kempermann, G., Kuhn, H.G., Palmer, T.D., Winkler, J., Thal, L.J. and Gage, F.H. 2000. Proliferation and Differentiation of Progenitor Cells Throughout the Intact Adult Rat Spinal Cord. *The Journal of Neuroscience*. **20**(6), pp.2218-2228.
- Huang, A.L., Chen, X., Hoon, M.A., Chandrashekar, J., Guo, W., Trankner, D., Ryba, N.J. and Zuker, C.S. 2006. The cells and logic for mammalian sour taste detection. *Nature*. **442**(7105), pp.934-938.
- Hubbard, Jeffrey M., Böhm, Urs L., Prendergast, A., Tseng, P.-En B., Newman, M., Stokes, C. and Wyart, C. 2016. Intraspinal Sensory Neurons Provide Powerful Inhibition to Motor Circuits Ensuring Postural Control during Locomotion. *Current Biology*. **26**(21), pp.2841-2853.

- Hugnot, J.P. and Franzen, R. 2011. The spinal cord ependymal region: a stem cell niche in the caudal central nervous system. *Frontiers in bioscience (Landmark edition)*. [Online]. **16**, pp.1044-1059.
- Hülsmann, S., Oku, Y., Zhang, W. and Richter, D.W. 2000. Metabotropic glutamate receptors and blockade of glial Krebs cycle depress glycinergic synaptic currents of mouse hypoglossal motoneurons. *Eur J Neurosci*. **12**(1), pp.239-246.
- Hunter, K. and Hölscher, C. 2012. Drugs developed to treat diabetes, liraglutide and lixisenatide, cross the blood brain barrier and enhance neurogenesis. *BMC Neurosci*. **13**, p33.
- Hunyady, B., Krempels, K., Harta, G. and Mezey, E. 1996. Immunohistochemical signal amplification by catalyzed reporter deposition and its application in double immunostaining. *J Histochem Cytochem*. **44**(12), pp.1353-1362.
- Ito, D., Imai, Y., Ohsawa, K., Nakajima, K., Fukuuchi, Y. and Kohsaka, S. 1998. Microglia-specific localisation of a novel calcium binding protein, Iba1. *Brain Res Mol Brain Res*. **57**(1), pp.1-9.
- Iwamoto, Y. and Sasaki, S. 1990. Monosynaptic excitatory connexions of reticulospinal neurones in the nucleus reticularis pontis caudalis with dorsal neck motoneurons in the cat. *Exp Brain Res*. **80**(2), pp.277-289.
- Jalalvand, E., Robertson, B., Wallen, P. and Grillner, S. 2016. Ciliated neurons lining the central canal sense both fluid movement and pH through ASIC3. *Nat Commun*. **7**, p10002.
- Jalalvand, E., Robertson, B., Wallén, P., Hill, R.H. and Grillner, S. 2014. Laterally projecting cerebrospinal fluid-contacting cells in the lamprey spinal cord are of two distinct types. *J Comp Neurol*. **522**(8), pSp1.
- Johansson, C.B., Momma, S., Clarke, D.L., Risling, M., Lendahl, U. and Frisen, J. 1999. Identification of a neural stem cell in the adult mammalian central nervous system. *Cell*. **96**(1), pp.25-34.
- Kalle, W.H., Hazekamp-van Dokkum, A.M., Lohman, P.H., Natarajan, A.T., van Zeeland, A.A. and Mullenders, L.H. 1993. The use of streptavidin-coated magnetic beads and biotinylated antibodies to investigate induction and repair of DNA damage: analysis of repair patches in specific sequences of uv-irradiated human fibroblasts. *Anal Biochem*. **208**(2), pp.228-236.
- Katsurada, K., Maejima, Y., Nakata, M., Kodaira, M., Suyama, S., Iwasaki, Y., Kario, K. and Yada, T. 2014. Endogenous GLP-1 acts on paraventricular nucleus to suppress feeding:

- Projection from nucleus tractus solitarius and activation of corticotropin-releasing hormone, nesfatin-1 and oxytocin neurons. *Biochemical and Biophysical Research Communications*. **451**(2), pp.276-281.
- Kazemi, H. and Johnson, D.C. 1986. Regulation of cerebrospinal fluid acid-base balance. *Physiological Reviews*. **66**(4), pp.953-1037.
- Kempermann, G., Kuhn, H.G. and Gage, F.H. 1997. Genetic influence on neurogenesis in the dentate gyrus of adult mice. *Proc Natl Acad Sci U S A*. **94**(19), pp.10409-10414.
- Kolmer, W. 1921. Das „Sagittalorgan“ der Wirbeltiere. *Zeitschrift für Anatomie und Entwicklungsgeschichte*. **60**(3), pp.652-717.
- Koole, C., Pabreja, K., Savage, Emilia E., Wootten, D., Furness, Sebastian G.B., Miller, Laurence J., Christopoulos, A. and Sexton, Patrick M. 2013. Recent advances in understanding GLP-1R (glucagon-like peptide-1 receptor) function. *Biochemical Society Transactions*. **41**(1), pp.172-179.
- Koser, D.E., Moeendarbary, E., Hanne, J., Kuerten, S. and Franze, K. 2015. CNS cell distribution and axon orientation determine local spinal cord mechanical properties. *Biophys J*. **108**(9), pp.2137-2147.
- Lee, Y.-S. and Jun, H.-S. 2016. Anti-Inflammatory Effects of GLP-1-Based Therapies beyond Glucose Control. *Mediators of Inflammation*. **2016**, pp.1-11.
- Liang, H., Paxinos, G. and Watson, C. 2011. Projections from the brain to the spinal cord in the mouse. *Brain Struct Funct*. **215**(3-4), pp.159-186.
- Liu, X., Wang, Q., Haydar, T.F. and Bordey, A. 2005. Nonsynaptic GABA signaling in postnatal subventricular zone controls proliferation of GFAP-expressing progenitors. *Nat Neurosci*. **8**(9), pp.1179-1187.
- Marichal, N., García, G., Radmilovich, M., Trujillo-Cenóz, O. and Russo, R.E. 2009. Enigmatic Central Canal Contacting Cells: Immature Neurons in “Standby Mode”? *The Journal of Neuroscience*. **29**(32), pp.10010-10024.
- Martens, D.J., Seaberg, R.M. and Van Der Kooy, D. 2002. In vivo infusions of exogenous growth factors into the fourth ventricle of the adult mouse brain increase the proliferation of neural progenitors around the fourth ventricle and the central canal of the spinal cord. *European Journal of Neuroscience*. **16**(6), pp.1045-1057.
- McDaid, D., Park, A.L., Gall, A., Purcell, M. and Bacon, M. 2019. Understanding and modelling the economic impact of spinal cord injuries in the United Kingdom. *Spinal Cord*. **57**(9), pp.778-788.

- McIntire, S.L., Reimer, R.J., Schuske, K., Edwards, R.H. and Jorgensen, E.M. 1997. Identification and characterization of the vesicular GABA transporter. *Nature*. **389**(6653), pp.870-876.
- Meletis, K., Barnabe-Heider, F., Carlen, M., Evergren, E., Tomilin, N., Shupliakov, O. and Frisen, J. 2008. Spinal cord injury reveals multilineage differentiation of ependymal cells. *PLoS Biol.* **6**(7), pe182.
- Moore, S.A. 2016. The Spinal Ependymal Layer in Health and Disease. *Veterinary Pathology*. **53**(4), pp.746-753.
- Moreno-Manzano, V., Rodríguez-Jiménez, F.J., García-Roselló, M., Laínez, S., Erceg, S., Calvo, M.T., Ronaghi, M., Lloret, M., Planells-Cases, R., Sánchez-Puelles, J.M. and Stojkovic, M. 2009. Activated spinal cord ependymal stem cells rescue neurological function. *Stem Cells*. **27**(3), pp.733-743.
- Nauli, S.M., Pala, R. and Kleene, S.J. 2016. Calcium channels in primary cilia. *Curr Opin Nephrol Hypertens*. **25**(5), pp.452-458.
- Nomura, H., Turco, A.E., Pei, Y., Kalaydjieva, L., Schiavello, T., Weremowicz, S., Ji, W., Morton, C.C., Meisler, M., Reeders, S.T. and Zhou, J. 1998. Identification of PKDL, a novel polycystic kidney disease 2-like gene whose murine homologue is deleted in mice with kidney and retinal defects. *J Biol Chem*. **273**(40), pp.25967-25973.
- Ohsawa, K., Imai, Y., Sasaki, Y. and Kohsaka, S. 2004. Microglia/macrophage-specific protein Iba1 binds to fimbrin and enhances its actin-bundling activity. **88**(4), pp.844-856.
- Orrenius, S. and Nicotera, P. 1994. The calcium ion and cell death. *J Neural Transm Suppl*. **43**, pp.1-11.
- Orts-Del'Immagine, A., Seddik, R., Tell, F., Airault, C., Er-Raoui, G., Najimi, M., Trouslard, J. and Wanaverbecq, N. 2016. A single polycystic kidney disease 2-like 1 channel opening acts as a spike generator in cerebrospinal fluid-contacting neurons of adult mouse brainstem. *Neuropharmacology*. **101**, pp.549-565.
- Orts-Del'Immagine, A., Trouslard, J., Airault, C., Hugnot, J.P., Cordier, B., Doan, T., Kastner, A. and Wanaverbecq, N. 2017. Postnatal maturation of mouse medullo-spinal cerebrospinal fluid-contacting neurons. *Neuroscience*. **343**, pp.39-54.
- Orts-Del'immagine, A., Wanaverbecq, N., Tardivel, C., Tillement, V., Dallaporta, M. and Trouslard, J. 2012. Properties of subependymal cerebrospinal fluid contacting neurones in the dorsal vagal complex of the mouse brainstem. *J Physiol*. **590**(16), pp.3719-3741.

- Orts-Del'Immagine, A., Cantaut-Belarif, Y., Thouvenin, O., Roussel, J., Baskaran, A., Langui, D., Koëth, F., Bivas, P., Lejeune, F.-X., Bardet, P.-L. and Wyart, C. 2020. Sensory Neurons Contacting the Cerebrospinal Fluid Require the Reissner Fiber to Detect Spinal Curvature *Current Biology*. **30**(5), pp.827-839.e824.
- Peterson, B.W., Maunz, R.A., Pitts, N.G. and Mackel, R.G. 1975. Patterns of projection and branching of reticulospinal neurons. *Exp Brain Res*. **23**(4), pp.333-351.
- Porter, A.G. and Jänicke, R.U. 1999. Emerging roles of caspase-3 in apoptosis. *Cell death & differentiation*. **6**(2), pp.99-104.
- Prendergast, A., Jim, K.K., Marnas, H., Desban, L., Quan, F., Djenoune, L., Roussel, J., Cantaut-Belarif, Y., Sahu, S. and Bardet, P.-L. 2019. Central sensory neurons detect and combat pathogens invading the cerebrospinal fluid. *Available at SSRN 3404255*.
- Protein atlas. The human protein atlas. [Online]. [Accessed 30 August 2021]. Available from: <https://www.proteinatlas.org/ENSG00000107593-PKD2L1/tissue/kidney>
- Que, Q., Guo, X., Zhan, L., Chen, S., Zhang, Z., Ni, X., Ye, B. and Wan, S. 2019. The GLP-1 agonist, liraglutide, ameliorates inflammation through the activation of the PKA/CREB pathway in a rat model of knee osteoarthritis. *Journal of Inflammation*. **16**(1), p13.
- Ren, Y., Ao, Y., O'Shea, T.M., Burda, J.E., Bernstein, A.M., Brumm, A.J., Muthusamy, N., Ghashghaei, H.T., Carmichael, S.T., Cheng, L. and Sofroniew, M.V. 2017. Ependymal cell contribution to scar formation after spinal cord injury is minimal, local and dependent on direct ependymal injury. *Scientific Reports*. **7**(1), p41122.
- Rexed, B. 1954. A cytoarchitectonic atlas of the spinal cord in the cat. *Journal of Comparative Neurology*. **100**(2), pp.297-379.
- Rosenberg, A.B., Roco, C.M., Muscat, R.A., Kuchina, A., Sample, P., Yao, Z., Greybuck, L.T., Peeler, D.J., Mukherjee, S., Chen, W., Pun, S.H., Sellers, D.L., Tasic, B. and Seelig, G. 2018. Single-cell profiling of the developing mouse brain and spinal cord with split-pool barcoding. *Science*. **360**(6385), pp.176-182.
- Ross, M.E., Park, D.H., Teitelman, G., Pickel, V.M., Reis, D.J. and Joh, T.H. 1983. Immunohistochemical localization of choline acetyltransferase using a monoclonal antibody: a radioautographic method. *Neuroscience*. **10**(3), pp.907-922.
- Selden, J.R., Dolbeare, F., Clair, J.H., Nichols, W.W., Miller, J.E., Kleemeyer, K.M., Hyland, R.J. and DeLuca, J.G. 1993. Statistical confirmation that immunofluorescent detection of DNA repair in human fibroblasts by measurement of bromodeoxyuridine incorporation is

- stoichiometric and sensitive. *Cytometry: The Journal of the International Society for Analytical Cytology*. **14**(2), pp.154-167.
- Shaner, N.C., Campbell, R.E., Steinbach, P.A., Giepmans, B.N., Palmer, A.E. and Tsien, R.Y. 2004. Improved monomeric red, orange and yellow fluorescent proteins derived from *Discosoma* sp. red fluorescent protein. *Nat Biotechnol*. **22**(12), pp.1567-1572.
- Sharma, D., Verma, S., Vaidya, S., Kalia, K. and Tiwari, V. 2018. Recent updates on GLP-1 agonists: Current advancements & challenges. *Biomedicine & Pharmacotherapy*. **108**, pp.952-962.
- Staderini, R. 1894. Sopra un nucleo di cellule nervose interstiziali tra i nuclei di origine del vago e dell'ipoglosso. *Monitore Zoologico Italiano*. **8**(5), pp.178-183.
- Sternberg, J.R., Prendergast, A.E., Brosse, L., Cantaut-Belarif, Y., Thouvenin, O., Orts-Del'Immagine, A., Castillo, L., Djenoune, L., Kurisu, S., McDearmid, J.R., Bardet, P.L., Boccara, C., Okamoto, H., Delmas, P. and Wyart, C. 2018. Pkd2l1 is required for mechanoreception in cerebrospinal fluid-contacting neurons and maintenance of spine curvature. *Nat Commun*. **9**(1), p3804.
- Stoeckel, M.-E., Uhl-Bronner, S., Hugel, S., Veinante, P., Klein, M.-J., Mutterer, J., Freund-Mercier, M.-J. and Schlichter, R. 2003. Cerebrospinal fluid-contacting neurons in the rat spinal cord, a γ -aminobutyric acidergic system expressing the P2X2 subunit of purinergic receptors, PSA-NCAM, and GAP-43 immunoreactivities: Light and electron microscopic study. *Journal of Comparative Neurology*. **457**(2), pp.159-174.
- Strachan, E., Mallia, A.K., Cox, J.M., Antharavally, B., Desai, S., Sykaluk, L., O'Sullivan, V. and Bell, P.A. 2004. Solid-phase biotinylation of antibodies. *J Mol Recognit*. **17**(3), pp.268-276.
- Thorens, B., Porret, A., Bühler, L., Deng, S.P., Morel, P. and Widmann, C. 1993. Cloning and functional expression of the human islet GLP-1 receptor. Demonstration that exendin-4 is an agonist and exendin-(9-39) an antagonist of the receptor. *Diabetes*. **42**(11), pp.1678-1682.
- Trapp, S. and Hisadome, K. 2011. Glucagon-like peptide 1 and the brain: central actions-central sources? *Auton Neurosci*. **161**(1-2), pp.14-19.
- Watson, C. and Harrison, M. 2012. The Location of the Major Ascending and Descending Spinal Cord Tracts in all Spinal Cord Segments in the Mouse: Actual and Extrapolated. *The Anatomical Record*. **295**(10), pp.1692-1697.

Weiss, S., Dunne, C., Hewson, J., Wohl, C., Wheatley, M., Peterson, A.C. and Reynolds, B.A. 1996. Multipotent CNS Stem Cells Are Present in the Adult Mammalian Spinal Cord and Ventricular Neuroaxis. *The Journal of Neuroscience*. **16**(23), pp.7599-7609.

Wheeler, M.B., Lu, M., Dillon, J.S., Leng, X.H., Chen, C. and Boyd, A.E., 3rd. 1993. Functional expression of the rat glucagon-like peptide-I receptor, evidence for coupling to both adenylyl cyclase and phospholipase-C. *Endocrinology*. **133**(1), pp.57-62.

Wiedenmann, B., Franke, W.W., Kuhn, C., Moll, R. and Gould, V.E. 1986. Synaptophysin: a marker protein for neuroendocrine cells and neoplasms. *Proc Natl Acad Sci U S A*. **83**(10), pp.3500-3504.

Wu, Z., Autry, A.E., Bergan, J.F., Watabe-Uchida, M. and Dulac, C.G. 2014. Galanin neurons in the medial preoptic area govern parental behaviour. *Nature*. **509**(7500), pp.325-330.

Wyart, C., Del Bene, F., Warp, E., Scott, E.K., Trauner, D., Baier, H. and Isacoff, E.Y. 2009. Optogenetic dissection of a behavioural module in the vertebrate spinal cord. *Nature*. **461**(7262), pp.407-410.

Xu, W., Lakshman, N. and Morshead, C.M. 2017. Building a central nervous system: The neural stem cell lineage revealed. *Neurogenesis (Austin)*. **4**(1), pe1300037.

Zhang, D. and Lv, G. 2018. Therapeutic potential of spinal GLP-1 receptor signaling. *Peptides*. **101**, pp.89-94.

Zhang, S. and Cui, W. 2014. Sox2, a key factor in the regulation of pluripotency and neural differentiation. *World J Stem Cells*. **6**(3), pp.305-311.

Zobel, E.H., Ripa, R.S., von Scholten, B.J., Rotbain Curovic, V., Kjaer, A., Hansen, T.W., Rossing, P. and Størling, J. 2021. Effect of liraglutide on expression of inflammatory genes in type 2 diabetes. *Scientific Reports*. **11**(1), p18522.